Martin Håbet Tangen

Rapid Prototyping for Estimating Hydrodynamic Coefficients of Scaled Experiments on Subsea Structures during Lifting Operations

NTNU
Norwegian University of
Science and Technology

Martin Håbet Tangen

Rapid Prototyping for Estimating Hydrodynamic Coefficients of Scaled Experiments on Subsea Structures during Lifting Operations

NTNU
Norwegian University of
Science and Technology

Rapid Prototyping for Estimating Hydrodynamic Coefficients of Scaled Experiments on Subsea Structures during Lifting Operations

Background

The offshore sector must always work to find new innovative methods. Subsea technology seems to be the future of the offshore industry. However, there are often significant expenses connected to the estimation of dynamical forces affecting a subsea structure during maritime operations. Therefore, a more innovative method for estimating the dynamic coefficients for subsea structures could be of great interest to the offshore industry.

An innovative solution to estimate the dynamic forces on a subsea structure could be with the use of rapid prototyping. A typical rapid prototyping technique is 3D printing. If a 3D model of a subsea structure could be 3D printed and used for scaled experimental testing, this could be an economic advantage compared to today's methods. The method will simulate the physical properties of a real operation and could have the potential to recreate accurate dynamical forces.
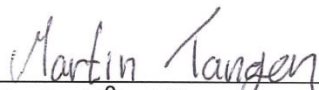
Scope

The scope of this thesis will be somewhere within the boundaries of the three topics of rapid prototyping, subsea lifting operations, and experimental methods. The project will aim at using down-scaled objects. Performing experimental tests on these objects will acquire data for damping and added mass, or as drag and added mass coefficients.

Objectives / Research Questions

The main objective of this thesis is to develop a method where rapid prototyping is used to estimate hydrodynamic forces on subsea structures. This will be done by performing experimental tests on 3D printed scaled subsea structures in the towing tank at NTNU Ålesund. Further, the method must be validated to check to what extent the results are applicable for an estimation of the dynamic forces on a full-scale model. Scale effects must be evaluated to acquire comparable results.

RQ1: How can 3D printed objects improve today's methods for estimating hydrodynamic coefficients?

RQ2: How to analyze and validate hydrodynamic coefficients from scaled experimental tests?

RQ3: How does the scale effect influence the hydrodynamic coefficients?

Martin Håbet Tangen
Student
MSc Product- and System Design
PHONE +47 45 46 92 16
E-mail tangen93@hotmail.com

Professor Vilmar Æsøy
Supervisor - Master Program

Abstract

The offshore industry must always strive for better technological choices. Hydrodynamical forces affecting maritime operations are partly based on experience since the estimation of complex geometries can be challenging and time-consuming. This master thesis presents and discusses the development of a method used to estimate hydrodynamical coefficients of subsea structures during maritime operations, including installation and maintenance. The estimation is conducted by experimental methods performed on 3D printed geometries in the towing tank at NTNU Ålesund.

A new and improved experimental test setup was designed to conduct experiments on 3D printed subsea structures. The new setup has been designed and assembled. While the existing setup allowed for an upward force on a submerged object, the new setup may apply both an upward and downward force. There are two types of experiments conducted: forced oscillation experiments and forced lifting experiments.

Tests were first conducted using simple geometries. Later an attempt to produce real-life subsea structures was performed using the available 3D printer technology at NTNU Ålesund. Simple reference geometries are used to verify the method itself, rather than verifying each tested geometry. For verification, structures where either theoretical or previous experimental data could be acquired is used.

The test objects are scaled down to fit the physical limitations of the towing tank. As a result of conducting down-scaled experiments, the measured values ultimately had to be re-scaled to full-size for practical use. Scale effects of different geometries can affect the flow and forces acting on a structure. Therefore, the forces are compared to several different scaled objects. The results are then used to evaluate how the added mass and damping change with the scale of the object.

The final result is a set of values for added mass and damping for different geometries. These results are then used, in combination with the reference data, to conclude if the method is feasible.

Sammendrag

Offshorenæringen må alltid strekke seg etter bedre teknologiske løsninger. Dynamiske krefter som påvirker maritime-operasjoner er delvis basert på erfaring på grunn av at estimeringen av komplekse geometrier kan være krevende og tidskonsumerende. Denne masteroppgaven presenterer og diskuterer utviklingen av en metode som brukes til estimeringen av hydrodynamiske koeffisienter for subsea konstruksjoner under, maritime-operasjoner som installasjon og vedlikehold. Estimeringen er utført med eksperimentelle metoder, utført ved bruk av 3D-printede geometrier i slepetanken ved NTNU Ålesund.

Et nytt og forbedret testoppsett er designet for å kunne utføre eksperimenter på 3D-printede subsea strukturer. Det nye oppsettet er designet og montert. Hvor det opprinnelige oppsettet kunne påføre en løftende kraft på et neddykket objekt, kan det nye påføre både en løftende og senkende kraft. Det har blitt utført to typer eksperimenter: tvunget oscillering og tvunget løft.

De første eksperimentene ble utført med enkle geometrier. Senere ble det forsøkt å fremstille ekte subsea strukturer ved å benytte den tilgjengelige teknologien ved NTNU Ålesund. Istedenfor å verifisere hvert enkelt eksperiment så er det heller forsøkt å verifisere metoden i seg selv. Enkle referanse geometrier er benyttet til å verifisere den eksperimentelle metoden. Dette har vært geometrier hvor teoretisk eller tidligere eksperimentell data er benyttet.

Testobjektene er nedskalert for å være tilpasset de fysiske begrensingene i slepetanken. Ettersom at eksperimentene er utført på nedskalerte modeller, er målingene oppskalert igjen. Skalaeffekter kan påvirke strømming og krefter som virker på en geometri. Derfor er kreftene sammenliknet for ulike skalerte objekter. Resultatet er videre benyttet for å evaluere hvordan demping og added mass er påvirket av skalaeffekter.

Resultatet er et sett av resultater med verdier for added mass og demping for ulike geometrier. Resultatene er videre brukt, i kombinasjon med referansedata, for å konkludere om metoden kan benyttes.

Preface

The research presented in this master thesis was conducted during spring 2019 at the Norwegian University of Science and Technology in Ålesund (NTNU), Department of Ocean Operations and Civil Engineering, Faculty of Engineering, to earn the degree of Master of Science in Product- and System Design.

This thesis contains physical model experiments, test setup development, and evaluation of 3D printed objects used to estimate hydrodynamical forces. This thesis builds on a previous master thesis at NTNU, where I assisted the author Qian Yu during the spring of 2018. She did experimental research to investigate hydrodynamical coefficients on cylinders and mudmats. This started my reflection that 3D printed objects could be a way of saving both energy and resources in the process of finding hydrodynamical coefficients for maritime operations.

In the course of my research, I have gained a considerable amount of knowledge in several fields. During the development of a test rig and a couple of hundred experimental tests, I have learned the importance of thoroughness and that nothing is made perfect the first time, but if you keep trying you can make it in the end. Software coding in MATLAB was something I had minimal experience with before the work of this thesis. Many hours have been spent to develop scripts extracting and processing the required data. At the end of my thesis, I must say I have learned a great deal that will help me throughout my working career.

It is with great pleasure, I would like to acknowledge the guidance from my supervisor Prof. Vilmar Æsøy. For always believing in me and providing me with highly qualified ideas and support whenever needed, in addition to many inspiring conversations. In addition to my supervisor, I would like to show my appreciation for all the support given by Prof. Karl Henning Halse within the field of hydrodynamics, Associate Prof. Henry Piehl within the field of programming and hydrodynamics, and Engineer André Tranvåg for all the help given in the workshop.

I am thankful to my fiancé, Kristine for her patience and support throughout the course of this work. Finally, I would like to thank all my fellow students for making my time at NTNU Ålesund unforgettable; it would not have been the same without every single one of you.

NTNU – Ålesund

June 2019

Martin Håbet Tangen

Table of Contents

List of Figures

List of Tables

List of Abbreviations

2D	*Two-Dimensional*
3D	*Three-dimensional*
AM	*Additive Manufacturing*
CAD	*Computer-Aided Design*
CAE	*Computer-Aided Engineering*
CCW	*Counterclockwise*
CFD	*Computational Fluid Dynamics*
DNV-GL	*Det Norske Veritas Germanischer Lloyd*
FDM	*Fused Deposition Modelling*
FIR	*Finite Input Response*
G-code	*Numerical Control Programming Language*
LOESS	*Locally Estimated Scatterplot Smoothening*
MSL	*Mean Sea Level*
NTNU	*Norwegian University of Science and Technology*
PLA	*Polylactic Acid*
PVA	*Polyvinyl Alcohol*
RQ	*Research Question*
SLS	*Selective Laser Sintering*
STL	*Stereolithography*
U.S	*United States of America*

List of Symbols

λ	Scale Factor	[-]
ν	Kinematic Viscosity	[m^2/s]
ρ	Density	[kg/m^3]
μ	Discharge Coefficient	[-]
ω	Angular Velocity	[rad/s]
φ	Phase Shift	[rad]
a	Acceleration	[m/s^2]
A	Cross-Section Area	[m^2]
$A0$	Theoretical Added Mass for Simplified Geometry	[kg]
$A1$	Added Mass Force Amplitude	[N]
$A2$	Damping Force Amplitude	[N]
A_{33}	Hydrodynamical Added Mass in Heave	[kg]
B	Damping	[N/(m/s)]
$B1$	Liner Damping	[N/(m/s)]
$B2$	Quadratic Damping	[$N/(m/s)^2$]
C_A	Added Mass Coefficient	[-]
C_D	Drag Coefficient	[-]
C_M	Inertia Force Coefficient	[-]
F	Force	[N]
F_a	Force Due to Added Mass	[N]
F_b	Buoyancy Force	[N]
F_d	Force Due to Drag	[N]
Fr	Froude Number	[-]
g	Gravitational constant	[9.81 m/s^2]
G	Gravitational Force of the Object in Air	[N]
H	Height	[m]
k	Geometrical coefficient	[-]
KC	Keulegan-Carpenter Number	[-]
μKC	Porous KC Number	[-]
L	Characteristic Linear Length	[m]
M	Oscillating Mass of System and Object	[kg]
p	Perforation	[-]
Re	Reynolds Number	[-]
t	Time	[s]
T	Oscillating Object Period	[s]
$T1$	Tension Force from Upper Wire	[N]
$T2$	Tension Force from Lower Wire	[N]
u	Velocity	[m/s]
$\dot{u}$	Acceleration	[m/s^2]
V	Volume	[m^3]
V_{ref}	Reference Volume	[m^3]
W	Width	[m]
Z	Amplitude of Oscillation	[m]
$\dot{Z}$	Velocity	[m/s]
$\ddot{Z}$	Acceleration	[m/s^2]

1 Introduction

1.1 Problem

Since the oil and gas crisis in 2014, the offshore sector has been forced to search for even more economical solutions for how things are done. Even if there might seem to be an increase in offshore commitment over the last period, the industry must still strive for even better technological choices. Subsea technology is one of the technologies that may reduce costs for the offshore industry even more. The first Norwegian subsea template was installed in the North Sea at the Tommeliten gas field, back in 1988 (Solheim, 1989). This new technology brought new possibilities to the offshore industry, as extraction from fields at greater depth and in challenging environments. However, until recent years the limited recovery from subsea wells compared to traditional platform operated wells have been a setback for subsea technology (Underwater Technology Foundation, 2018). The gap between subsea and traditional wells have decreased, and subsea oil and gas production seems to be the future for the offshore industry.

Despite the positive sides related to subsea oil and gas extraction, several new challenges emerged — some related to maintenance at vast depths, and others related to the installation of the subsea structures. For the offshore industry to be able to install the subsea structures as smoothly and safely as possible, the dynamic forces affecting the operation must be known.

The estimation of dynamic forces is often based on the Morison equation. In this equation, the hydrodynamical properties of an object can be defined by a drag coefficient and an added mass coefficient (Morison, et al., 1950). These are not necessarily easy to acquire, since they may change according to velocity and acceleration.

Historically, it seems that dynamic forces in maritime operations are partly based on experience instead of accurate calculations. For subsea structures, the dynamic forces are hard to estimate correctly due to complex geometries. Some software has been created to solve the complicated operation, but there are several physical properties which are not included in these numerical simulations that appear in real life.
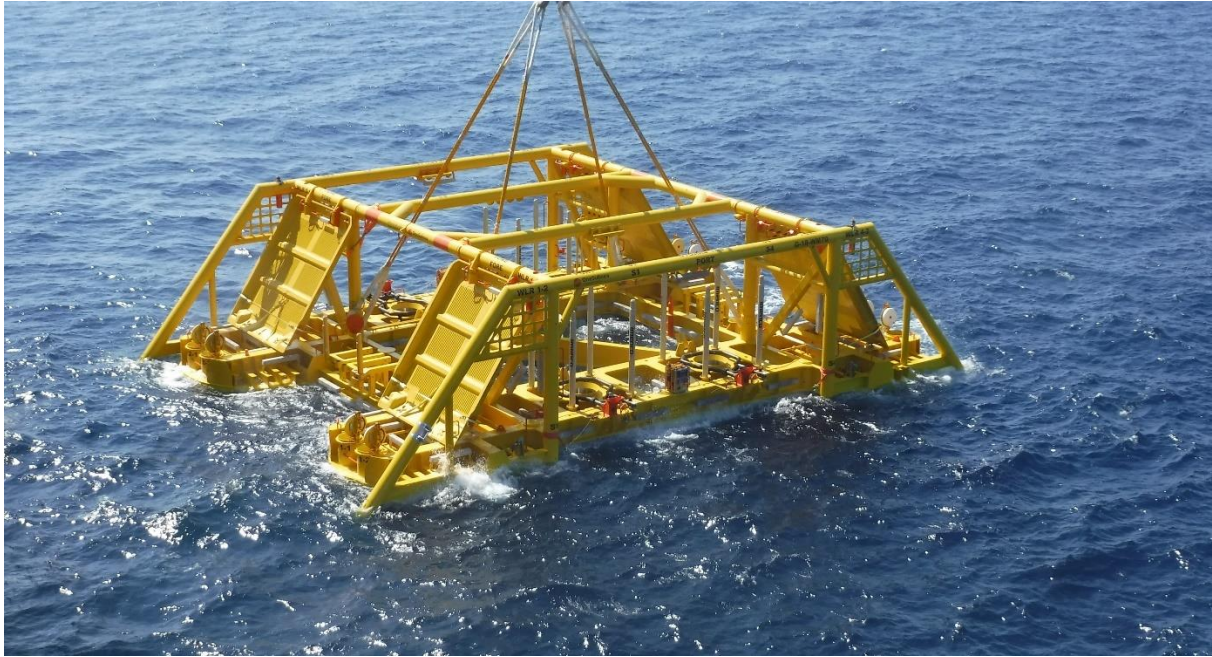
Figure 1.1 - Subsea template being deployed
Photo: Ashtead Technology

Therefore, physical experiments are the most accurate method of achieving the correct hydrodynamic forces affecting this type of complex geometry. At the same time, building full-scale models of the size of a real subsea structure, like the one in Figure 1.1, and paying lease on an offshore vessel is highly expensive and time-consuming. Therefore, a more innovative and cost-saving method for estimating dynamic forces could be of great benefit to the offshore industry.

1.2 Motivation

An innovative solution to estimate the hydrodynamic forces on a subsea structure could be with the use of rapid prototyping. Rapid prototyping is a technique where parts relatively quick can be produced with the help of computer-aided design (CAD). A typical rapid prototyping technique is 3D printing. If a digital 3D computer model of a subsea structure could be 3D printed and used for scaled testing, this could be profitable compared to full-scale tests or time-consuming computational fluid dynamics (CFD) simulations. The method of scaled experiments will recreate the physical properties of the real operation and could have the potential to simulate accurate dynamical forces.

There are multiple 3D printing technologies available today. One technology that NTNU Ålesund has invested in is several machines with fused deposition modeling (FDM). Objects made utilizing this technology can be made in a large variety of materials; the most common material is polylactic acid (PLA) (All3DP, 2018). This is a low-cost material that also generates proper quality objects. The machines using fused deposition modeling are relatively cheap compared to other 3D printing methods. A large variety of geometries can be produced, like the example in Figure 1.2.

The motivation for this research originated from a research project at NTNU Ålesund. The research project will benefit if the method of finding hydrodynamic forces from 3D printed objects is proven plausible. By making a method for how a 3D CAD model can be directly produced by a 3D printer or with minor geometrical adjustments before experimentally tested, this could be of great interest for the offshore industry. The price for investing in a 3D printer and the material and time needed is almost neglectable in comparison to today's either costly experimental tests or advanced and time-consuming CFD simulations.

How the dynamic forces affect a subsea structure must be known to be able to perform lifting operations safely and with correct assumptions. The results could be used to implement better predictions for such as active heave compensation, prediction of splash zone forces, and landing forces.

Figure 1.2 - 3D printed object
Credit: 3D Hubs

1.3 Scope

The scope of this thesis will be somewhere within the boundaries of the three topics of rapid prototyping, subsea lifting operations, and experimental methods, as illustrated in Figure 1.3. The project will aim at using scaled-down 3D printed subsea structures and performing experimental tests on these objects to acquire data for drag- and added mass, or as coefficients.

There is a large variety of subsea structures used for subsea lifting operations. Therefore, this field is narrowed down and limited to a few simple subsea structures, like a subsea template and a suction anchor. The focus will not be to analyze as many structures as possible, but rather select a few and do thorough research on these particular designs.

Rapid prototyping may refer to several techniques. In this research, the technology used is the additive manufacturing technique of 3D printing, or more accurately fused deposition modeling. The availability of 3D printers is limited by the available machines at NTNU Ålesund. This is due to an ideal thought that a useable model can be made with the equipment at hand, and not by outsourcing the production to others.

Experimental research will be limited to scaled-down experiments in the towing tank at NTNU Ålesund. This is tests where the target is to acquire hydrodynamic data or coefficients in the form of drag- and added mass. Two different experiments will be conducted, one as a combination of tests with constant speed and constant acceleration, and the other with oscillating movement. All tests are of fully submerged test objects.
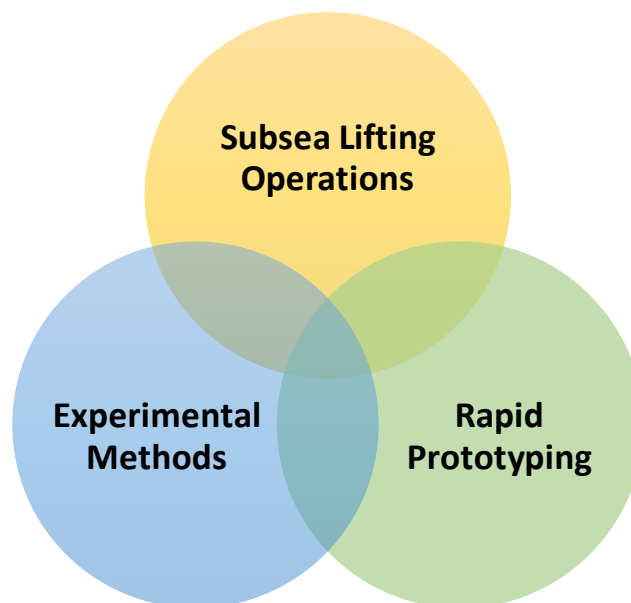
Figure 1.3 - Scope illustrated through VENN-diagram

1.4 Objective and Research Questions

The main objective of this thesis is to develop and test a method for how rapid prototyping can be used to estimate hydrodynamic coefficients of subsea structures. This will be done by performing experimental tests on various structures, including 3D printed scaled subsea structures, in the towing tank at NTNU in Ålesund. Scale effects must be evaluated to acquire comparable results between the experiments conducted.

To be able to execute accurate tests, an improved test setup from the existing setup in the towing tank is needed. The existing system uses two wires to apply a lifting force to the test object. The new system should be designed to both apply a force upwards and downwards to the test object. A downward force will make the system able to perform forced oscillating movement experiments on low-density objects, like 3D printed geometries.

The use of 3D printing to produce scaled models may result in several challenges. Subsea structures are large constructions. Therefore, the structures must be scaled to an appropriate size for the towing tank and the 3D printer. A 10 mm plate scaled 1:100 will be too thin to be produced and for experimental purposes in the test tank. Depending on how the CAD model is constructed, this could be a challenging problem to solve.

The research questions are the underlying targets for the master thesis. Answering or discussing these questions will be the focus of the report. The research questions are as follows:

RQ1: How can 3D printed objects improve today's methods for estimating hydrodynamic coefficients?

RQ2: How to analyze and validate hydrodynamic coefficients from scaled experimental tests?

RQ3: How does the scale effect influence the hydrodynamic coefficients?

1.5 Thesis structure

This thesis is structured with a literature review in chapter 2 following this introductory chapter. Chapter 2 describes the theoretical knowledge utilized throughout this research. Starting with the fundamentals of rapid prototyping and 3D printing. The process from design to the finished model is explained, with related 3D printing technologies and essential knowledge within the field. Then the basic theory for the experimental methods used in this thesis is presented. Next, some background of subsea lifting operations is presented. The background describes generic on subsea structures, operations, and more detailed information on subsea templates. Then the related work of a previous master thesis within the same field is summarized, among other related work.

Chapter 3 presents the methodology of the thesis. Starting with an overall description of the experimental approach for the research. Followed by the development of the new experimental test setup utilized to conduct all the experiments. Then, the two different experimental test methods are presented with related theory. Next, the methodology regarding the design and fabrication of 3D printed structures is presented. Finally, the work done with real-life subsea structures is presented.

Chapter 4 contains the experimental model test study. Starting with the presentation of the different test geometries the experiments are conducted with. Details for each geometry and control variables are presented. Next, the smoothing and fitting of the recorded data series are explained and followed by the data analysis regarding how the hydrodynamical forces and coefficients are calculated from the already smoothed data.

Chapter 5 presents the results and the discussion of the results acquired. Each geometry is split into separate sub-chapters. The results are then compared to other experimental or theoretical data, where this could be found.

Chapter 6 concludes the research conducted in this thesis. Furthermore, the research questions are addressed before the future work that would bring this research even further is presented.

2 Literature Review

2.1 Rapid Prototyping

Rapid prototyping is a technique for manufacturing that was developed in the 1980s (Gardan, 2015). This technique aims at converting ideas into physical prototypes in a short period with minimum investment. Multiple iterations with prototyping and refinement are often needed before the final product is designed as desired. This iterative process is illustrated in Figure 2.1. By producing physical objects of a product under development, the engineers can perform functionality tests or use the object for visualization purposes. Presenting a new product to the leadership of a company or a customer by showing a physical prototype can be of great benefit. Another field of use could be the utilization of scaled prototypes for physical testing – like hydrodynamic forces on a subsea structure.
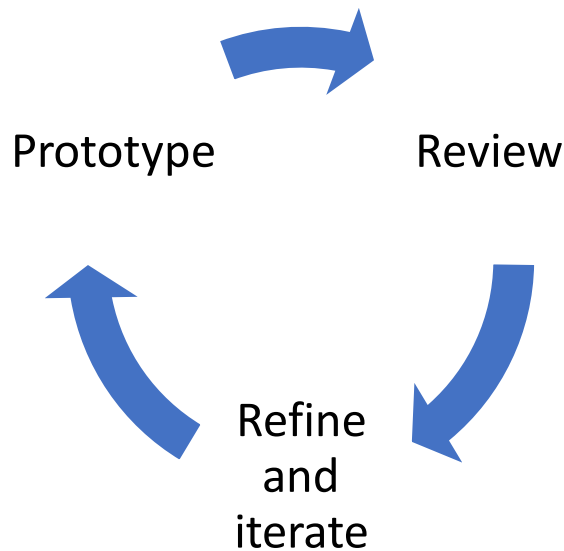
Figure 2.1 - Generic process for rapid prototyping

A manufacturing process often used for rapid prototyping is additive manufacturing. This technology creates objects by producing layer by layer. This type of production technology makes it possible to produce almost any shape. Geometries that are impossible to make from traditional subtractive methods can be made with additive manufacturing, which results in several new possibilities related to design.

Today additive manufacturing is used mostly for short-term prototypes, but also to manufacture small-scale products (rapid manufacturing) and tooling applications (rapid tooling) (Stampfl & Hatzenbichler, 2014). An example of rapid tooling is the use of additive manufacturing to produce a geometry that will be utilized to create a mold. The mold can then be used to produce multiple objects which are sold as end-use parts.

3D printing is a commonly well-known term where machines produce objects with additive manufacturing. 3D printers are often used for rapid prototyping. The reason for this is the low cost and rapid production time these machines offer, in addition to the geometrical possibilities the additive manufacturing technique presents. The objects produced from a 3D printer are made from a 3D computer-aided design (CAD) file. The CAD file is then converted into a format adapted for 3D printing, most often a stereolithography file (STL). An STL file only describes the surface geometry of a three-dimensional object, by forming triangles according to the surface (Chua, et al., 2003). Each triangle is described by three nodes and a perpendicular vector (Figure 2.2). Neither color, texture, or other attributes are expressed in this type of file.
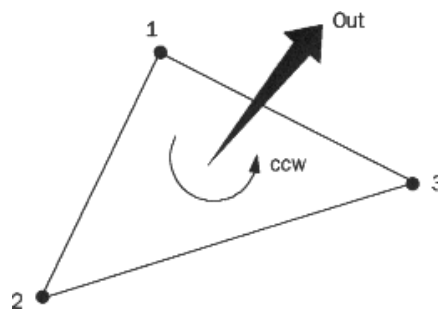
Figure 2.2 - STL file format, consisting of triangles
Credit: Fabbers.com

A separate software processes the STL file into a code which works as a production recipe for the 3D printer, known as slicing. Since the file format only processes the surface, the software automatically generates an internal structure inside the part to give the part the strength needed, known as the infill. In the software, multiple parameters can be tuned and adjusted to achieve the desired quality of the end product. Typical parameters are layer height of each layer for the additive process, infill density, wall thickness, and the building speed (Brockotter, 2018).

The automatically generated code from the slicing software (or additive manufacturing specific software) is then uploaded to the 3D printer, and the product is produced. The time to produce an object is directly related to the size of the object constructed. The additive layer process can differ from minutes to days, depending on the size. The building process is automatic, which makes for an automatic production process where no mechanical expertise is needed; only some finishing work may be needed on the final product. A typical, extended rapid prototyping process cycle is shown in Figure 2.3.
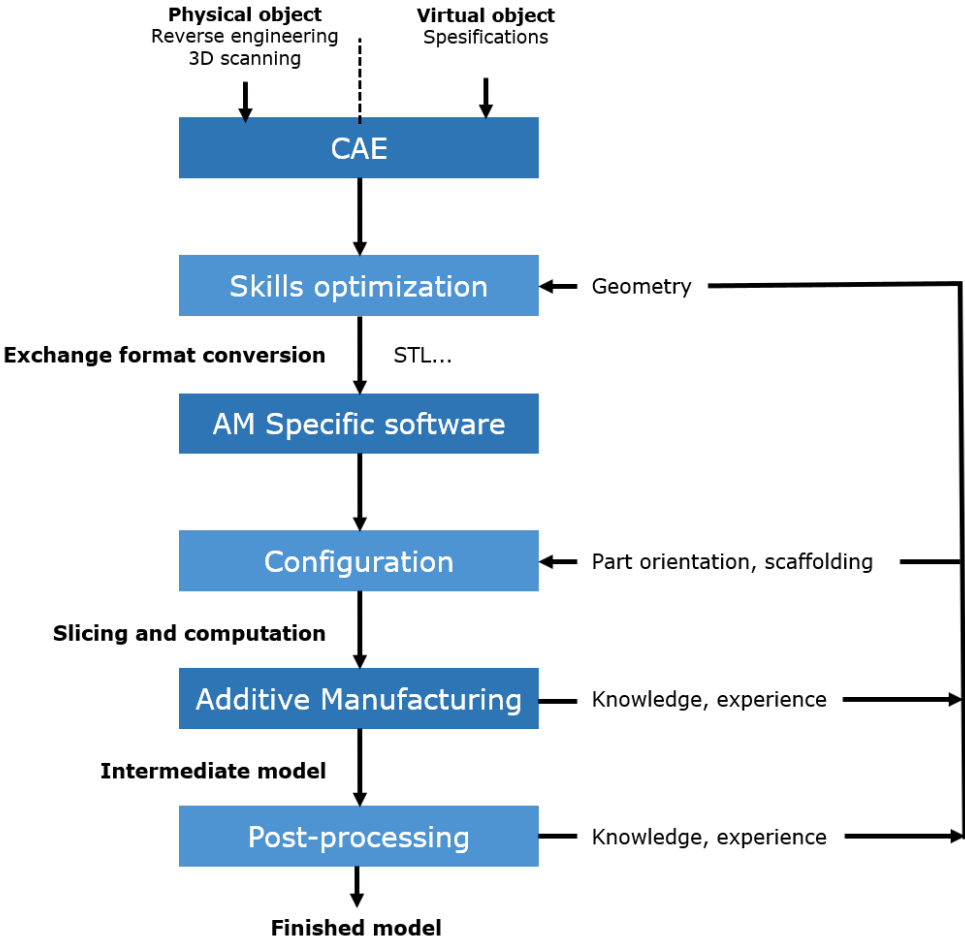
Figure 2.3 - Rapid prototyping process cycle
Credit: (Gardan, 2015)

2.1.1 Fused Deposition Modelling

There are lots of different technologies available for additive manufacturing and 3D printing. The most used technologies are Fused Deposition Modelling (FDM), Stereolithography & Digital light processing, and Selective laser sintering (Statista, 2018). FDM is the most popular. The reason for the FDM popularity may be related to both that it is relatively easy to use and often cheaper compared to other 3D printing technologies. The majority of 3D printers available at NTNU Ålesund are FDM printers. A brand printer like Ultimaker sells 3D printers in a price range between about 25 000 NOK and 80 000 NOK (price from Ultimaker home page, spring 2019). Larger non-branded printers can be acquired for less than 10 000 NOK. Making FDM 3D printers available for both large companies and the general public.
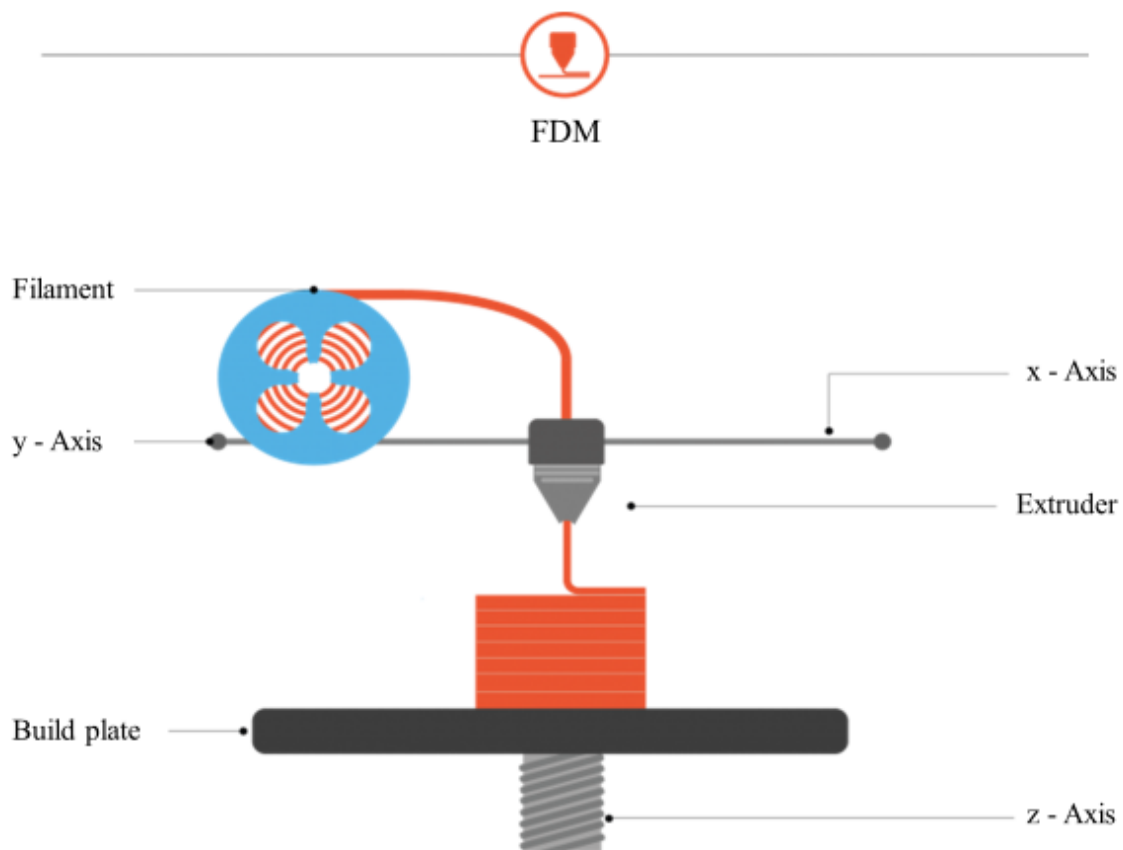
Figure 2.4 - Fused Deposition Modelling illustration
Credit: Fab Academy

Fused deposition modeling is a technique where the filament is extruded through an extruder and built layer by layer (Figure 2.4). The filament is stored on storage rolls, typically with 100 meters of material, or more, on each roll. The extruder can be moved around in a two-dimensional plane (x- and y-direction), moved by two gantries connected at the extruder nozzle. The pattern results in a single layer of the whole geometry, typically with a 0.10 mm height. As one layer is complete, the build plate is lowered (in z-direction) the same height as a layer, before layer two can be constructed.

Since FDM builds layer by layer, the produced parts will get an anisotropic material structure. An anisotropic material results in different strength properties in different directions of the object. Therefore, dependent on what the produced part will be used for the production orientation is essential. Assuming that each layer is built from the alternating filament in straight x- and y-direction; the strength of a 3D printed object is around 30% lower in z-direction compared to x- and y-direction. While if the material is loaded in the tangential direction of x-and y-direction, the strength increases around 11% compared to x- and y-direction (3D Matter, 2015).

A disadvantage of FDM is that geometries with a larger overhang angle than 45° from the vertical plane cannot be produced without additional supporting, like the object in Figure 1.2. This results in some limitations for specific geometries that may be challenging to produce with FDM. The same material that the object is built from may be used as support material, but for complex geometries, it is close to impossible to remove it without destroying the object itself. Polyvinyl Alcohol (PVA) is a material that can be used as a support material for complex geometries. The PVA will be extruded through a separate nozzle to support the structure under production. Polyvinyl alcohol dissolves in water, which makes it easy to remove the support structure. However, the use of PVA may reduce the surface quality of the object, and it drastically increases the production time of an object.

2.1.2 Material – Polylactic Acid (PLA)

Polylactic acid (PLA) is the most commonly used filament material used for 3D printing (MatterHackers, 2017). One of the most beneficial properties of PLA is related to that it is a relatively easy filament to achieve good results with. The material is also eco-friendly since it is made of corn-starch and has a quite low energy demand for fabrication, compared with traditional petroleum-based plastics (MatterHackers, 2017). There are also many companies producing PLA filaments, which results in low and competitive prices.

2.1.3 CAD- and Slicing tools

3D printed parts originate from computer-aided designed software. There are many CAD software available today. One of these is Siemens NX, which is the software utilized in this thesis. The CAD software from Siemens is in addition to a CAD software also a computer-aided engineering software with multiple other features as well, as tools for 3D printing optimization of parts (Siemens, 2018). In Siemens NX a modeled geometry can be converted into an STL format file which can be further processed in a slicing software for 3D printers.

To turn an STL file into a g-code, which is the production recipe for a 3D printer, a slicing software is needed. Ultimaker printers are delivered with their slicing software that must be installed on a computer, known as Cura. This software is used to tune different parameters discussed briefly in chapter 2.1 Rapid Prototyping. Depending on the different settings, a customized g-code will be made which will decide how the printer will build the object.

2.1.4 Selective Laser Sintering

Selective laser sintering (SLS) is a technique where an energy beam, or laser, is used to fuse small powdered particles of material into three-dimensional objects. Sintering is the process for creating objects from powder, which is something that has been done for thousands of years with bricks, porcelain, and jewelry (Palermo, 2013). Objects made with SLS can be made in a wide range of materials of both polymers and metal.

The process of SLS consists of two main steps being repeated multiple times. A 0.1 mm high layer of powder is laid out in the printer; then the laser sinters the powder according to the geometry desired. Next, another 0.1 mm layer of powder is laid upon the previous layer before the laser sinters again. This is repeated until the geometry is finished. The overall process is presented in Figure 2.5.

One of the main advantages of SLS printing is that it does not require a support structure (Flynt, 2019). This is due to that the object is produced in powder, and therefore fully supported at all times under production. Therefore, complex structures may be produced in an SLS printer without the need for any additional support. The disadvantage of SLS printing is that it is more expensive compared with FDM.
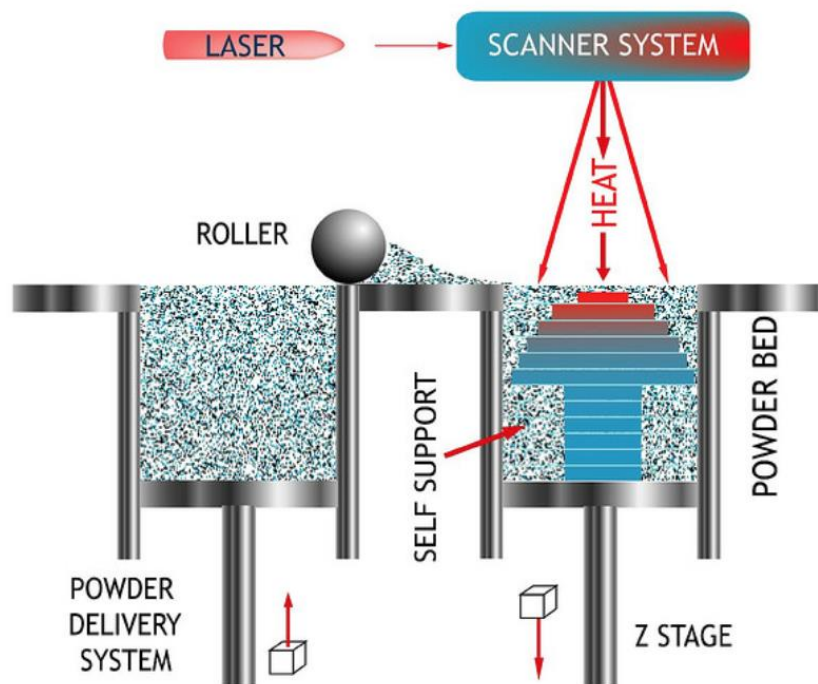
Figure 2.5 - Selective Laser Sintering illustration
Credit: Embodi3D

2.2 Experimental methods

2.2.1 Model scale testing

Experimental tests can be done at many scales. Since the experiments in this thesis are conducted in the towing tank at NTNU Ålesund, the test objects must be scaled to a smaller size. The process of performing a full-scale experimental test is costly or almost impossible (Knott, 1993). An often more convenient way to do tests on large scale structures is model-scale testing. The test object is then scaled down to a smaller, cheaper, and faster-produced product which may be used to investigate the desired data.

The forces affecting a scaled model may be adjusted to another model with the same shape, but with another scale. The scaling can be done with the Reynolds number (Knott, 1993). The number describes the relationship between inertia and viscosity. With the use of the Reynolds equation, it is possible to estimate hydrodynamic forces like drag and lift for full scaled objects, from down-scaled experiments. Reynolds equation is shown below in equation 2.1.

$$Re = \frac{u \cdot L}{\nu} \tag{2.1}$$

In which:

Re = Reynolds number [-]
u   = Flow velocity [m/s]
L   = Characteristic linear dimension [m]
ν = Kinematic viscosity [m^2/s]

The Reynolds number can also be used to calculate if the flow around an object is laminar, turbulent or in the transient zone between the two. For external flows, the flow is turbulent when the Reynolds number is higher than about $5\text{x}10^5$. For internal flows, Reynolds numbers below 2300 results typically in a laminar flow, while flows with a Re between 2300 and 4000 are in the transient area between laminar and turbulent. Flows with a Reynolds number above 4000 are generally turbulent (Reynolds, 1883).

Froude scaling is another method to scale hydrodynamic values. The Froude number is a dimensionless number defined as a relation between inertia forces and gravitational forces (Journée & Massie, 2001). The number is used to compare the wave making resistance between bodies of various shape and size but may also be used about submerged objects. The definition of the Froude number is shown below in equation 2.2.

$$Fr = \frac{u}{\sqrt{g \cdot L}} \tag{2.2}$$

In which:

Fr = Froude number [-]
g   = Gravitational constant [9.81 m/s^2]

The Froude number can be used to scale the desired values between the different scaled test objects and a full-scale model. By scaling the length for similarly shaped objects with $\lambda = L_{Structure}/L_{Model}$, the remaining scaling factors will be as presented in Table 2.1 (Solaas, 2017).

Table 2.1 - Scaling factors

Length	Time	Velocity	Accele-ration	Mass	Added Mass	Force	Linear Damping	Quadratic Damping
[m]	[s]	[m/s]	[m/s^2]	[kg]	[kg]	[N]	[N/(m/s)]	[N/(m/s)^2]
λ	$\lambda^{1/2}$	$\lambda^{1/2}$	1.0	λ^3	λ^3	λ^3	$\lambda^{5/2}$	λ^2

2.2.2 Estimating hydrodynamic coefficients with experimental methods

For the estimation of hydrodynamic coefficients from experimental tests, the Morison's equation can be utilized. The equation is used to calculate the added mass forces and the viscous drag forces resulting from separation and boundary layer friction (Morison, et al., 1950). If the force is recorded in an experimental test, the equation can be used to calculate the drag coefficient C_D and the inertia force coefficient C_M. Morison's equation is presented in equation 2.3.

$$F = \frac{1}{2}\rho C_D A u|u| + \rho C_M V \dot{u}$$ (2.3)

In which:

ρ = Mass density of fluid [kg/m^3]
C_D = Drag coefficient [-]
A = Cross-sectional area in flow direction [m^2]
u = Flow/object velocity [m/s]
C_M = Inertial force coefficient, $C_M = C_A + 1$, where the number 1 is the hydrostatic force component in accelerated fluid, and C_A the added mass coefficient [-]
V = Volume of submerged body [m^3]
$\dot{u}$ = Flow/object acceleration [m/s^2]

The hydrodynamic drag and added mass coefficients, C_D and C_A, can also be determined in an oscillating flow. This was done by Keulegan and Carpenter in 1958 (Keulegan & Carpenter, 1958). From their studies and experiments, they discovered that their results could be plotted as a function for a dimensionless number, they called the Keulegan-Carpenter number. The equation for this number is shown in equation 2.4.

$$KC = \frac{u \cdot T}{L}$$ (2.4)

In which:

KC = Keulegan Carpenter number [-]
T = Oscillating object period [s]

Many objects are perforated, and therefore a more suitable dimensionless value is used for such geometries called the porous Keulegan-Carpenter number (Mentzoni, et al., 2018), shown in equation 2.5.

$$\mu KC_{Por} = \frac{Z}{L}\frac{(1-p)}{2p^2}$$ (2.5)

In which:

Z = Amplitude of oscillation [m]
p = Perforation [-]
μ = Discharge coefficient [-]

For oscillating movements, the velocity of an object may be expressed as the equivalent oscillation velocity (Solaas, 2017), which is defined as in equation 2.6:

$$\frac{16}{3}\cdot\frac{Z}{T}$$ (2.6)

Even if the coefficients from Morison's equations are quite practical in some cases, they may be hard to calculate for complex geometries since they are directly linked to the cross-section area and the volume of the submerged body. A complex geometry might consist of different cross-section areas and a perforated volume. Therefore, it might be more practical to express the added mass of a structure in kg, or dimensionless in other methods than Morrison's, and the drag (or damping) as one linear term B1 (N/(m/s)) and one quadratic term B2 (N/(m/s)^2) – as done in SINTEF's MOVE reports (Solaas, 2017). When expressed in kg and N/(m/s), no specification of the geometry is needed. The linear damping is equal to B(Z=0), and the quadratic is equal to the slope of the curve. An example presenting two different approximations for linear and quadratic damping may be seen in Figure 2.6. Where approximation 1 is better for small equivalent oscillation velocities, while approximation 2 is better from lager velocities.
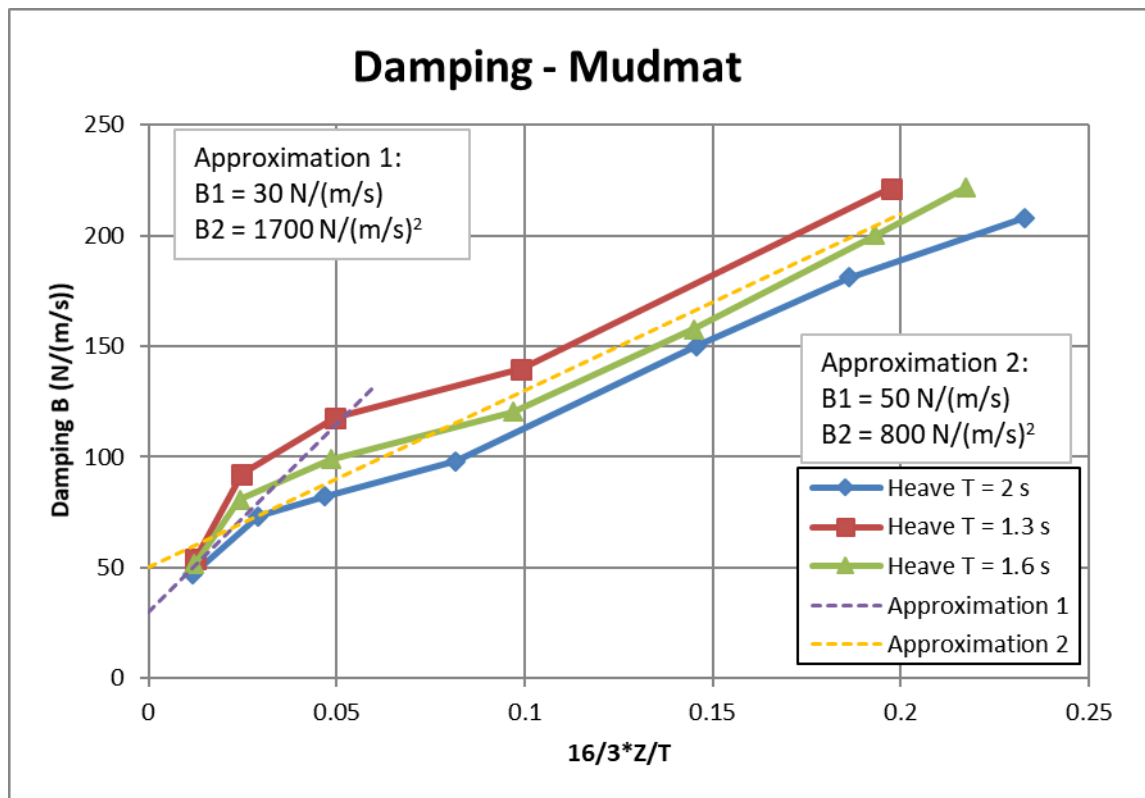
Figure 2.6 - Example of linear- B1 and quadratic B2 damping
Credit: (Solaas, 2017)

The drag and inertia do not necessarily affect the hydrodynamical force with equal values. In some cases, one may be such dominant that the other could be neglected. The KC number gives a clear indication of which is dominant. This is well explained by Journée and Massie in "Offshore Hydrodynamics" as follows:

> *For low values of KC (KC < 3), the inertia force is dominant. The flow 'does not travel far enough' relative to the cylinder diameter to generate much of a boundary layer not to mention vortices; potential flow theory is still applicable. Drag can simply be neglected.*

> *For the next range until drag becomes significant (3 < KC < 15); one will often linearize the drag.*

> *There is a range of KC (15 < KC < 45) in which one cannot really avoid using the full Morison equation with its nonlinear drag.*

> *For high values of KC (KC > 45), the drag force is dominant. The vortex shedding frequency becomes high compared to the wave frequency, so the flow tends to behave more and more like a uniform flow. Inertia can be neglected. Indeed, the limit KC towards infinite corresponds to a constant current.*

(Journée & Massie, 2001).

2.3 Subsea lifting operations

2.3.1 Generic on subsea structures

As briefly discussed in chapter 1.1, the first use of subsea technology in Norway was installed in the North Sea at the Tommeliten gas field, back in 1988 (Solheim, 1989). The use of subsea plants at the seabed can be used to expand the area an oil platform can collect oil. Figure 2.7 illustrates how a subsea factory can be positioned to supply the platform with gas and oil. Subsea structures can also be used without a platform, then the oil or gas is transported directly to shore.
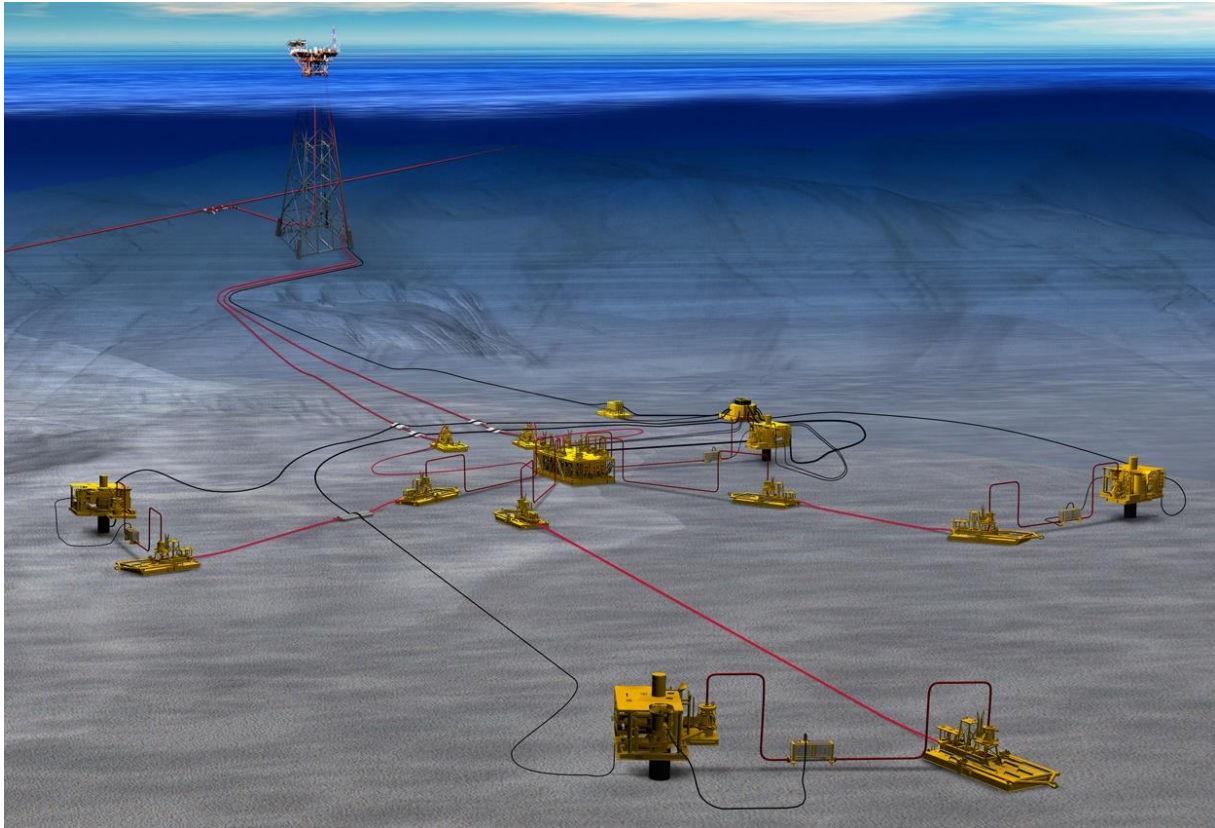
Figure 2.7 - Subsea field connected to the platform
Credit: Jeff Whiteley

Another benefit for Subsea plants is that they can be used to extract oil and gas at more significant depths than a traditional platform. There is a significant growth in deep water and ultra-deep-water petroleum production today, according to the U.S Energy Information Administration (Manning, 2016). The production at depths greater than 125 meters increased by 25% from 2005 to 2015. The Energy Information Administration has defined depths up to 125 meters as shallow waters, deep water as 125-1500 meters and ultra-deep-water as depths greater than 1500 meters. The deepest subsea well is located at a depth of more than 2900 meters, in the Gulf of Mexico (Tippee, 2016).

A subsea production plant like the one in Figure 2.7 typically consists of a subsea well, seabed wellhead, subsea production tree, a subsea tie-in to flowline system, and control facilities to operate the well (Bai & Bai, 2018). The factory can differ depending on if the oil/gas is pumped straight to shore, to a platform or a ship.

2.3.2 Subsea templates

A typical subsea structure is a subsea template (Figure 2.8). They are used for several purposes as a guide, hang off and support to drilling, and to the wellhead conductor, but also as a base for subsea trees, manifolds and other equipment (DNV-GL, 2014). The design for the template will vary with where it is located and how it is installed, in addition to other choices. According to DNV-GL, the foundation of a template is based on the seabed condition where typical foundation features are:

- *Mudmats* *as the foundation and provide bearing capacity to avoid settlements.*
- *Washout sleeves* *to avoid shortfall and fracture in seabed during 36" drilling*
- *Skirts* *to penetrate seafloor for resist later forces and to provide friction against heave during installation*
- *Mini* *Suction piles* *or large singe suction pile to support vertical and horizontal loads on the manifold*
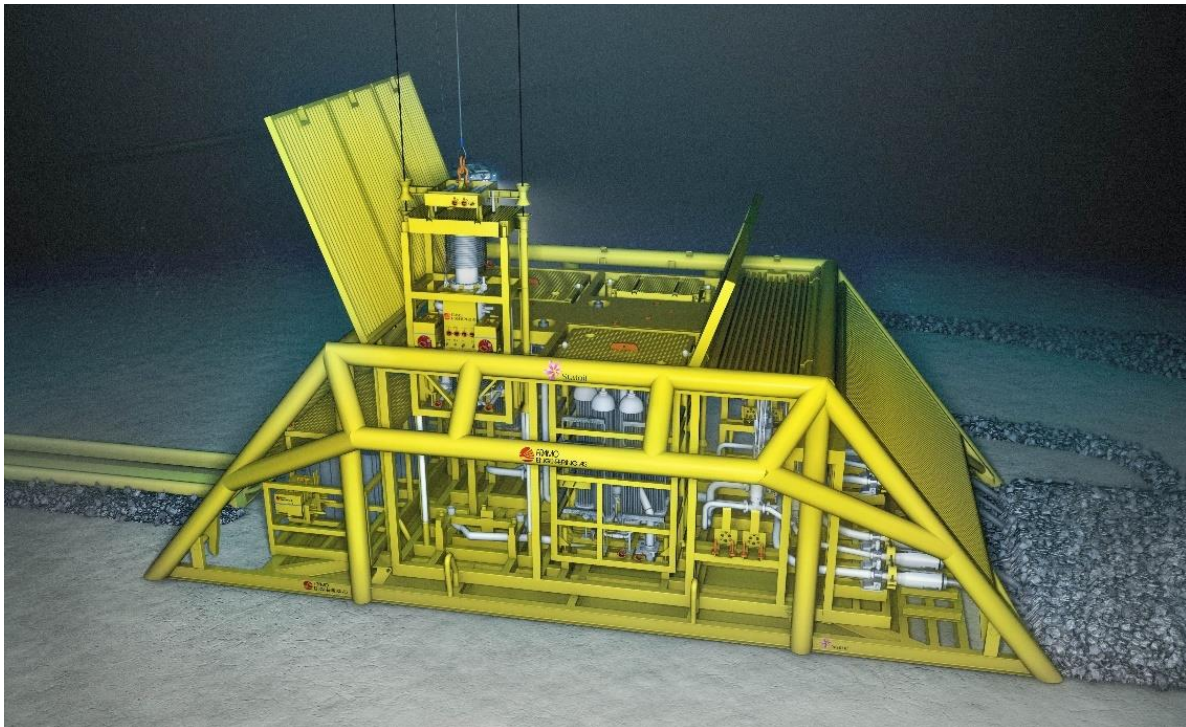
Figure 2.8 - Subsea equipment being lowered into a subsea template
Credit: Equinor

The dimensions of the subsea template variates according to the amount of equipment installed, among other factors. Some of the most abundant templates can reach heights of around 30 meters (FishSafe, 2018). The four large subsea templates used to hold the manifold extracting gas from the Ormen Lange gas field are 44 meters long, 33 meters wide, and 15 meters high (NorskOljeMuseum, 2015). While the subsea templates installed at the Goliat field, located in the northern part of the Norwegian Sea, are 33 meters long, 23 meters wide, 25 meters high and weighs about 300 tons each.

2.3.3 Subsea Lifting Operations

A subsea operation may be divided into different operational phases. To move the structure from the offshore vessel to the seabed, the structure must first be moved in the air, then through the splash zone, and then through the water until it is landed on the seabed. During the different phases, different forces are affecting the structure and the wire holding it. To make sure that the wire will hold and that the subsea structure does not break they must both be dimensioned to withstand the dynamic forces affecting the structure. The different phases are shown in Figure 2.9.
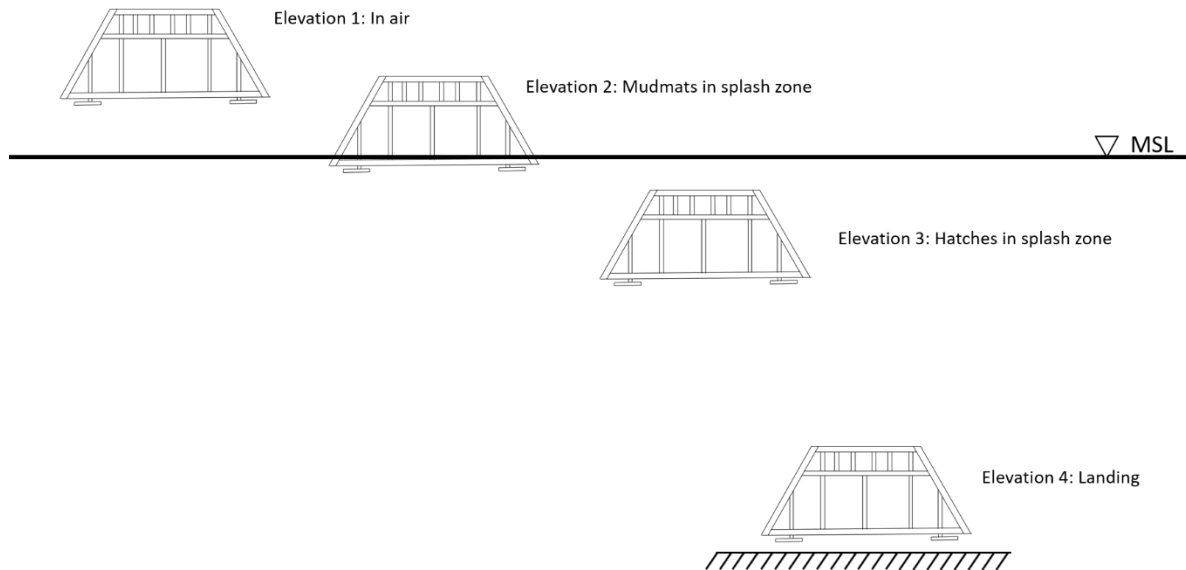
Figure 2.9 - Different phases of a subsea lifting operation
Credit: Technip

When the subsea structure is in the air, there are mainly two forces acting on the structure – the gravitational force pulling it down and the wire force holding it up. In the splash zone, waves may apply large forces to the structure. Active heave compensation may reduce the forces by making the structure oscillate according to the wave movement. During the lowering between the surface and the seabed forces from heave- and roll motion of the ship along with drag and other hydrodynamical forces will affect the structure. By knowing all forces acting on the structure during operation, this will result in safer operations, which may be executed faster and at lower costs.

2.4 Related Works

2.4.1 Master Thesis by Qian Yu

The spring of 2018, Qian Yu wrote a master thesis on "Estimate Dynamic Factors for Subsea Lifting Operation by Experimental Method – Rapid Prototyping" (Yu, 2018). Yu studied the international study program of ship design, at NTNU Ålesund. Her thesis is the last work done about NTNU's research for estimating hydrodynamic forces on subsea structures, by more innovative methods.

Her objective was to present and validate a new experimental method to find the added mass- and drag coefficient and then analyze different factor effects on these. Furthermore, to carry out an experiment to find C_A and C_D for subsea modules. She would verify the results by CFD analysis and other analytical- and numerical methods, like Artificial Neural Networks Prediction.

By conducting experiments, Qian Yu managed to validate both drag- and added mass coefficient for different geometries. Mainly cylinders where tested, both alone and together to discover how the flow around one cylinder could affect the flow around another positioned in the wake-field. A squared cube and a mudmat were also tested to acquire results from other geometries as well. In the end, she concluded that the methods used in the thesis had proven to be suitable for estimating hydrodynamic forces.

The experiments were conducted in the test tank at NTNU in Ålesund. Both force and displacement were logged by sensors and computer software. Figure 2.10 illustrates one of the tests where a cylinder is submerged in the test tank and tested with an oscillating movement. The recorded force results were then processed to remove noise from the measured data. This was done with several methods as finite impulse response (FIR) filtering, Fourier series methods, and MATLAB fitting tools.
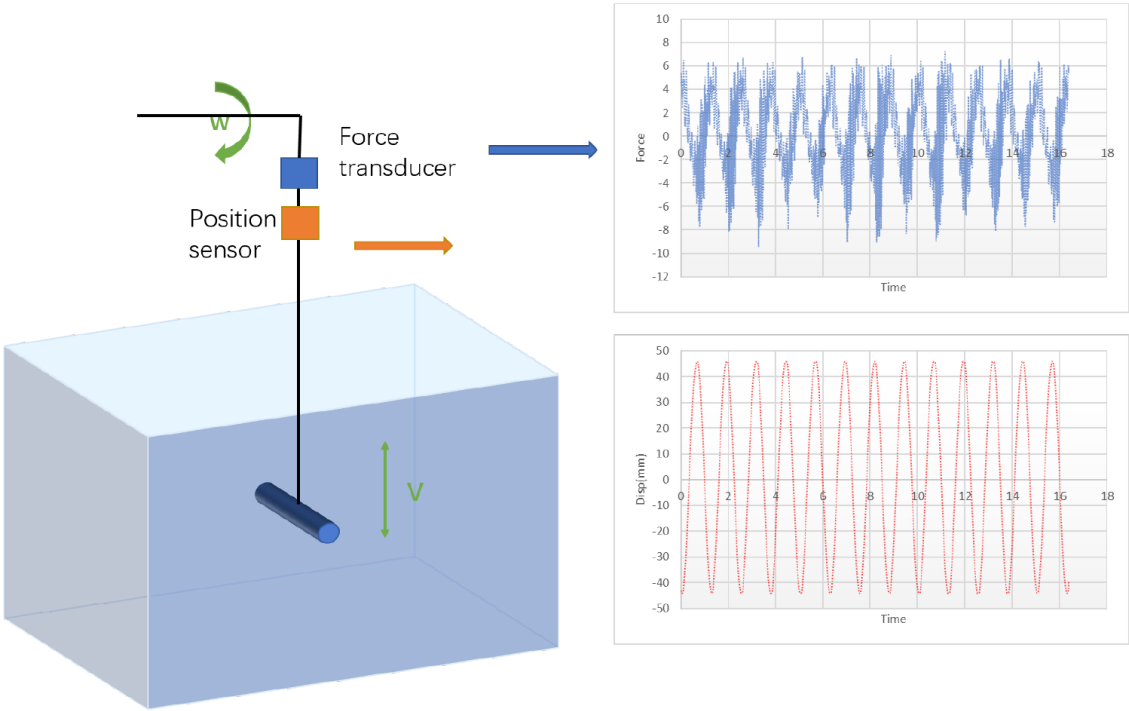
Figure 2.10 - Experimental process sketch and results
Credit: Qian Yu

After the plots were processed (like in Figure 2.11), the drag- and added mass coefficient was resolved by a least square method. This method was dependent on an algorithm, where the algorithm runs a high amount of combinations of the drag- and added mass coefficient until the correct combination is found, giving the coefficients for the geometry.
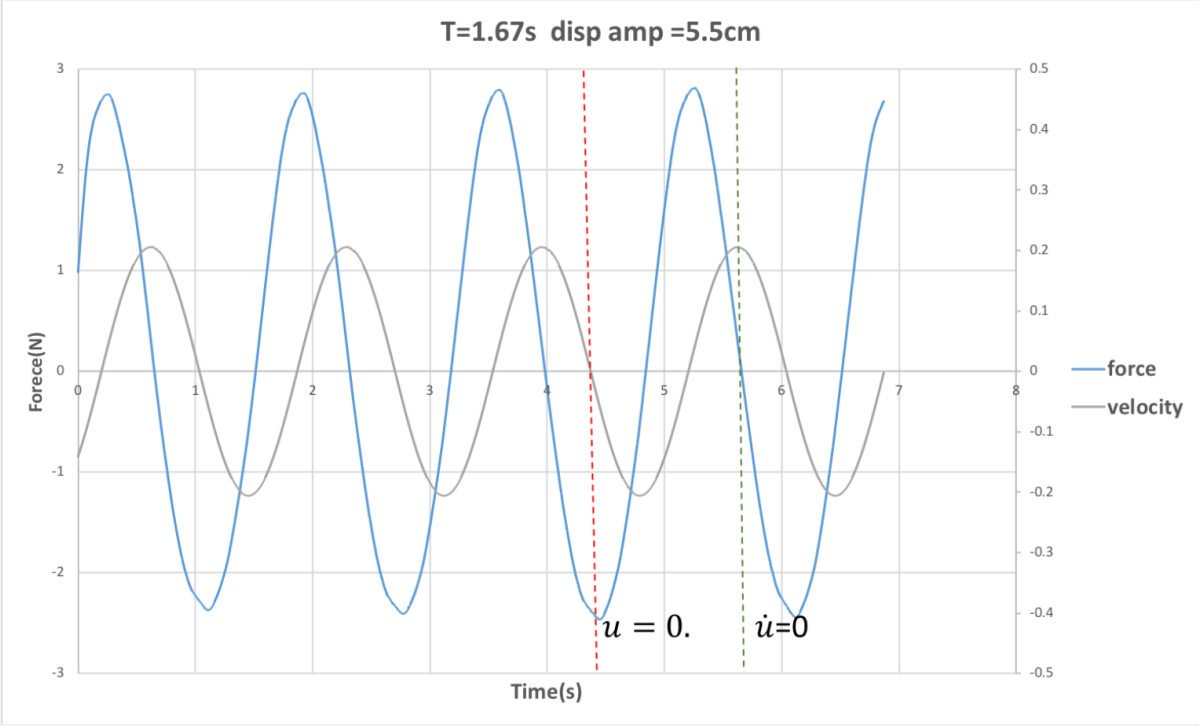
Figure 2.11 - Processed plots for force and velocity
Credit: Qian Yu

Yu did not manage to perform the rapid prototyping part of the thesis as planned. In the end, no 3D printed subsea structure was produced or tested. However, she was able to 3D print a cube and perform experiments on it.

The research done by Yu will help this thesis to answer the research questions. Less time can be spent to verify the method on cylinders and more on setting up a method for the use of rapid prototyping to estimate the hydrodynamical characteristics.

2.4.2 DNV-RP-H103

The DNV report RP-H103 is a recommended practice for modeling and analysis of maritime operation (DNV-GL, 2011). Particularly lifting operations of deep-water operations are presented, along with other aspects of lifting operations. The report is used as a source for hydrodynamical equations and previous studies.

In the report, the added mass- and drag coefficient of perforated plates are presented versus the perforation percentage. This is especially useful since there already is a mudmat structure available, acquired during the research by Qian Yu. The mudmat may then be used as a reference where the results are compared with the experiments found in DNV-RP-H103. The coefficients from the DNV-GL report are presented in Figure 2.12. In each plot, there are three datasets, one is experimental data, and two are CFD calculations. It is not stated which is what.
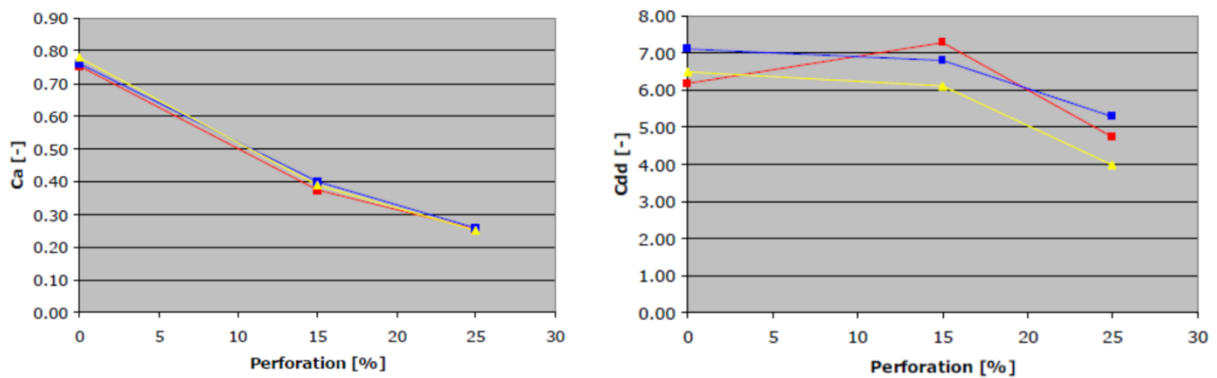
Figure 2.12 - Added mass- and drag coefficient from DNV-GL-H103

3 Methodology

3.1 Assumptions

Scaled experimental tests have been conducted to estimate hydrodynamic coefficients for subsea structures. The test objects are made innovatively, using 3D printers. The printers available at NTNU Ålesund are several Ultimaker printers. Also, a new larger printer was acquired in relation to this thesis, a 500x500x500 mm size printer named Creality CR-10 S5. This printer allowed for about three times larger test objects compared to the Ultimaker. The project has only utilized the Creality and the Ultimaker printer to simulate a scenario where all test objects are manufactured in-house.
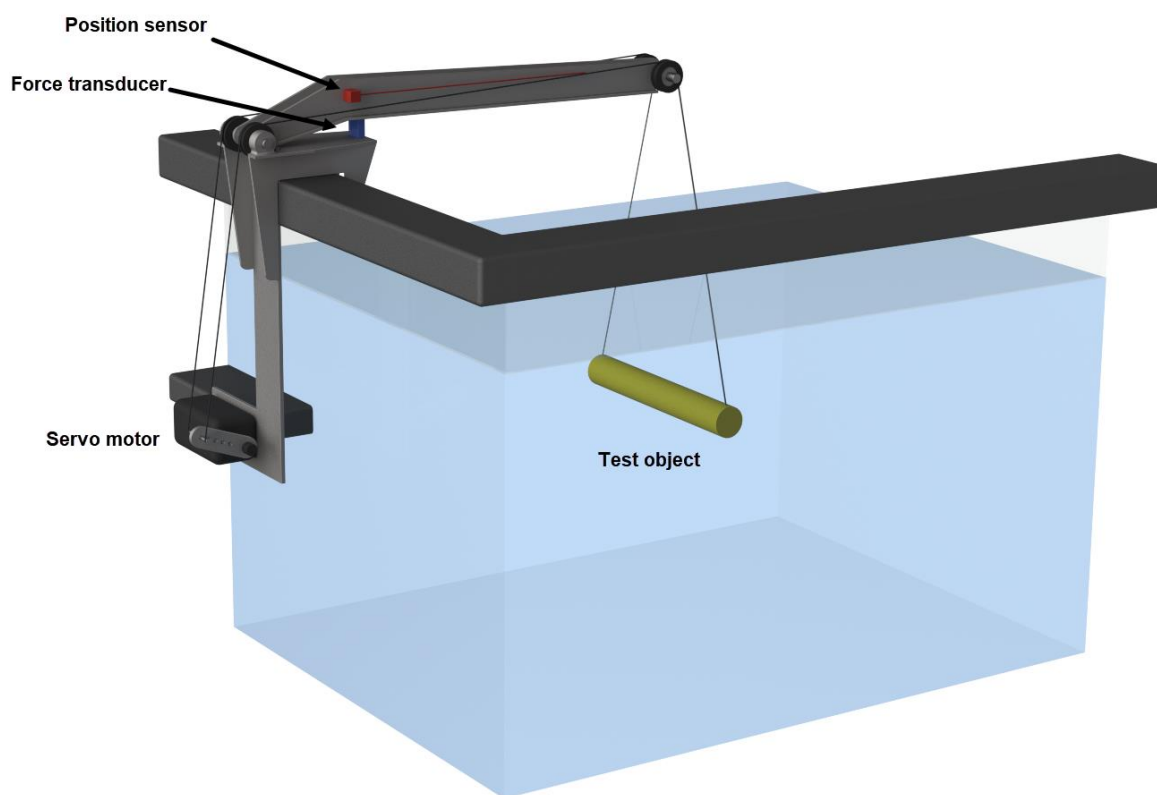
Figure 3.1 – Initial experimental test setup

The tests are performed in the towing tank at NTNU Ålesund. The tank has a length of 10.9 meters, the width is 2.0 meters and the depth around 0.9 meters. Next to the tank, there is a small crane, operated by an electric motor and computer software. It is this crane that has been utilized to test the different 3D printed objects and estimate the drag and added mass coefficients. The initial experimental test setup of the thesis is illustrated in Figure 3.1.

The test objects are mainly 3D printed objects since the use of rapid prototyping is in the essence of the thesis. A mudmat made of stainless steel have also be used, but this was only as a reference, used to verify the new test setup and method. All 3D printed parts were made of Polylactic acid (PLA) material.

For all experiments, the tests were conducted in a vertical motion, with the test objects oriented in the normal direction, i.e. the subsea structure was oriented as in real life. The tests conducted were two types of experiments. One where the test object was raised from the bottom of the tank with constant speed or constant acceleration, while the other was with an oscillating movement. The fluid was fresh water, and all experiments were conducted submerged and in calm waters with no waves.

3.2 Experimental approach

To explain the methodology better, the experimental process is shown as a research workflow chart in Figure 3.2. The flow chart is set up showing the different stages needed to conduct the experiments and to acquire the hydrodynamic forces for a subsea structure. The experimental process can be divided into three main looping stages. When the targeted result is achieved for one loop, the next loop can be initialized.

- Experimental test setup development (stage 1-4)
- Verification of experimental test setup and method (stage 5-8)
- Experimental tests of 3D printed subsea structures (stage 9-13)
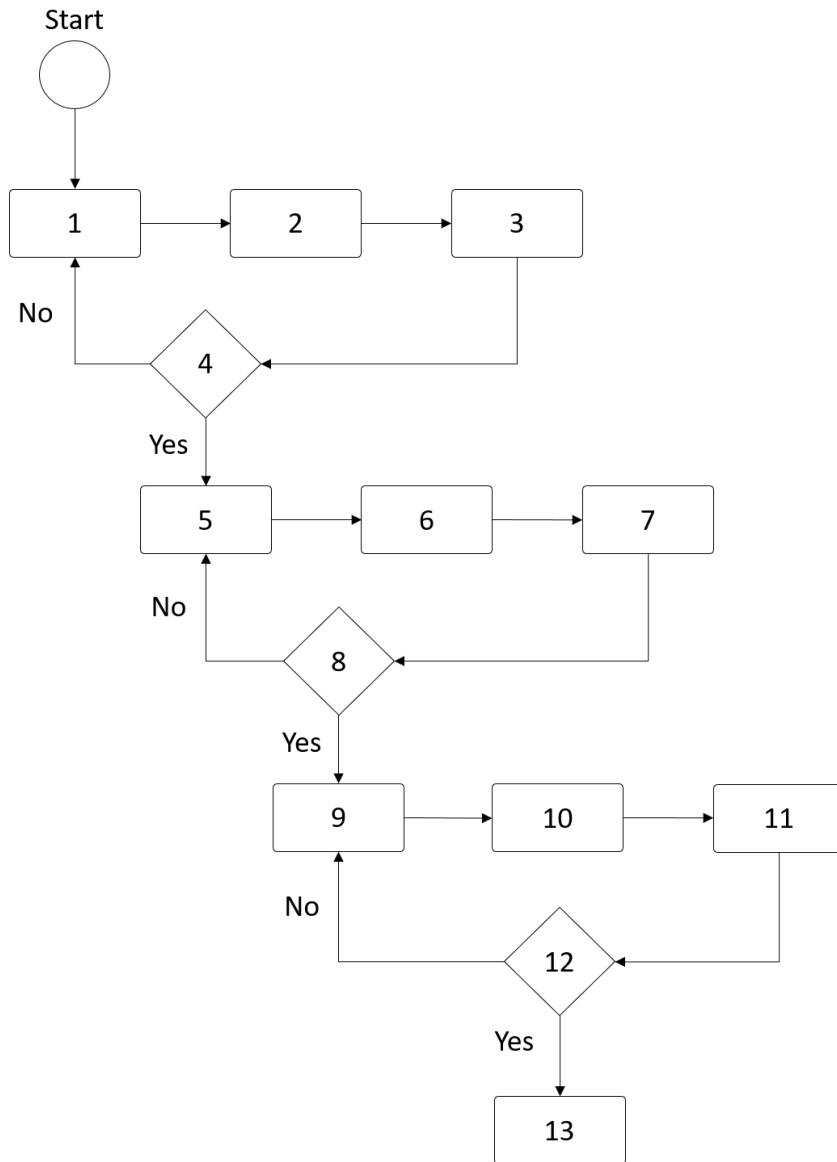
Figure 3.2 – Research workflow

1. Design new test setup
2. Perform simple experimental test in towing tank with reference results and analyze
3. Evaluate setup
4. Decision – Is the test setup good enough?
5. Model simple test objects with 3D printing / use existing objects
6. Perform experimental tests in towing tank and analyze the result
7. Evaluate results
8. Decision – Is the result valid?
9. Make subsea model more/less advanced
10. Perform experimental tests in towing tank and analyze the result
11. Evaluate
12. Decision – Are all experiments complete?
13. Discuss results

3.3 Experimental test setup development

The first main stage for the experimental tests was to develop a new and improved test setup in the towing tank at NTNU Ålesund (step 1-4 Figure 3.2). The goal for the new setup was for it to be able to apply a pulling force both up and down in vertical direction. This will be an improvement from the initial setup, which only could apply an upward force. Meaning that the old setup could not perform tests on objects with a lower density than water, as 3D printed parts.

The first thoughts for the new test setup were that it either had to be pulled downwards or pushed from above. After several sketches of different solutions, the selected design was a solution where the test object would be pulled down with wires attached to the object in one end, and with the other end on the outside of the tank pulled down with a counterweight. The first sketch of the new system is shown in Figure 3.3.
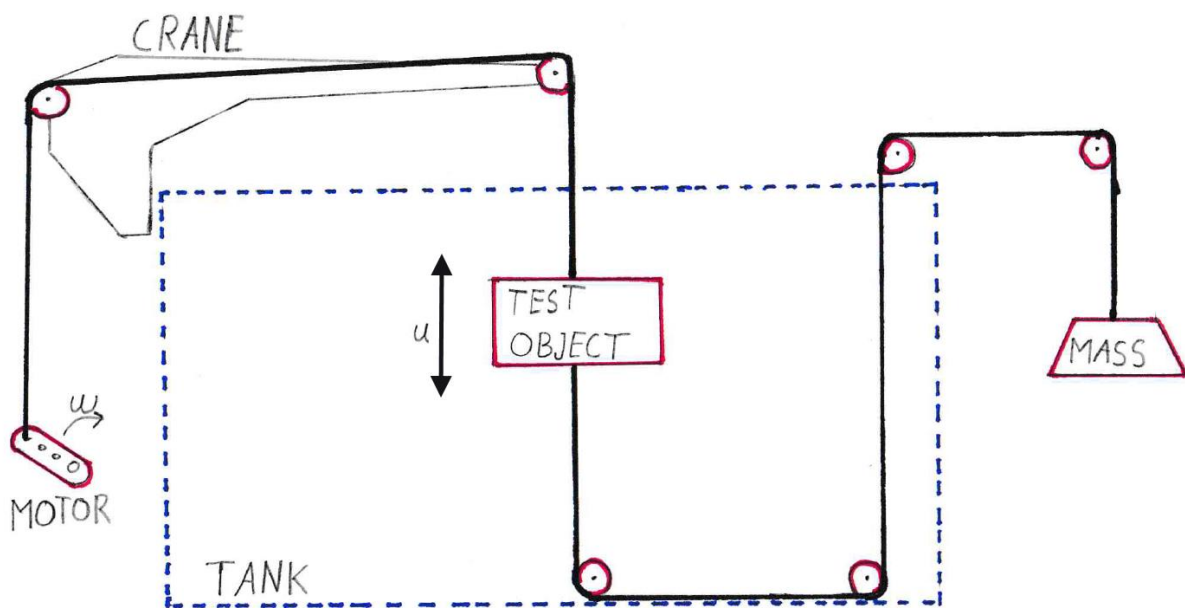
Figure 3.3 - Early sketch of the new experimental setup

A more detailed 3D CAD file was made in Siemens NX. In NX the setup was designed through several iterations before the final design was ready, and 2D production drawings were made and set into production. The final design of the pulldown system consists of two main parts. The first, a plate in the bottom of the tank where two pulleys may be mounted with different spacing to lead the wires back up from the bottom. The second part is located at the top edge of the tank, leading the wires over the edge on two pulleys and down to the counterweight keeping the wires tensioned. The two parts are then connected with two L-beams. The final improved experimental test setup is presented in Figure 3.4 and Figure 3.5, while detailed 2D production drawings are found in Appendix 3.
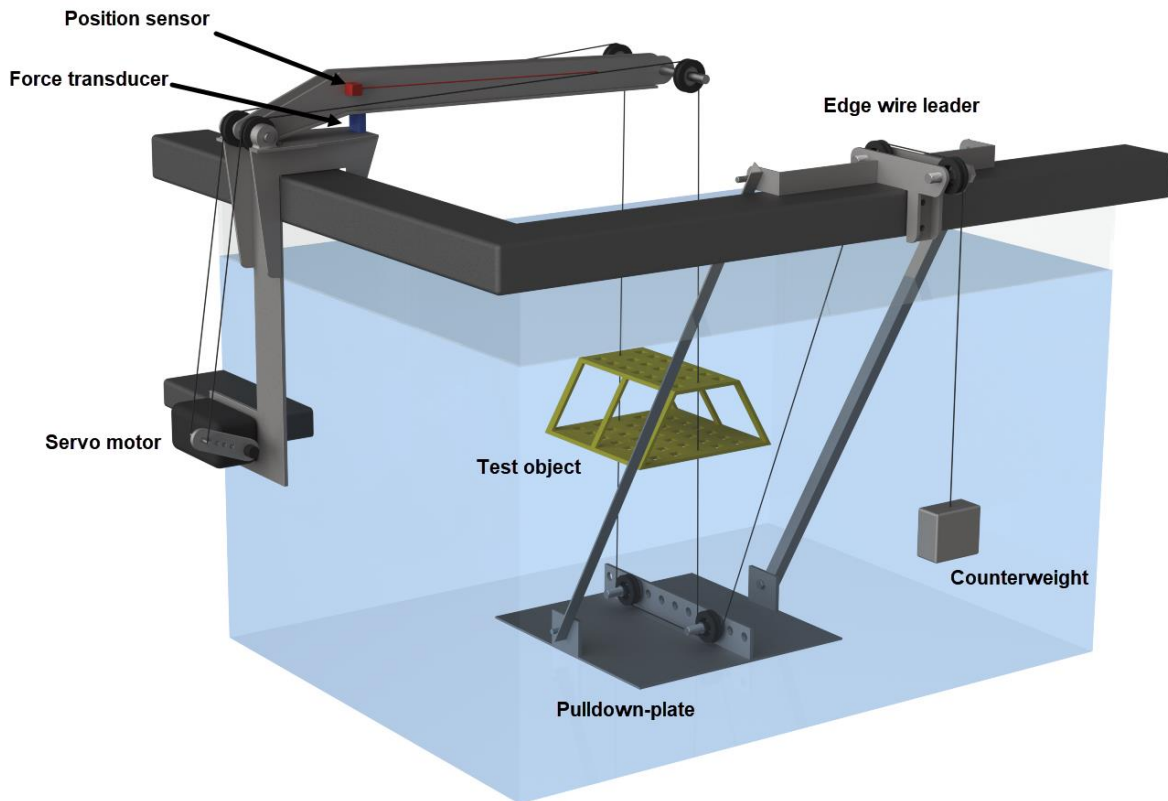
Figure 3.4 - New experimental test setup
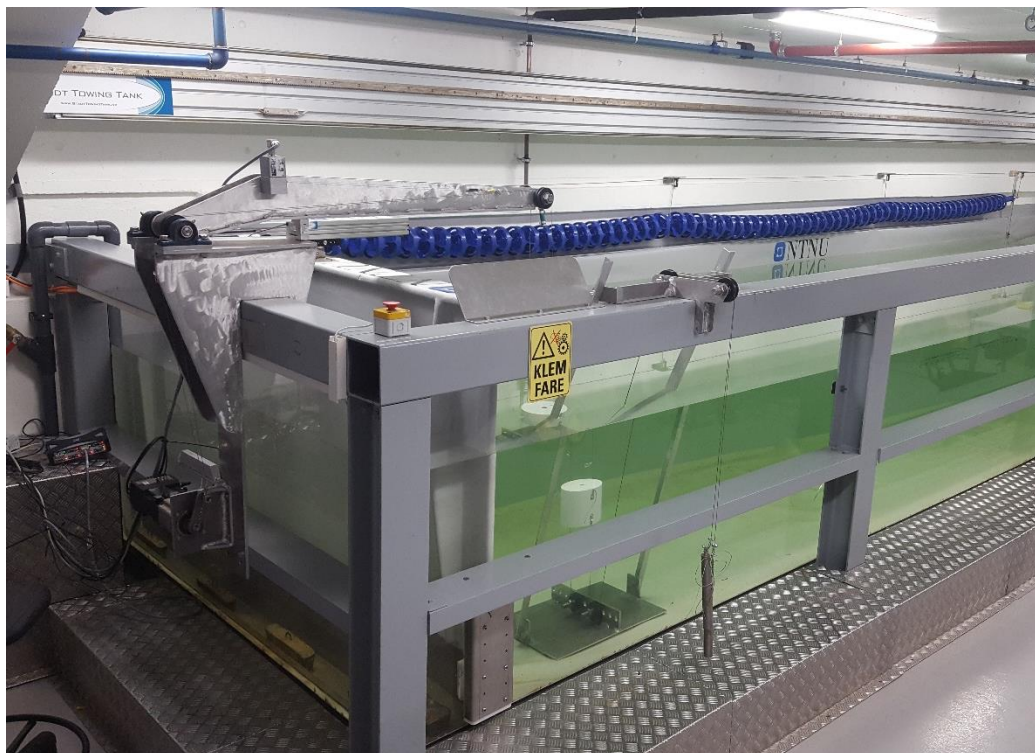
Figure 3.5 - Picture of the new experimental test setup

Following, the different components from Figure 3.4 will be presented:

- Position sensor – ASM cable extension position sensor, used to log the position.
- Force transducer – Tensile/compress force transducer S2M (1000 N), used to log the force.
- Servo motor – Servo motor MAC800 D2, used to control the movement of the system.
- Pulldown-plate – Adjustable pulldown plate with two pulleys to lead the wire back up.
- Counterweight – Two pieces, each 1.15 kg, to keep wires tensioned and to pull the object down.
- Edge wire leader – Part used to lead the wire from the inside of the tank to the outside over two pulleys
- Test object – Experimental test object, connected to the wires at four points.

A new force sensor was acquired, with a smaller load range of 200 N, compared with the initial of 1000 N. The reason for this was to see if a cell with a smaller load range would give more accurate results in the way of a less noisy signal. However, reference tests showed that there were no differences in the signal. Calculations and experiments also showed that the 200 N load cell would operate at the edge of its range, meaning that it could experience forces larger than 200 N. Therefore, the 1000 N load cell was used during all experiments throughout the thesis.

After the new setup was installed, several oscillating reference tests were conducted to verify the setup. However, the results were not usable due to vibrations and large friction forces in the system, as shown in Figure 3.6. The force shifted as the velocity went from positive to negative (happens when the position is at its peak), which implies friction in the system.
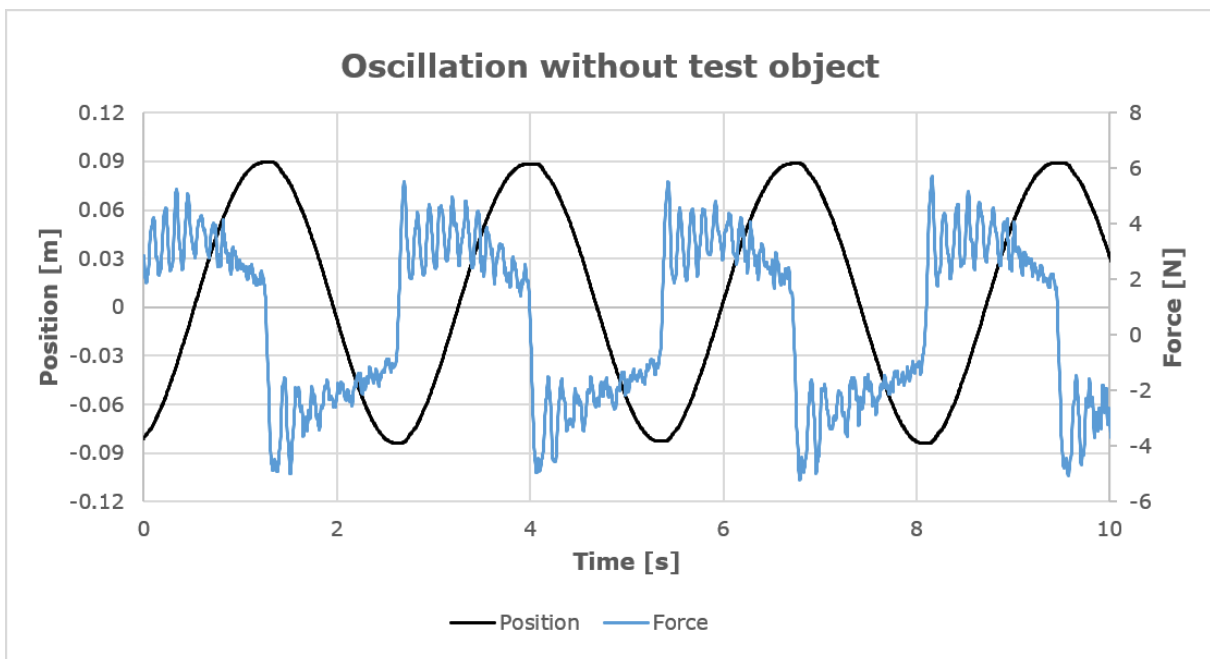
Figure 3.6 - Oscillation without test object, before improvements

Several changes and improvements were done to improve the results to remove noise and friction. The crane was fixed with new bolts to the tank-frame and all other bolts where re-tightened. All pulleys were initially supported by two roller-bearings filled with grease. To remove friction in the bearings, the pulleys with two roller bearings was reduced to one bearing, and all the grease was removed from the bearing. In the initial setup, the wires vertically aligned at the tip of the crane was not parallel. Therefore, a new and longer axle was made to fit the pulleys with a wider distance at the tip of the crane, reducing both friction and noise. These changes, along with others, were applied to the system throughout several iterations.

The improvements resulted in a better force plot with less friction and noise. The results from an identical experiment performed in Figure 3.6 can be seen in Figure 3.7. After the improvements, the most significant force acts when the acceleration is at its peak (at the same time as the position is at its peak). This is the force required to accelerate the system and the counterweight at the end of the wire. The peak force for oscillating experiments is ultimately reduced with around 60 %, to around 1.5 N; for the reference test with the largest amplitude possible (85 mm) and a period of 2.7 seconds. From these results, it was concluded that the test setup seemed satisfactory for the intended purpose. During experiments on different structures, the non-hydrodynamical forces are removed from the final test results for oscillating experiments. This will be explained further in this chapter.
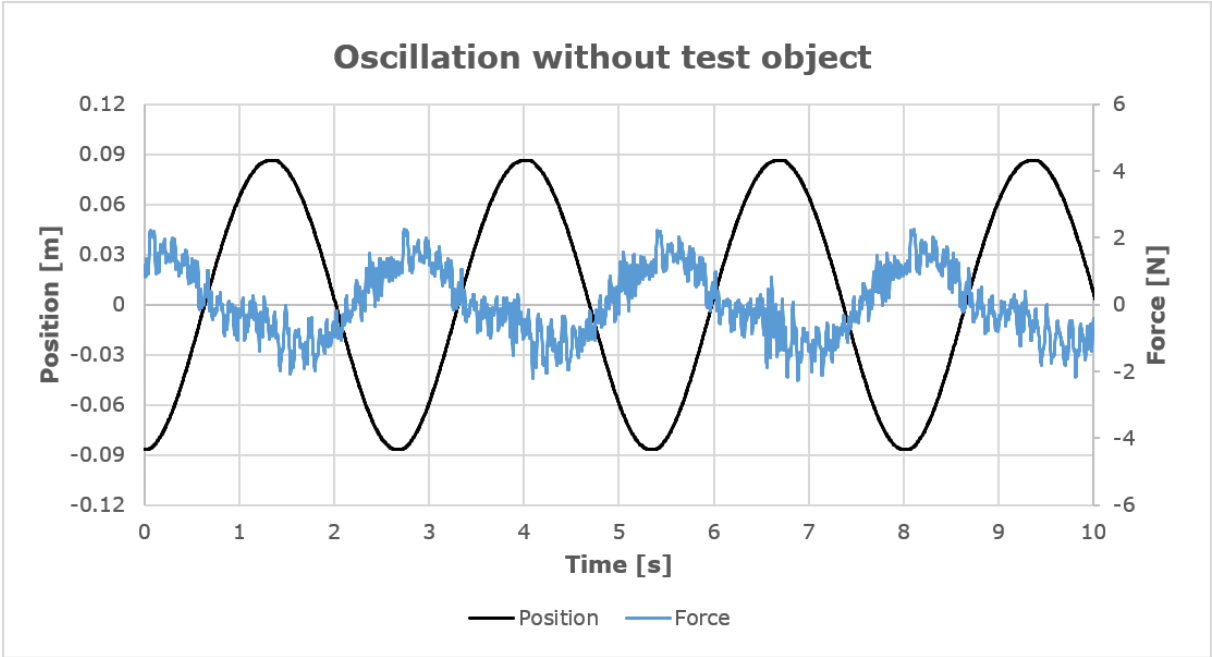
Figure 3.7 - Oscillation without test object, after improvements

3.4 Experimental test methods

When the new experimental setup was completed and set up in the towing tank, several verification experiments had to be conducted (step 5-12 in Figure 3.2). These were tests both about the data collected and functionality of the setup, but also in regards of the quality of 3D printed parts to verify that it is possible to use simple 3D printed objects to estimate hydrodynamical characteristics. The method regarding the design and fabrication of 3D printed parts itself will be further presented in chapter 3.6.

Before experimental tests could be conducted, specific preparations were required. This includes sensor calibration for both the position sensor and the position sensor and zero balance for both sensors. It is essential that the sensors are accurately calibrated to be able to extract reliable data from the experiments. To calibrate and set zero balance for the position sensor, several measurements are done at different distances to set reference points needed in the software. Afterward, several other reference measurements are conducted to verify the calibration. The process is somewhat similar for the force sensor, but with different masses attached to the wires to set reference points and to verify the calibration.

When the new setup was verified with several tests, more advanced geometries could be 3D printed and tested (step 9-13 in Figure 3.2). This was various subsea geometries, starting with small and simple structures, and then stepwise larger structures. This way, both the structural strength of the object and the experiment could be verified with different scaled objects. This would also show how the scale effect influences the hydrodynamic coefficients.

When all experiments were complete, the method and the final results could be evaluated. It is vital that the results are evaluated before new experiments are conducted; this was done to assure the quality of the experiments. The thesis should, in the end, try to discuss and conclude if the method of utilizing 3D printing to estimate hydrodynamic coefficients is either proven to be successful or not.

As stated earlier, two different experiments were conducted in the tank, lifting experiments and oscillation experiments. This was done to evaluate two different experimental methods that could be utilized to acquire hydrodynamic data from 3D printed objects.

3.4.1 Forced oscillation experimental tests

In a forced oscillation experiment the test object is forced to move up and down in an oscillating movement at different amplitudes and periods. This test is used since both the added mass and damping may be extracted from the measured data. A typical and simplified test setup is illustrated in Figure 3.8.
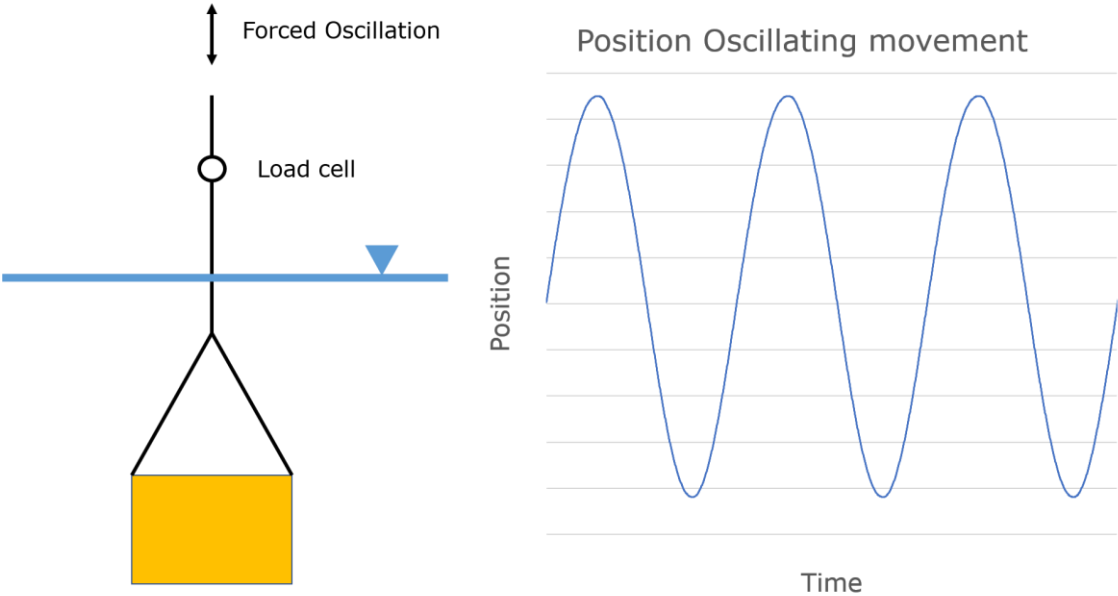
Figure 3.8 - Simplified test arrangement for oscillating experiments

The forces acting on a test object during submerged forced oscillating experimental tests may be split into force components. By managing to split these forces into different components, it is possible to estimate the hydrodynamical characteristics for different complex geometries. The various forces acting on the object in an instant while moving upwards are presented in Figure 3.9.
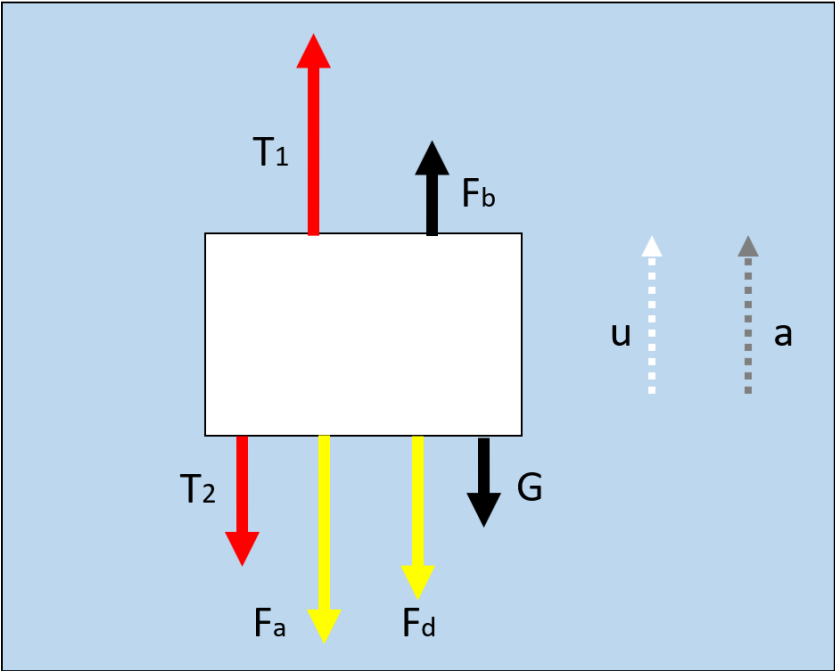
Figure 3.9 - Forces acting on test object during oscillating experimental tests

In which:

T_1 = Tension force from upper wire (motor) [N]
T_2 = Tension force from lower wire (mass) [N]
F_b = Buoyancy force [N]
G = Gravitational force of the object in air [N]
F_a = Force due to added mass [N]
F_d = Force due to drag [N]

By performing a zero balance of the force sensor when the test object is submerged, and at rest, the gravitational (for a non-moving object) and buoyancy force is subtracted from the measured data.

The oscillating movement of a structure may be described with a sinusoidal equation, shown in equation 3.1.

$$Z(t) = Z \cdot \sin(\omega t + \varphi) \qquad (3.1)$$

In which:

Z(t) = time series of the model position [m]
ω   = angular velocity [rad/s]
t   = time [s]
φ = phase shift [rad]

While the forces could be described with a single sinusoidal term as well, it is more practical to express the force of an oscillating movement with both a sinus term and a cosine term. The velocity and acceleration of an oscillating movement will be shifted 90°. By separating the force this way, the force will also be split into one term for inertia forces and one for damping forces. The oscillation forces are represented with equation 3.2.

$$A_1 \cdot \sin(\omega t) + A_2 \cdot \cos(\omega t) = F(t) \qquad (3.2)$$

In which:

A_1 = Amplitude of added mass [N]
A_2 = Amplitude of damping [N]
F(t)   = time series of the model force [N]

The forces acting on a structure may also be described in term of mass and damping as in equation 3.3.

$$(M + A_{33})\ddot{Z}(t) + B\dot{Z}(t) = F(t) \qquad (3.3)$$

In which:

M = oscillating mass of the system and object [kg]
A_{33} = hydrodynamical added mass in heave [kg]
B = linearized damping [N/(m/s)]
$\dot{Z}$(t)   = time series of the model velocity [m/s]
$\ddot{Z}$(t)   = time series of the model acceleration [m/s^2]
$F(t)$ = time series of the force in the lifting wire [N]

To estimate the hydrodynamical forces and coefficients for a particular geometry, all forces except hydrodynamical forces must be subtracted. This could be done analytically, but it would require knowledge about specifics such as the friction and inertia of all bearings, pulleys, wires and test object. Therefore, the oscillating experiments are done in two variations for each case: one with the test object submerged and one in air, resulting in equation 3.4.

Next, the test data is aligned with the same phase, and then the forces from the experiment in the air are subtracted from the submerged experiment leaving only hydrodynamical forces due to added mass (A_{33}) and damping (B). Ultimately, the damping can be split into linear (B1)- and quadratic (B2) damping (equation 3.5).

$$(M + A_{33}) \cdot \ddot{Z}(t) + B_{submerged} \quad \cdot \dot{Z}(t) = F_{submerged}(t)$$

$$- \quad (M) \quad \cdot \ddot{Z}(t) + B_{dry} \quad \cdot \dot{Z}(t) = F_{dry}(t)$$

$$= \quad (A_{33}) \quad \cdot \ddot{Z}(t) + B_{hydrodynamical} \cdot \dot{Z}(t) = F_{hydrodynamical}(t) \qquad (3.4)$$

$$F_{damping} = B1 \cdot \dot{Z}(t) + B2 \cdot \left(\dot{Z}(t)\right)^2 \qquad (3.5)$$

In which:

B1 = Linear damping [Ns/m]
B2 = Quadratic damping [Ns^2/m^2]

The added mass may be converted into a dimensionless number for complex structures by dividing the added mass (A_{33}) by the analytical added mass A_0 of a similar, but simplified geometry. For a perforated plate, that would be the added mass A_0 of a solid plate, while for a subsea structure that could be a solid cube with similar dimensions (Solaas, 2017).

For solid objects where the cross-section and volume are easier calculated, as solid boxes or cylinders, the hydrodynamic coefficients Ca and Cd may be calculated by modifying Morison's equation (Eq. 2.3) into equation 3.6 and 3.7. If the linear damping is equal to zero, the drag coefficient may be calculated by equation 3.8.

$$Ca = \frac{A_{33}}{\rho \cdot V} \qquad (3.6)$$

$$Cd = \frac{2 \cdot B_{hydrodynamical}}{\rho \cdot A \cdot u} \qquad (3.7)$$

$$Cd = \frac{2 \cdot B_2}{\rho \cdot A} \qquad (3.8)$$

3.4.2 Forced lifting experimental tests

In a forced lifting experiment, the test object is raised from the bottom of the tank to the surface at different velocities and accelerations. A typical and simplified test setup is illustrated in Figure 3.10.
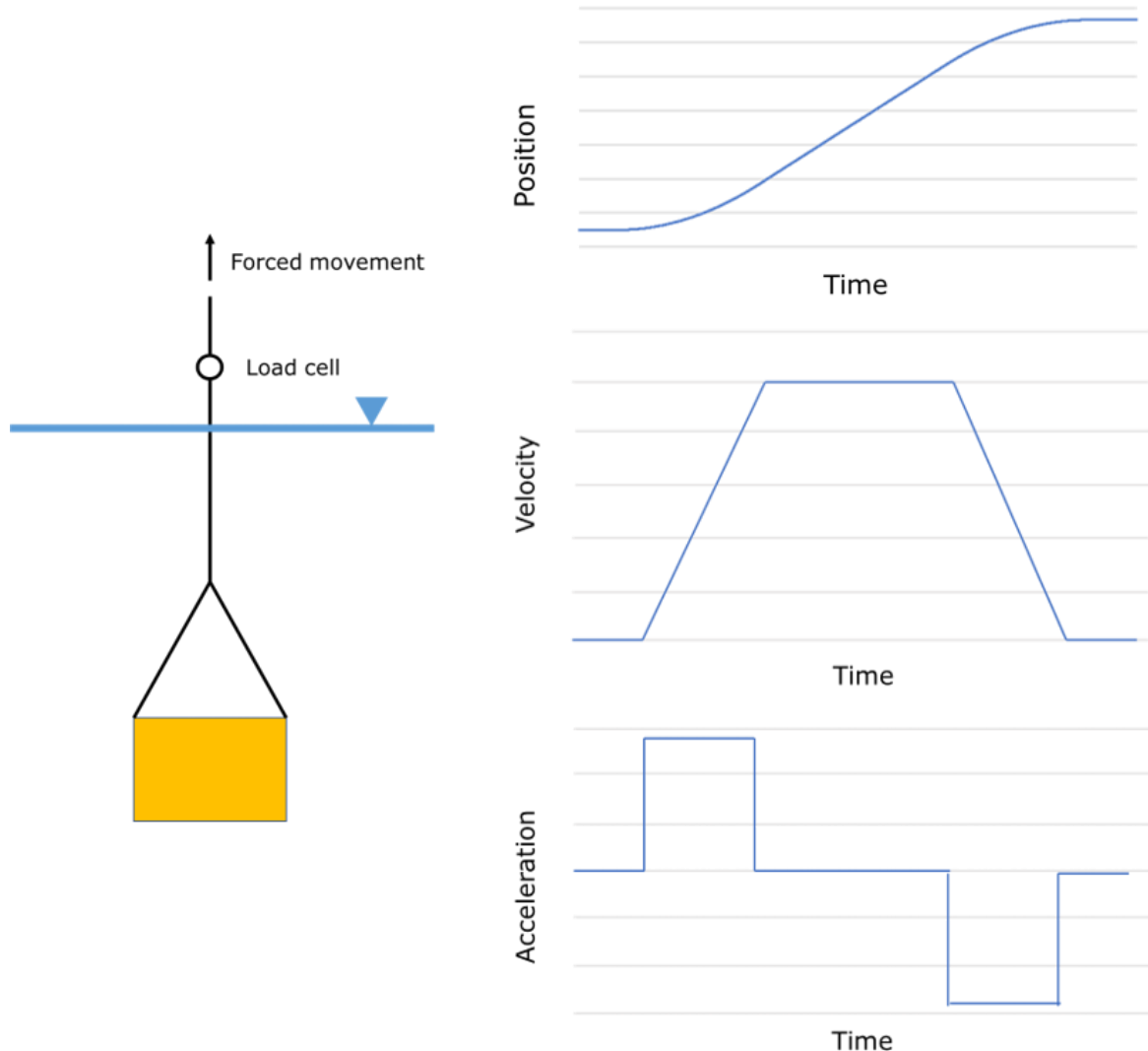
Figure 3.10 – Simplified test arrangement for lifting experiments

While the pure hydrodynamical forces are found by subtracting the values logged in an experiment in air from a submerged experiment, this was not possible for lifting experiments due to limitations of the setup. There is not enough height above the water surface under the crane to perform lifting operations in air. Therefore, the friction and inertia forces of the system had to be subtracted analytically.

At first, several experiments were conducted with the pulldown system, but it was proven too challenging to subtract the friction and inertia forces of the system to get good results. Therefore, the lifting experiments are done without the pulldown system, but with additional masses fixed to the test objects; where the object had a lower density than water. These changes result in that only the inertia forces from the object, and the additional mass must be subtracted from the test results. The remaining pulleys are attached to the crane, and its friction and inertia forces will not affect the measured force.

The forces affecting the test object during lifting operations would be as for the oscillating experiments, but without the force from the lower wire (T_2 in Figure 3.9). By performing a zero balance of the force sensor when the test object is submerged, and at rest, the gravitational force (for a non-moving object) and buoyancy forces are subtracted from the measured data.

The damping is acquired from the section of the lifting movement where the object is moving at a constant velocity and with an acceleration equal to zero. At this point, there are no added mass forces or other inertia forces, which result that the measured force is exclusively damping (equation 3.9). Ultimately, the damping can be split into linear (B1)- and quadratic (B2) damping, as in equation 3.5

$$B_{hydro} \cdot \dot{Z}(t) = F_{damping}(t) \tag{3.9}$$

When the damping is known, the added mass can be estimated where the acceleration is constant. Experiments with constant acceleration could either be conducted in a separate experiment or during the accelerating phase before reaching constant velocity. The added mass may then be calculated by taking the measured force and then subtract the damping part of the force and the inertia due to the mass of the object, leaving the added mass exclusively (equation 3.10).

$$F_{measured}(t) - F_{inertia} - F_{damping}(t) = F_{added\ mass}(t)$$

$$\left((M + A_{33}) \cdot \ddot{Z}(t) + B_{hydro} \cdot \dot{Z}(t)\right) - M \cdot \ddot{Z}(t) - B_{hydro} \cdot \dot{Z}(t) = F_{added\ mass}(t) \tag{3.10}$$

$$A_{33} \cdot \ddot{Z}(t) = F_{added\ mass}(t)$$

As for an oscillating movement, the added mass (A_{33}) for a complex geometry may be converted into a dimensionless number if desired by dividing A_{33} by A_0. While for simpler geometries, the hydrodynamic added mass and drag coefficient may be calculated with equation 3.6 and 3.7. If the linear damping is equal to zero, the drag coefficient may be calculated by equation 3.8.

$$Ca = \frac{A_{33}}{\rho \cdot V} \tag{3.6}$$

$$Cd = \frac{2 \cdot B_{hydrodynamical}}{\rho \cdot A \cdot u} \tag{3.7}$$

$$Cd = \frac{2 \cdot B_2}{\rho \cdot A} \tag{3.8}$$

3.5 Real life subsea models

To evaluate if the method for 3D printing complex subsea structures could be used to acquire hydrodynamical characteristics, a couple of real subsea structures were acquired as CAD files. The files acquired are the property of TechnipFMC. There were several challenges with the printability of the structures. One of the main issues was that the CAD files were highly detailed. Both details such as small hydraulic piping, electric cables, bolts, which are all details that will be too small when scaled down for the printer to produce. Due to the small size of these components, the hydrodynamical forces and coefficients of the structure should not change too much by the removal of the components. One of the structures acquired is a subsea template (29 m x 29 m x 16 m), presented in Figure 3.11.
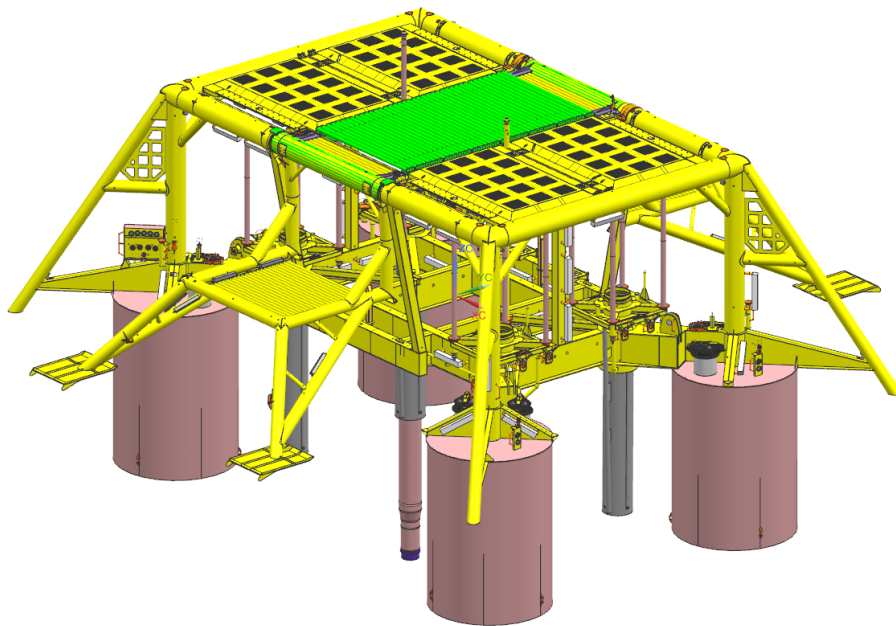
Figure 3.11 - Subsea template from TechnipFMC

The structure is highly detailed on several locations with components that need to be removed if one should attempt to 3D print the structure. An example of a detailed area is on top of the suction anchors, shown in Figure 3.12.
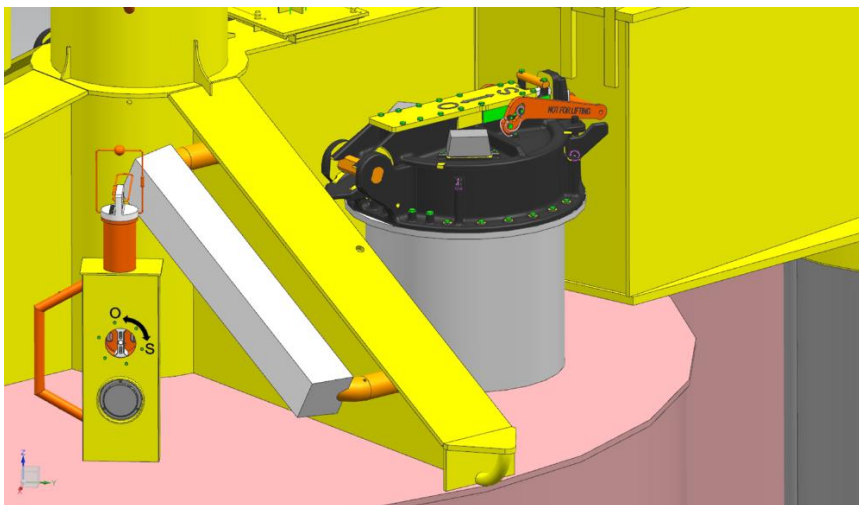
Figure 3.12 - Highly detailed area on the subsea template

To make the structure more 3D-printer friendly, a large amount of the small details was removed in Siemens NX, as illustrated in Figure 3.13. The acquired file was a STEP file. In this file, all the different components are assembled, which means that they may be un-assembled again. By going through each component and removing all the smallest details, a cleaner structure is the result.
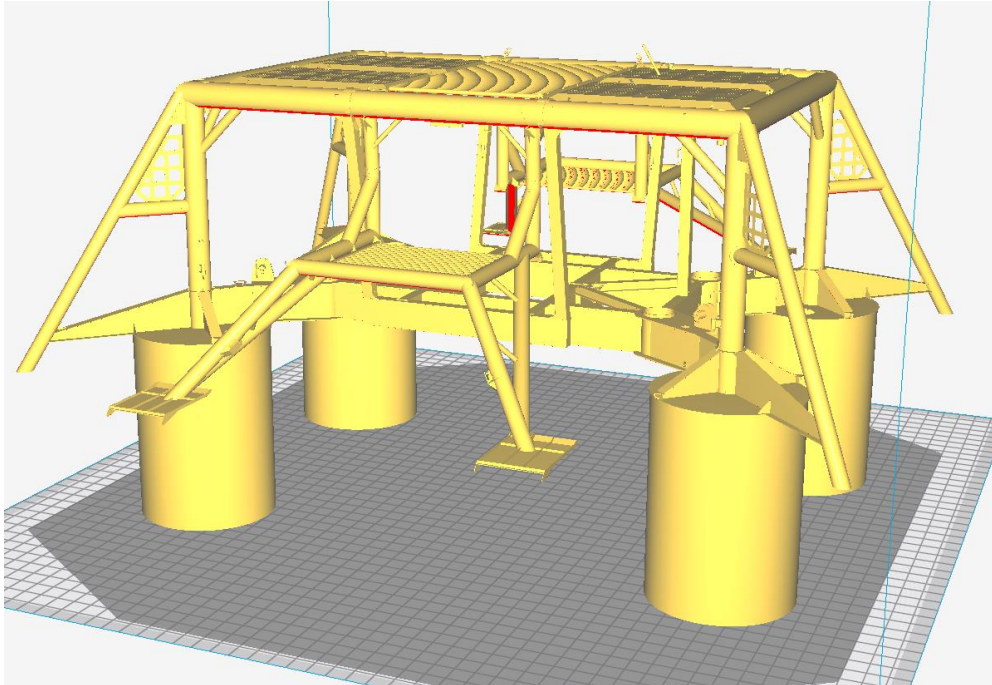
Figure 3.13 - Subsea template with fewer details imported to Cura

A printer with the possibility for water dissolvent support material (PVA) is essential when 3D printing complex structures with fused deposition modeling. A PLA support structure would be impossible to remove without destroying the structure. The only printer available at NTNU Ålesund with PVA is an Ultimaker 3 printer. The problem using this printer is the limited build volume of the printer. After small details are removed, the structure needs to be scaled 1:150 to fit the Ultimaker 3 printer. This results in that plates with an original thickness of 6 mm ends up being 0.04 mm, which is smaller than the nozzle diameter itself. Therefore, no printer at NTNU Ålesund can 3D print such a geometry at this scale.

Even a printer with the same build volume as the Creality CR-10 S5 (500 mm x 500 mm x 500 mm) would not have been able to scale the structure large enough to give the structure enough thickness to be produced.

Another smaller subsea structure was also acquired from TechnipFMC (9 m x 10 m x 7 m), presented in Figure 3.14 and Figure 3.15. The size of this structure could fit inside the Creality printer if scaled 1:20, which would make the thickness of the structure printable. Splitting the structure into several sections could allow for less support material, but more post-processing fixing the section together again. Still, PVA or SLS would be required to get a feasible 3D printed structure.
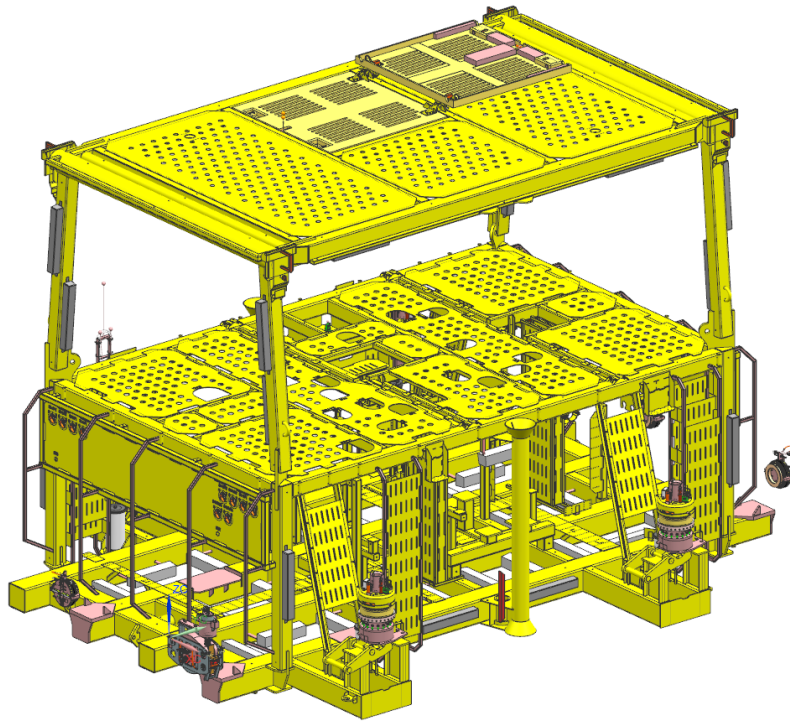
Figure 3.14 – Subsea structure, before removal of details and small components
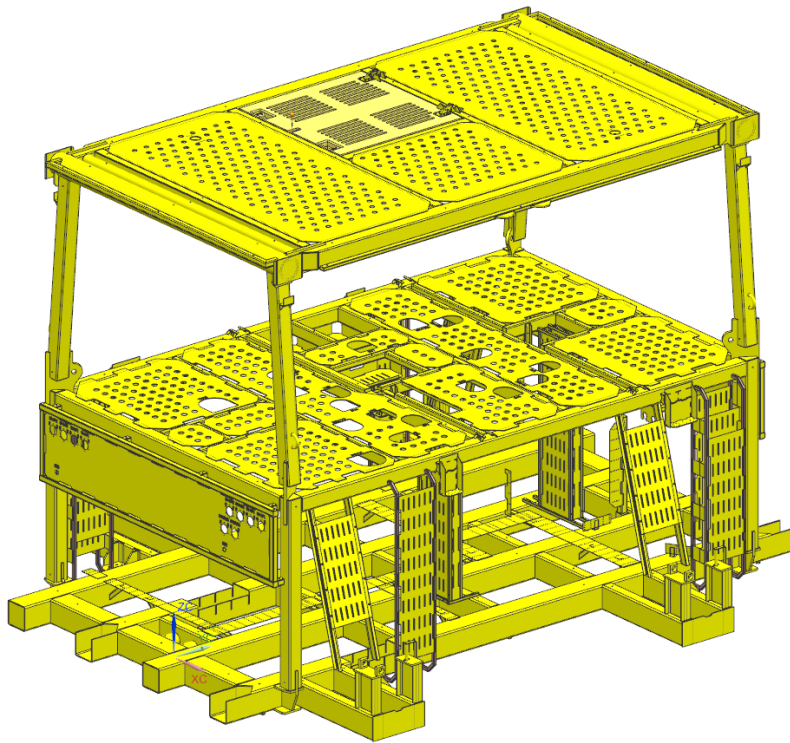
Figure 3.15 - Subsea structure, after removal of details and small components

3.6 Design and fabrication of simplified 3D printed structures

Since there is no possibility to 3D print the acquired real subsea structures, simplified structures had to be designed. The first step of designing a new geometry is to make the design in a 3D CAD software. The self-designed structures are designed to be well suited for 3D printing with fused deposition modeling. This means that the structures do not need any support structure for being fabricated. The result of a CAD model in Siemens NX is shown in Figure 3.16.
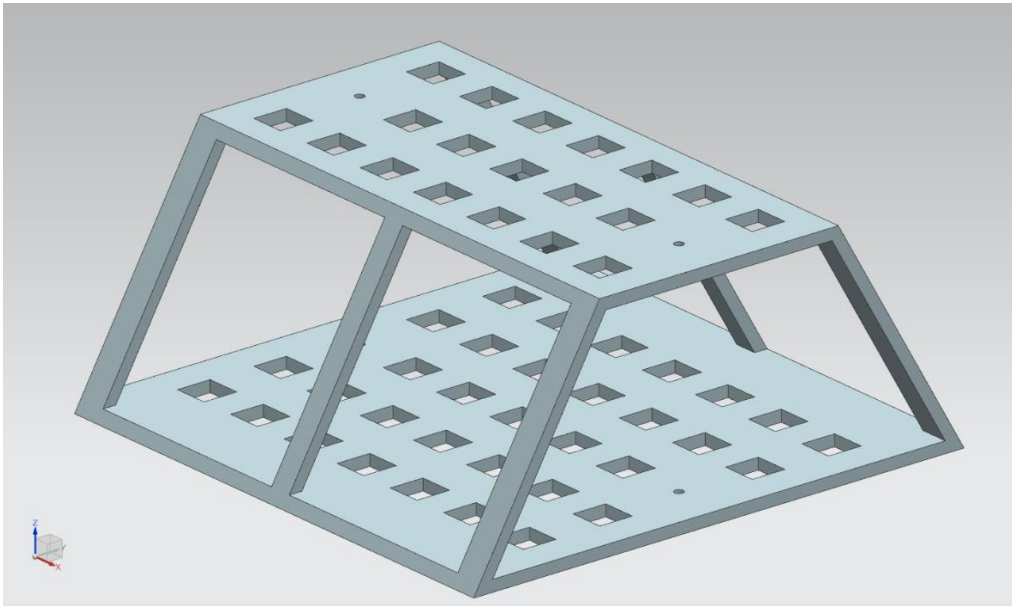
Figure 3.16 - 3D-model in Siemens NX

Next, the geometries are exported as an STL file, which may be processed in Cura. Several parameters were tuned to make the different test structure more suited for hydrodynamical experiments. It is essential that water does not leak into the inner structure of the test object – the infill. Therefore, the walls of the test objects are set up thicker than "typical" wall thicknesses. The layer height is also made smaller, to make a more compact outer wall. The essential parameters set in Cura is presented in Table 3.1 below.

Table 3.1 – Slicing parameters

Nozzle diameter	0.4 mm
Layer height	0.1 mm
Wall thickness	2 mm
Infill type	Grid
Infill density	20 %

Before completing the slicing, it is essential to evaluate how each structure should be orientated during the 3D printing to be best suited for this production method. The structure in Figure 3.16 would require a support structure to support the upper plate of the geometry. For this exact structure, it is possible to rotate the object 120° so that the bars supporting the top part of the geometry is faced down. With this new orientation shown in Figure 3.17, the structure may be printed without any need for the support structure.
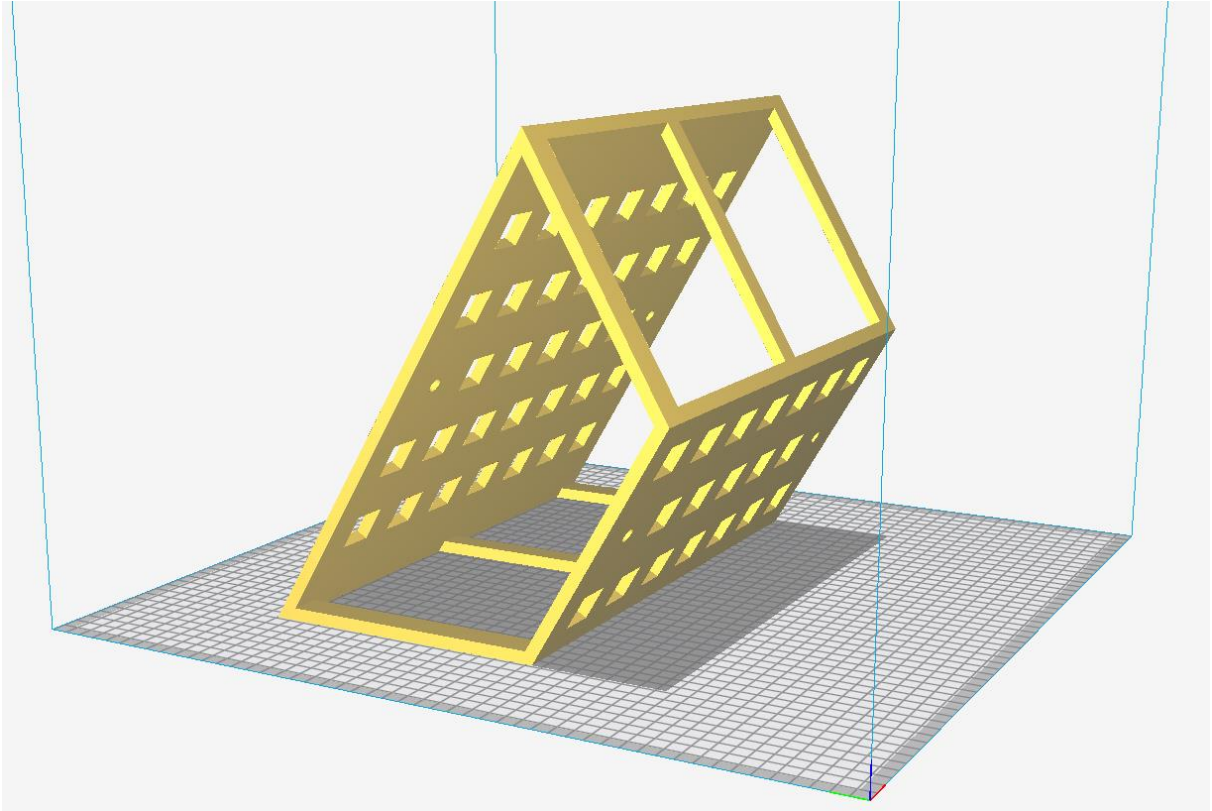
Figure 3.17 – 3D-model in Cura

When the slicing is complete, the g-code is uploaded to the Creality CR-10 S5 3D printer. Several settings must be set on the printer. The settings used in this thesis is presented below in Table 3.2.

Table 3.2 - 3D printer settings

Filament material	PLA
Filament diameter	1.75 mm
Nozzle temperature	200 °C
Bed temperature	60 °C
Print speed	50 mm/s
Fan speed	100 %

When the geometry is produced, a print without support structure will need none to very little post-processing before the object is test ready. The finished product is presented in Figure 3.18.

Figure 3.18 - 3D printed structure

4 Experimental Model Test Study

Experiments have been conducted on several test objects during this research. These test objects will be presented in this chapter. The chapter will also present the method used for smoothening and analysis.

4.1 Experimental tested models

The overall experimental matrix for the various test objects is presented in Table 4.1. While more detailed information will be given in the following sub-chapters.

Table 4.1 - Overall experimental matrix

Test object	Test method	Object dimensions (LxWxH) [m]	Object scale
Mudmat	Lifting and oscillation	0.83 x 0.51 x 0.019	-
Solid cube	Oscillation	0.15 x 0.15 x 0.15	-
Subsea template	Lifting and oscillation	6.75 x 6.75 x 3	1:20, 1:30, 1:45, 1:60
Suction anchor	Oscillation	5 x 5 x 4	1:20, 1:30, 1:40

4.1.1 Control variables for mudmat

The mudmat is utilized as reference geometry for both the lifting and oscillating experiments. The reason that this particular geometry is used for this is that several experiments have been conducted on similar geometries in other research from both SINTEF (Solaas, 2017), Yu (Yu, 2018) and DNV-GL (DNV-GL, 2011). The mudmat is presented in Figure 4.1, and the geometrical properties of the mudmat are presented in Table 4.2.
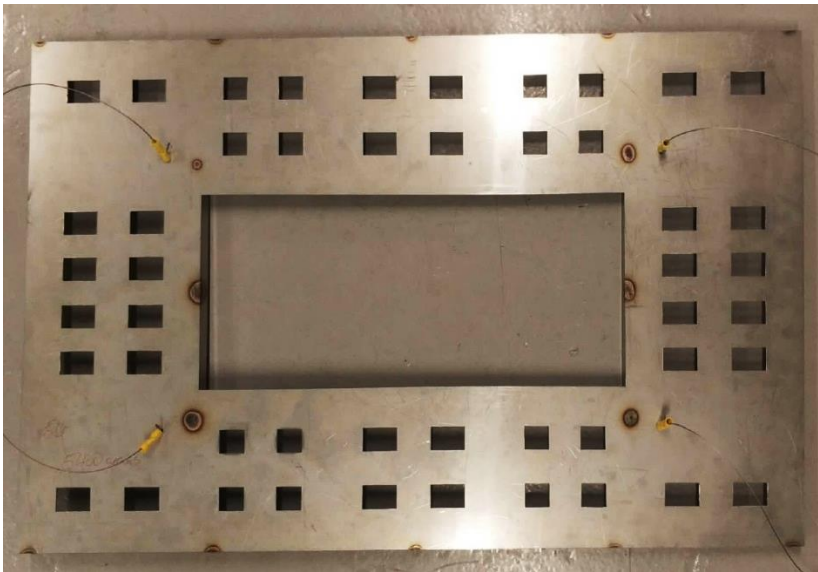
Figure 4.1 – Picture of mudmat

Table 4.2 - Geometrical properties of mudmat

Length	0.83 m
Width	0.51 m
Height	0.019 m
Perforation	29 %
Mass	5.37 kg

The oscillation experiments performed with the mudmat are done with seven different amplitudes and three different periods, presented in Table 4.3. All experiments are done both submerged and dry, as discussed in chapter 3, resulting in 42 experiments in addition to several additional tests for verification.

Table 4.3 - Control variables for oscillating experiments with mudmat

Displacement amplitude [m]	0.025 − 0.085 every 0.01
Period [s]	4; 3; 2.5

The forced lifting experiments were ultimately conducted at four different velocities and several different accelerations. In total, seven runs make up the final results, even though far more tests were conducted to verify the data and find the correct interval for both velocity and acceleration. The control variables for the forced lifting experiments are presented below in Table 4.4.

Table 4.4 - Control variables for forced lifting experiments

Max velocity [m/s]	Acceleration [m/s^2]
0.044	0.021
0.074	0.021
	0.041
0.096	0.021
	0.041
0.118	0.021
	0.082

4.1.2 Control variables for solid cube

A solid 3D printed cube has been used to conduct oscillating experiments on a simple geometry where the data could be compared with theoretical values. The cube is printed as a "square bucket" and later filled with polyurethane. This is a faster method, compared with printing the cube as a solid. The cube is presented in Figure 4.2, and the geometrical properties of the cube are presented in Table 4.5.
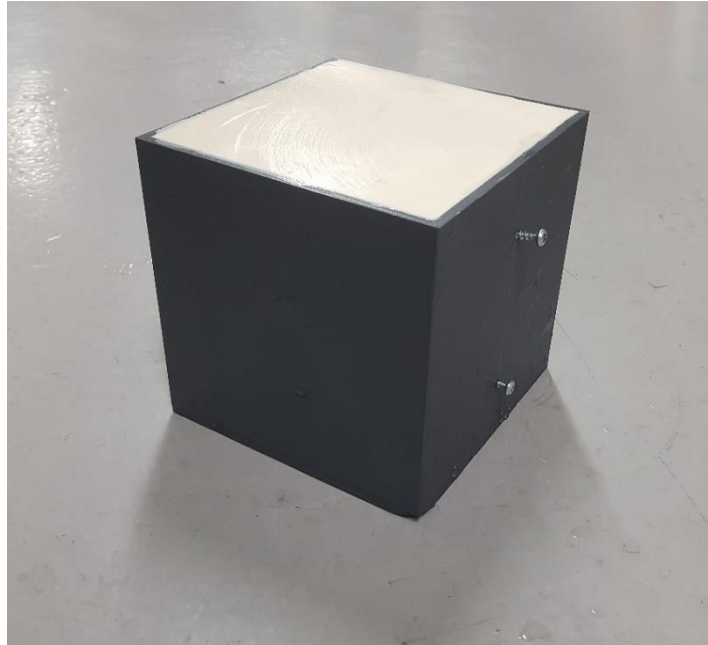
Figure 4.2 – 3D printed solid cube, filled with polyurethane

Table 4.5 - Geometrical properties of solid cube

Length	0.15 m
Width	0.15 m
Height	0.15 m
Mass	4.93 kg

The oscillation experiments performed with the solid cube are conducted with four different amplitudes and three different periods, presented in Table 4.6. All experiments were conducted both dry and submerged, resulting in a total of 24 test-runs, in addition to several additional tests for verification.

Table 4.6 - Control variables for oscillating experiments with solid cube

Displacement amplitude [m]	0.025 – 0.085 every 0.02
Period [s]	3; 2.5; 2

4.1.3 Control variables for subsea template

The self-designed simplified subsea template is used to verify the method of using 3D printed models to acquire hydrodynamical characteristics. The model has been produced in four different scales to evaluate the scale effects. The subsea templates are presented in Figure 4.3.
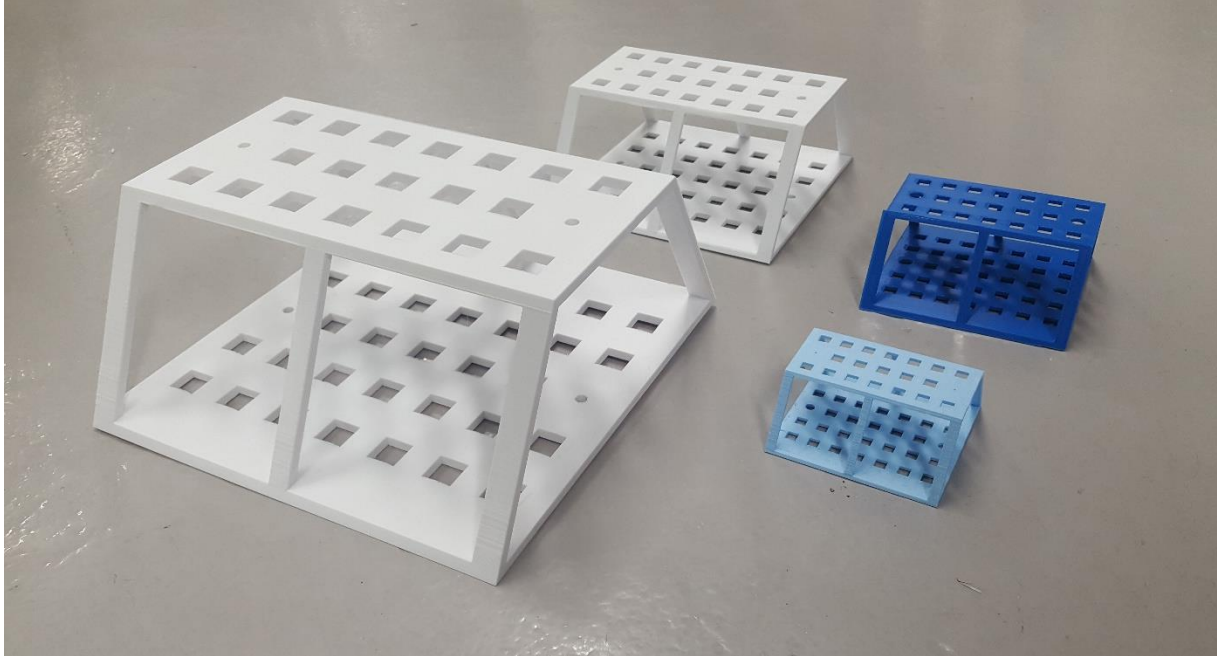
Figure 4.3 - 3D printed simplified subsea template

The geometrical properties are presented in Table 4.7. It is assumed that the real size of the template is 6.75 m x 6.75 m x 3 m. This is just an assumption used for comparison of different experimental results for different scales into values that could be realistic for a real size subsea structure. The added mass A0 is the theoretical added mass of a cube with the same footprint and height as the subsea structure (equation 4.1), which may be used to make the added mass dimensionless for the cube.

$$A0 = L \cdot W \cdot H \cdot k \cdot \rho \qquad (4.1)$$

In which:

L   = Length [m]
W   = Width [m]
H   = Height [m]
k   ≈ 1.4 for a cube with the same dimensions (DNV-GL, 2011) [-]
ρ   = density of water [kg/m^3]

Table 4.7 - Geometrical properties of the simplified subsea structure

Length	6.75 m			
Width	6.75 m			
Height	3 m			
Cross section perforation	16 %			
Scale	1:20	1:30	1:45	1:60
Mass (oscillation)	1005 g	364 g	128 g	37 g
Mass (lifting)	2995 g	-	-	-
A0 for scale 1:1	191.2 tons			

During experimental tests, the 1:60 scaled subsea structure broke, due to a too little structural strength. The other three was tested successful, and therefore the following control variables are only linked to the three largest objects.

The oscillation experiments performed with the subsea templates are done with four different amplitudes and four different periods, presented in Table 4.8. The larger objects are tested with the longest period of four seconds, while the smaller once are tested with three seconds as the most prolonged period. All experiments are done both submerged and dry, resulting in 96 test-runs in addition to several extra tests for verification.

Table 4.8 – Control variables for oscillating experiments of the subsea structure

Displacement amplitude [m]	0.025 – 0.085 every 0.02
Period [s]	4; 3; 2.5; 2; 1.67

The forced lifting experiments were conducted on the 1:20 scaled subsea template. To make it heavy enough to sink by itself, additional mass was attached to the structure. The tests were conducted at several different velocities and accelerations, presented in Table 4.9.

Table 4.9 – Control variables for forced lifting experiments

Max velocity [m/s]	Acceleration [m/s^2]
0.074	0.021
	0.041
0.096	0.041
	0.082
0.118	0.021
	0.041
	0.082

4.1.4 Control variables for suction anchor

The suction anchor is a geometry acquired from SINTEF (Solaas, 2017). SINTEF has conducted experiments on an identical geometry (but at a different scale), which gives the possibility to compare experimental results from 3D printed structures to other experiments. One of the printed suction anchors is presented in Figure 4.4.

Figure 4.4 – 3D printed suction anchor

The suction anchors are tested at three different scales, all 3D printed. The geometrical properties are presented in Table 4.10. The anchors are designed with one circular hole at the top (suction anchor in Figure 4.4 is turned upside-down), and with four holes on the side for attachment of the test setup. The added mass A0 is the theoretical added mass of a cylinder with the same dimensions as the suction anchor.

Table 4.10 – Geometrical properties of suction anchors

Diameter	5 m		
Height	4 m		
Perforation	2.56 %, one circular hole		
Scale	1:20	1:30	1:40
Mass	835 g	413 g	193 g
A0 for scale 1:1	148 tons		

The experiments conducted on the suction anchors are oscillation experiments, performed with four different amplitudes and at three different periods, presented in Table 4.11. All experiments are done both submerged and dry, resulting in 72 experiments in addition to several additional tests for verification.

Table 4.11 – Control variables for oscillating experiments on suction anchors

Displacement amplitude [m]	0.025 – 0.085 every 0.02
Period [s]	3; 2.5; 2

4.2 Data smoothening and fitting

4.2.1 Forced oscillation experiment

The recorded data from the various experiments are obtained in time series. Noise due to vibrations and hydrodynamic disturbance must be removed from the data before it may be analyzed. Note that the presented data from the oscillation experiments is just a section of the recorded data. All oscillating experiments are conducted with ten full oscillations.

The method used to smooth the results from the oscillating experiments is a nonlinear least square data fitting by the Gauss-Newton method. The method fits a particular function to the measured data, returning the desired variables. The fitting is done by minimizing the sum of the square residuals over a given interval (Stats Directe, 2019). In this case, the data is fitted to sinus functions, returning the amplitude, period, and phase shift of the position. The method is performed by code in MATLAB. The script related to forced lifting experiments is found in Appendix 2.

The measured position (seen to the left in Figure 4.5) is fitted to equation 3.1 (presented again below), returning the amplitude, period, and phase. The position is then re-plotted, starting from zero at time equals zero (seen in the right-hand plot in Figure 4.5). The amplitude and period are already known from the experimental setup and settings, but the phase shift will variate. The phase shift must be acquired from both the dry and submerged experiment before they are used to shift the dry and submerged force series to be synchronized.

$$Z(t) = Z \cdot \sin(\omega t + \varphi) \tag{3.1}$$
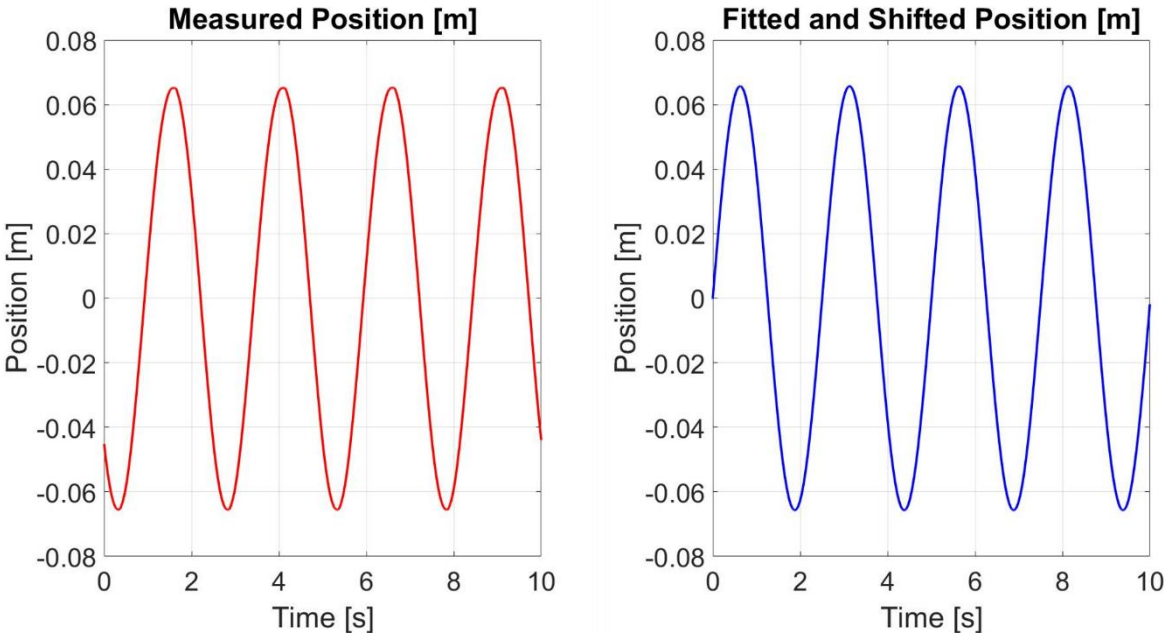
Figure 4.5 - Measured and fitted position from forced oscillation experiment

Next, both the dry and submerged data were fitted to equation 3.2 (presented again here). Returning the amplitude of the added mass force (A_1) and the amplitude of the damping force (A_2), before being shifted by utilizing the phase shift found from the position fitting.

$$A_1 \cdot \sin(\omega t) + A_2 \cdot \cos(\omega t) = F(t) \qquad\qquad (3.2)$$

With the submerged amplitudes A_1 and A_2 known, the fitted force series could be plotted together with the measured force series, seen to the left in Figure 4.6. The force is shifted according to the phase shift acquired from the position fitting (seen in the right-hand plot in Figure 4.6). The equivalent fitting and shift are performed on the dry force series and may be seen in Figure 4.7.
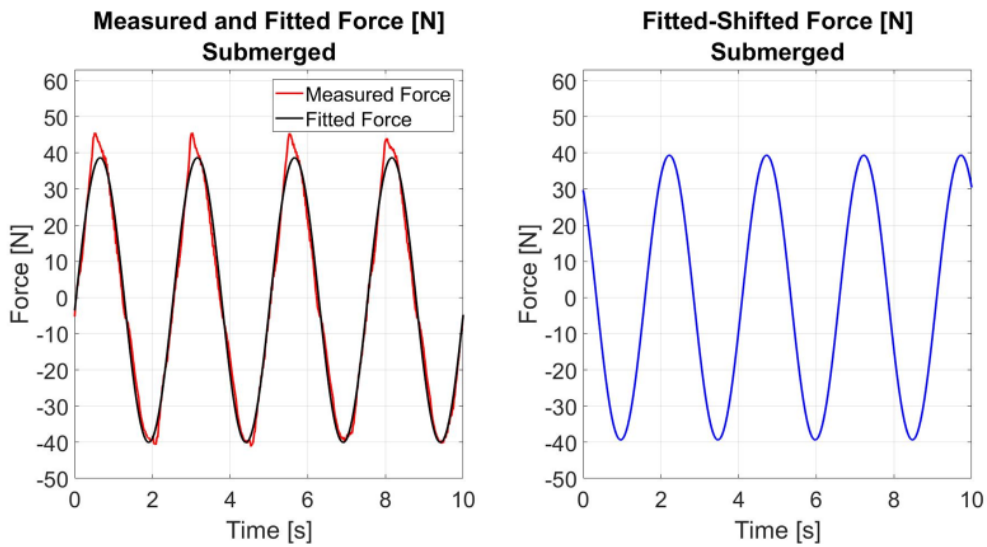
Figure 4.6 – Measured and processed force from submerged oscillation experiment
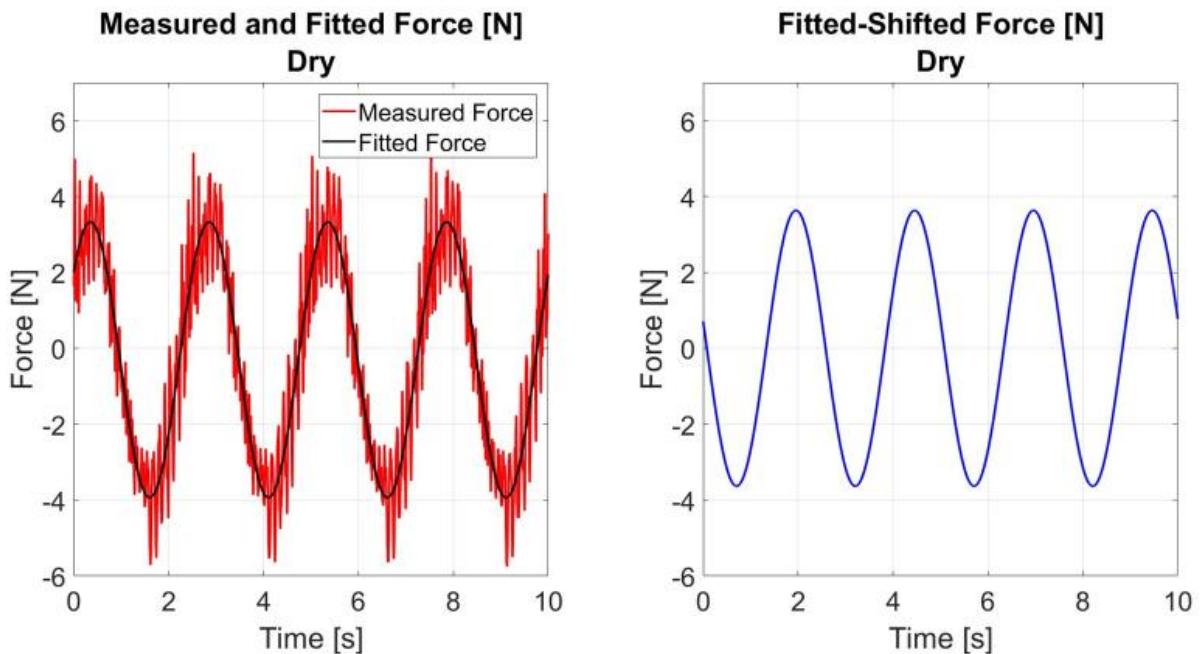
Figure 4.7 – Measured and processed force from dry oscillation experiment

With the fitted and shifted data, it is possible to process the data further to calculate the desired hydrodynamical characteristics for the different geometries. The analysis for forced oscillation experiments are found in chapter 4.3.1.

4.2.2 Forced lifting experiment

As for the forced oscillation experiments, the data from the lifting experiments must be smoothed. Rather than fitting a function to the data, the series are smoothed over an interval with the Locally Estimated Scatterplot Smoothing (LOESS), also known as Local Polynomial Regression. While the position series is quite smooth, the velocity and acceleration are derived from the position, and just small disturbances in the position will ruin the velocity and acceleration (Figure 4.8). Therefore, the position must be smoothed before the velocity may be calculated, and then the acceleration calculated from the smoothed velocity (Figure 4.9). After smoothing, reference calculations confirmed the velocity and acceleration series. The script used for smoothing and analysis is found in appendix 2.
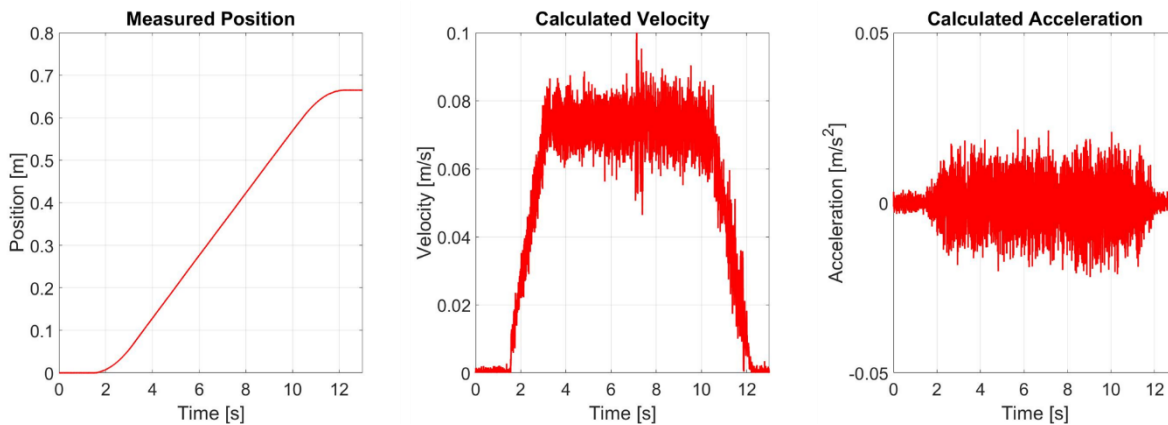
Figure 4.8 - Measured and calculated data without smoothing
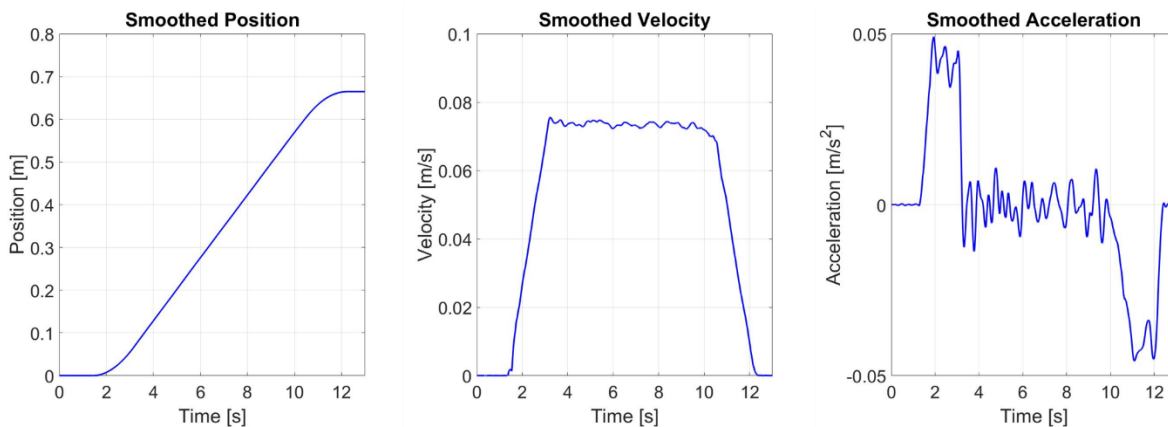
Figure 4.9 - Measured and calculated data with smoothing

The force series are also affected by noise. The noise occurs due to effects such as vibrations in the system, hydrodynamic disturbance. To be better able to process the force series, the data must be smoothed to remove some of the noise. The measured data before and after smoothing is presented in Figure 4.10.
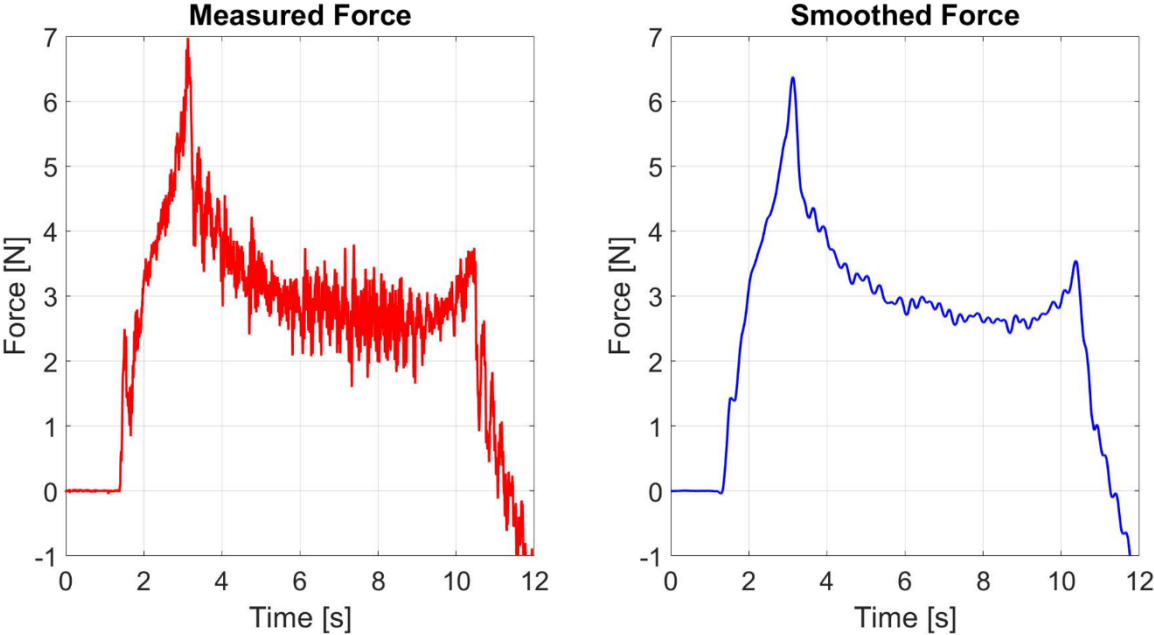
Figure 4.10 - Smoothing of force series, lifting experiments

With smoothed data, it is possible to process the data further to calculate the desired hydrodynamical characteristics for the different geometries. The data analysis for forced lifting experiments is found in chapter 4.3.2.

4.3 Data Analysis

4.3.1 Forced oscillating experiment

After the data series for the forced oscillation experiments are fitted to smooth sinus functions, the data may be processed to acquire the desired hydrodynamical characteristics for the different geometries. As explained in chapter 4.2.1, the fitting with the least-square method for dry and submerged data series returns the added mass force amplitude A_1 and the damping force amplitude A_2 (equation 3.2).

Data acquired from the forced oscillation experiment on the mudmat structure will be utilized in this sub-chapter to explain further the method used. The setup settings and the values acquired from the smoothening is presented in Table 4.12 and Figure 4.11.

Table 4.12 - Data from mudmat experiment, Z = 65mm, T = 2.5 s

Period	T	2.5 s
Amplitude	Z	65 mm
Added mass amplitude submerged	A_1 sub	25.8 N
Added mass amplitude dry	A_1 dry	3.6 N
Damping amplitude submerged	A_2 sub	29.7 N
Damping amplitude dry	A_2 dry	0.7 N
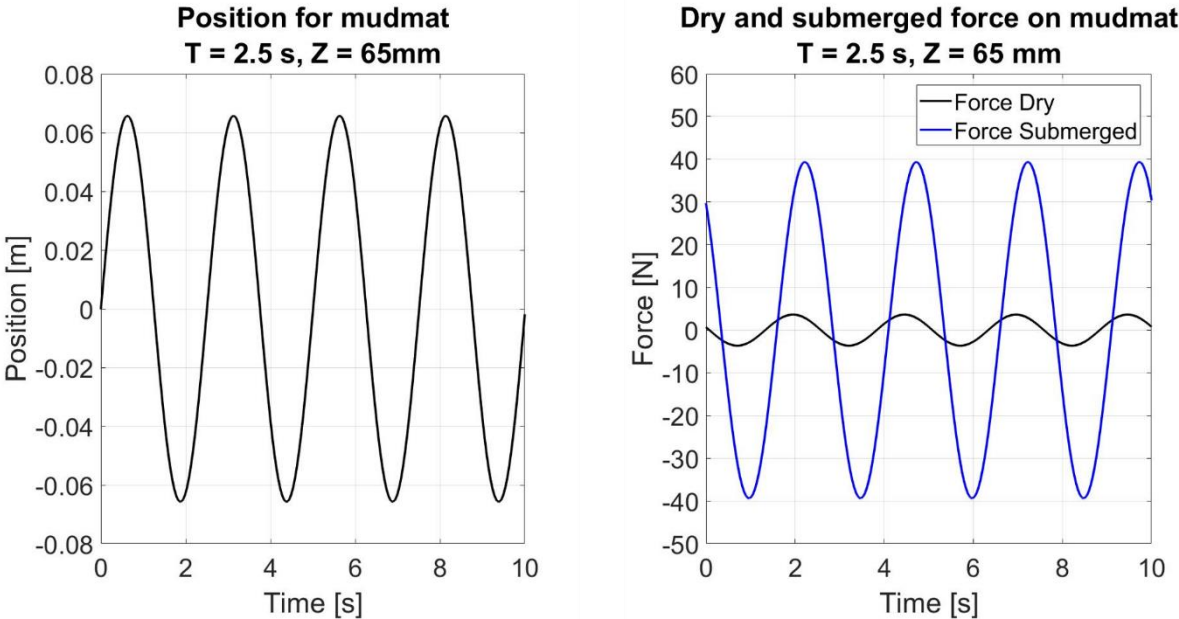
Figure 4.11 – Smoothed data from mudmat, T = 2.5 s, Z = 65 mm

Next, the hydrodynamical forces are calculated with equation 4.2 and 4.3, by subtracting the dry data from the submerged. Resulting in a hydrodynamical added mass (A_{1Hyd}) of 22.2 N, and hydrodynamical damping (A_{2Hyd}) of 29.0 N.

$$A_{1\,Hyd} = A_{1\,Sub} - A_{1\,Dry} \qquad (4.2)$$

$$A_{2\,Hyd} = A_{2\,Sub} - A_{2\,Dry} \qquad (4.3)$$

Then the added mass term of equation 3.2 is set equal to the added mass term in equation 3.4, resulting in equation 4.4. Next, the same is done with the damping terms, resulting in equation 4.6. For the added mass term, the added mass A_{33} is found at the time when the velocity is equal to zero and the acceleration at its peak (0.41 m/s^2 for the particular experiment) — resulting in the sinus term equal to one, leading to equation 4.5. The added mass is then calculated to 54.1 kg.

$$A_{1\,Hyd} \cdot \sin(\omega t) = A_{33} \cdot \ddot{Z}(t) \tag{4.4}$$

$$A_{33} = \frac{A_{1\,Hyd}}{\ddot{Z}(max)} \tag{4.5}$$

For the damping term, the damping B is found at the time when the acceleration is equal to zero, and the velocity is at its peak (0.16 m/s for the particular experiment) — resulting in the cosine term equal to one, leading to equation 4.7. The damping is then calculated to 177.7 Ns/m.

$$A_{2\,Hyd} \cdot \cos(\omega t) = B_{Hyd} \cdot \dot{Z}(t) \tag{4.6}$$

$$B_{Hyd} = \frac{A_{2\,Hyd}}{\dot{Z}(max)} \tag{4.7}$$

The added mass may then be converted into a dimensionless number by either using Morrison's equation with a reference volume for simple structures, for more complex geometries the added mass A_{33} could be divided by the theoretical added mass of a solid object with the same volume. For the mudmat both could be done, but in this case the Morrison's equation is used. The added mass coefficient can be calculated, with equation 3.6 (presented again below), to 0.27.

$$C_a = \frac{A_{33}}{\rho \cdot V_{Ref}} \tag{3.6}$$

In which V_{Ref} is calculated by equation 4.8.

$$V_{Ref} = \frac{\pi}{4} \cdot length^2 \cdot width \cdot perforation \tag{4.8}$$

The damping may also be done dimensionless with Morrison's equation and equation 3.7 (presented again below). The mudmat has an effective cross-section of 0.299 m^2, resulting in a drag coefficient of 7.1.

$$C_D = \frac{2 \cdot B}{\rho \cdot A \cdot u} \tag{3.7}$$

4.3.2 Forced lifting experiment

After the data series for forces lifting experiments are smoothed, the data may be processed to acquire the desired hydrodynamical characteristics for different geometries.

Data acquired from the forced lifting experiment on the mudmat structure will be utilized in this sub-chapter to explain further the method used. The setup settings are presented in Table 4.13, and the values acquired from the smoothing is presented in Figure 4.12.

Table 4.13 - Data from lifting experiment on mudmat

Max velocity	u_{max}	0.074 m/s
Acceleration	a	0.041 m/s^2
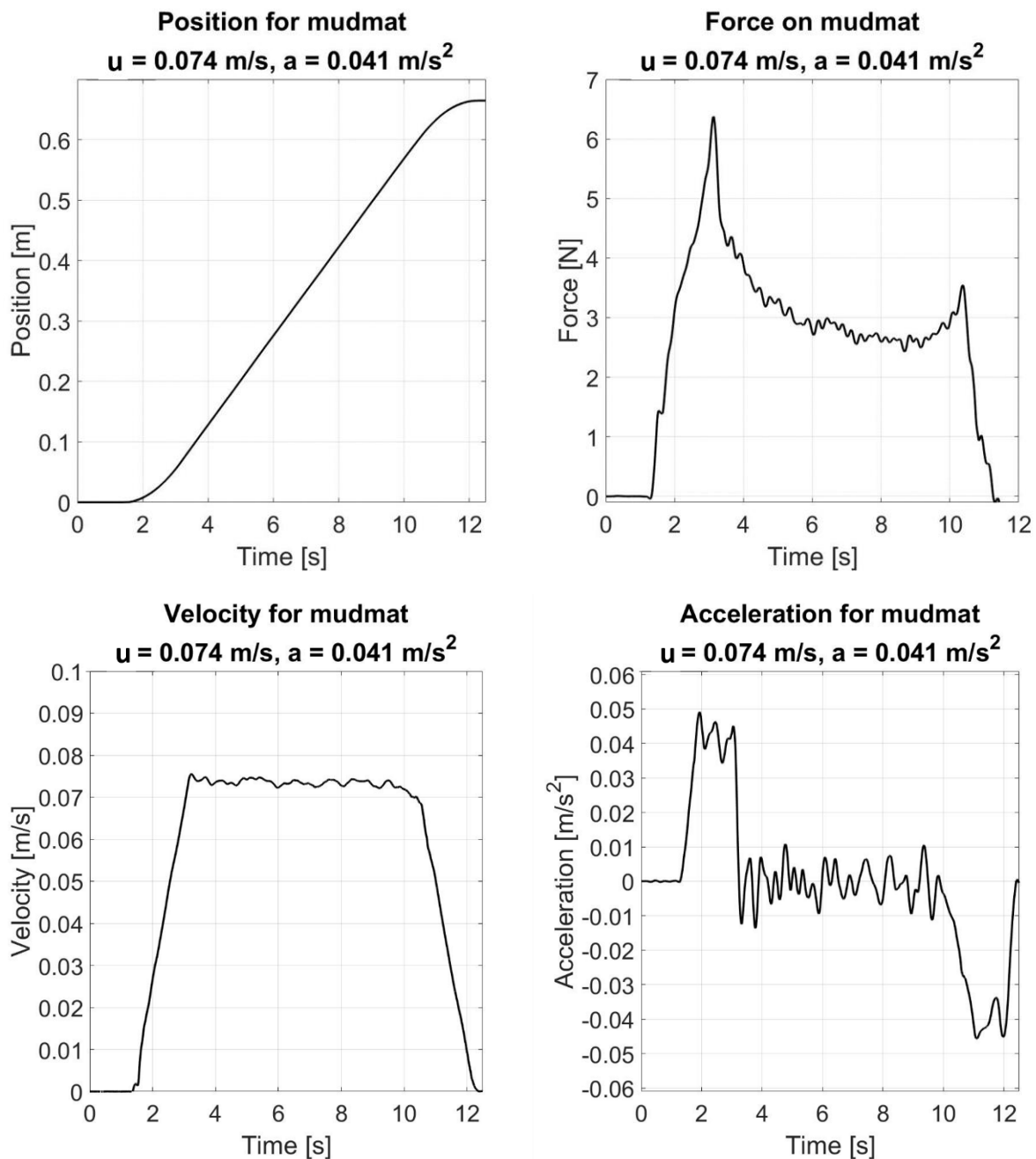
Figure 4.12 – Smoothed data for mudmat u = 0.074 m/s, a = 0.041 m/s^2

Next, damping may be calculated from the force plot in Figure 4.12. The calculation may be done from the approximate horizontal section where the velocity is constant, between 7 and 9.5 seconds into the time series. Before seven seconds, the flow has not developed properly, and after 9.5 seconds the surface starts to affect the force series. The average force between seven and nine seconds is measured to 2.65 N (Figure 4.13).
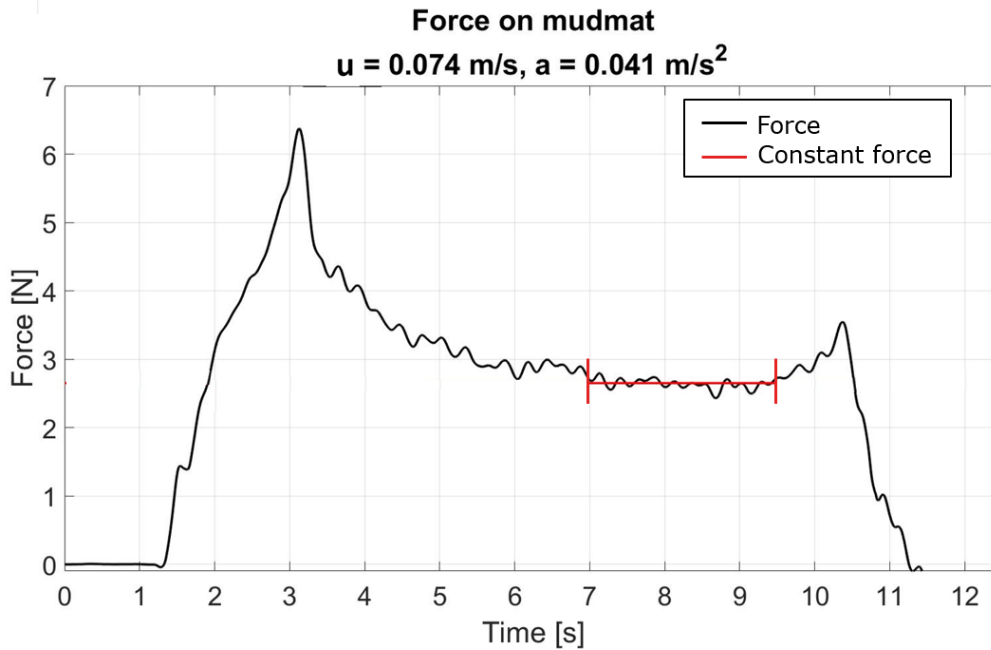
Figure 4.13 - Force series from mudmat experiment, u = 0.074 m/s, a = 0.041 m/s^2

By manipulating equation 3.9, the damping may then be calculated for the section between seven and nine seconds with equation 4.9, resulting in damping of 35.8 Ns/m.

$$B_{hydro} = \frac{F_{damping}(t)}{\dot{Z}(t)} \tag{4.9}$$

When the acceleration is equal to zero, the measured data is not affected by the mass of the object itself. However, when assessing the added mass, the inertia force of the object must be subtracted. This is done analytically by multiplying the measured acceleration with the mass of the object.

To be able to assess the added mass, the damping part of the force during acceleration must also be subtracted from the measured force. This is done by calculating the average added mass in MATLAB during the last 0.5 seconds of the acceleration phase (more accurate to use average due to noise). The force due to added mass is then calculated to 2.88 N by equation 4.10.

$$F_{measured}(t) - F_{inertia} - F_{damping}(t) = F_{added\ mass}(t)$$

$$\left((M + A_{33}) \cdot \ddot{Z}(t) + B_{hydro} \times \dot{Z}(t)\right) - M \cdot \ddot{Z}(t) - B_{hydro} \cdot \dot{Z}(t) = F_{added\ mass}(t)$$

(4.10)

The added mass in kg is then calculated, with equation 4.11, by dividing the force on the acceleration at that instant, resulting in an added mass of 70.2 kg.

$$A_{33} = \frac{F_{added\ mass}(t)}{\ddot{Z}(t)}$$

(4.11)

As for the oscillation experiments the added mass and the damping may be converted into a dimensionless number by using Morrison's equation (equation 3.6 and 3.7) with the reference volume V_R and the area A. Resulting in an added mass coefficient of 0.36, and a drag coefficient of 3.2.

5 Results and Discussion

The experiments are conducted according to the control variables listed in the previous chapter. However, not all the combinations listed gave good results and therefore are some of the combinations not included in this chapter. This is mostly experiments with long periods and small amplitudes (acceleration and velocity for lifting experiments), where the measured forces were too small to give reliable results. Some experiments with short periods and high amplitudes gave chaotic movement and are therefore also not included in the presented results in this chapter.

The results are presented as added mass [kg] and damping [Ns/m]. The damping is split into linear and quadratic damping, and an approximation is given for both (as presented in equation 3.5). The approximation for B1 and B2 is plotted manually to fit the damping as good as possible. In addition, the added mass and damping are made dimensionless where suited, as explained in chapter 3. All results are also presented in tables in appendix 1.

5.1 Forced lifting experiments

Results from forced lifting experiments are presented as added mass from equation 4.11 and damping from equation 4.9. When suited, the added mass and damping is made dimensionless with equation 3.6, 3.7, and 3.8.

The linear and quadratic damping is adapted to the measured results and given by equation 3.5, presented again below.

$$F_{damping} = B1 \cdot \dot{Z}(t) + B2 \cdot \left(\dot{Z}(t)\right)^2 \tag{3.5}$$

5.1.1 Mudmat experiments

The forced lifting experiments with mudmat was the first set of experiment conducted, used to verify the method of forced lifting. The results from the forced lifting experiment are presented in Figure 5.1 and Figure 5.2.
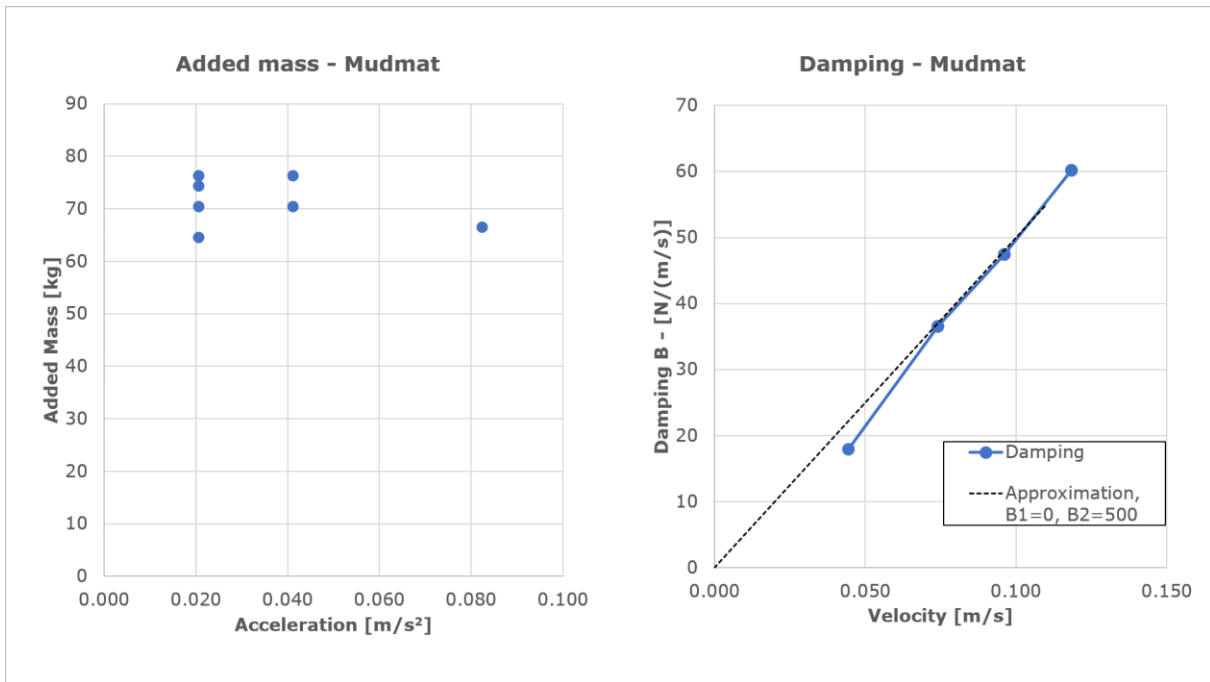
Figure 5.1 - Added mass and damping from mudmat – lifting experiments
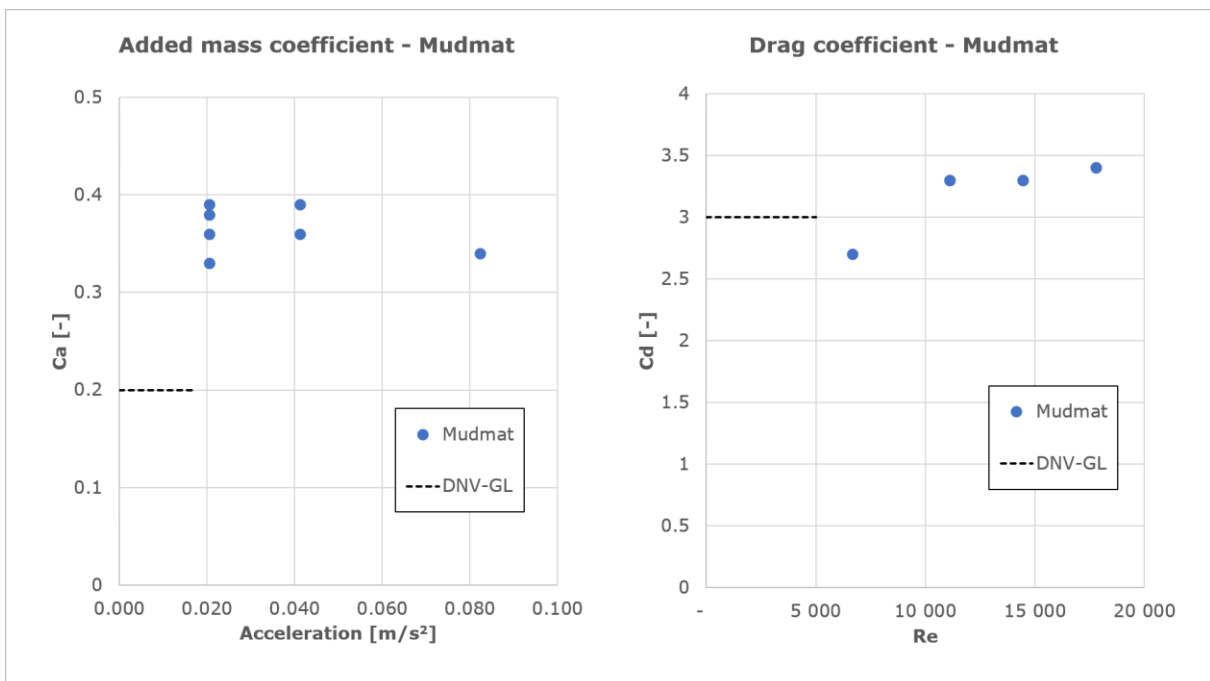
Figure 5.2 - Added mass and drag coefficient from mudmat – lifting experiment

If the data from DNV-GL-H103 in Figure 2.12 is extrapolated to 29%, the added mass coefficient should be around 0.2, and the drag coefficient between 2.5 - 3.5. The results from the experiments give an added mass coefficient around 0.35, which is a bit higher than the reference value. While the drag coefficient is within the expected interval.

The drag coefficient is calculated from the section of the lifting movement with constant velocity. The main challenge for the drag calculation is that the flow needs time to develop before a constant force is reached. Since the test tank has a limited height, this may be hard to achieve before the surface effect starts to affect the result. During the experiments, a short section with an approximated constant force could be achieved. At this stage, there are no inertia forces to subtract analytically. This gives for a scenario where the calculation of the drag coefficient should be quite precise.

On the other hand, the calculation of the added mass coefficient requires an analytical removal of inertia forces. During acceleration, the object could also be affected by the bottom effects of the tank-bed. Both the analytical removal of inertia and bottom effects results in a more uncertain calculation, which might be the reason for the deviation of the added mass coefficient. In addition, the result may be affected by bottom, surface, and wall effects. Even if the mudmat has the same cross-section and perforation, there is a chance that there still could be minor differences with the geometry – resulting in different values.

The approximate values from the results are presented in Table 5.1.

Table 5.1 - Results from forced lifting experiment on mudmat

Added Mass	Linear Damping	Quadratic Damping	Ca	Cd
70 kg	0 Ns/m	500 Ns^2/m^2	0.35	3.2

5.1.2 Subsea structure experiments

The results from the forced lifting experiment on the 1:20 scaled subsea structure is presented below in Figure 5.3 and Figure 5.4. To make an approximation for the drag coefficient, the cross-section of the lower plate of the subsea structure is used. In reality, the subsea structure has several cross-sections. To use the area of the lower plate is probably not according to standards, but if the same area is used later to estimate the full-scale forces, this could be used as an preliminary approximation.
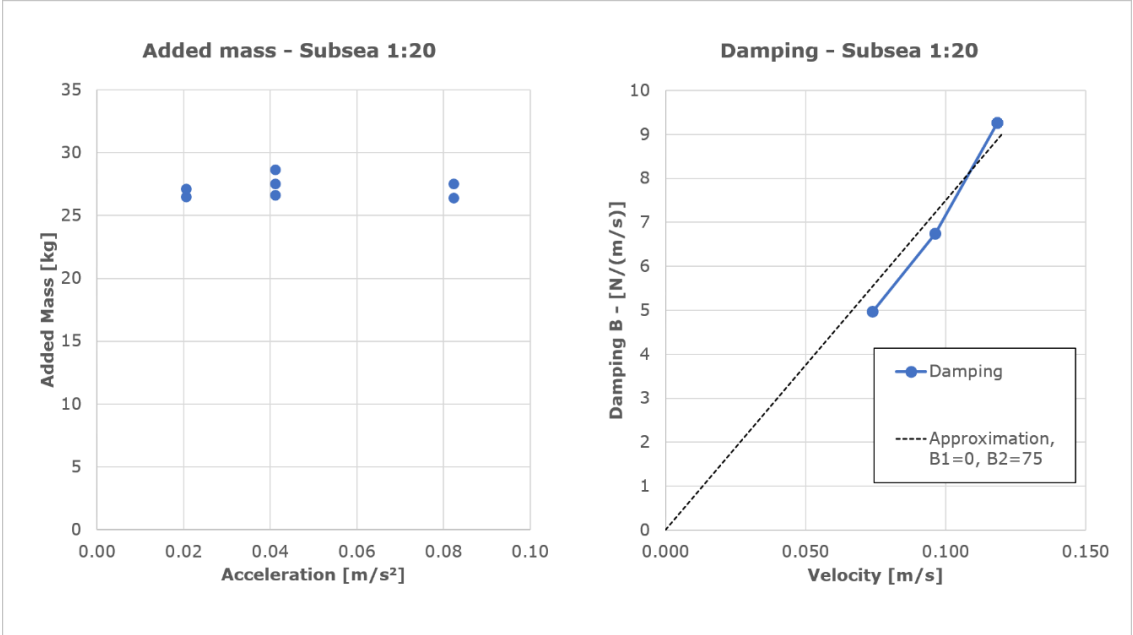
Figure 5.3 - Added mass and damping, 1:20 subsea structure - lifting experiment
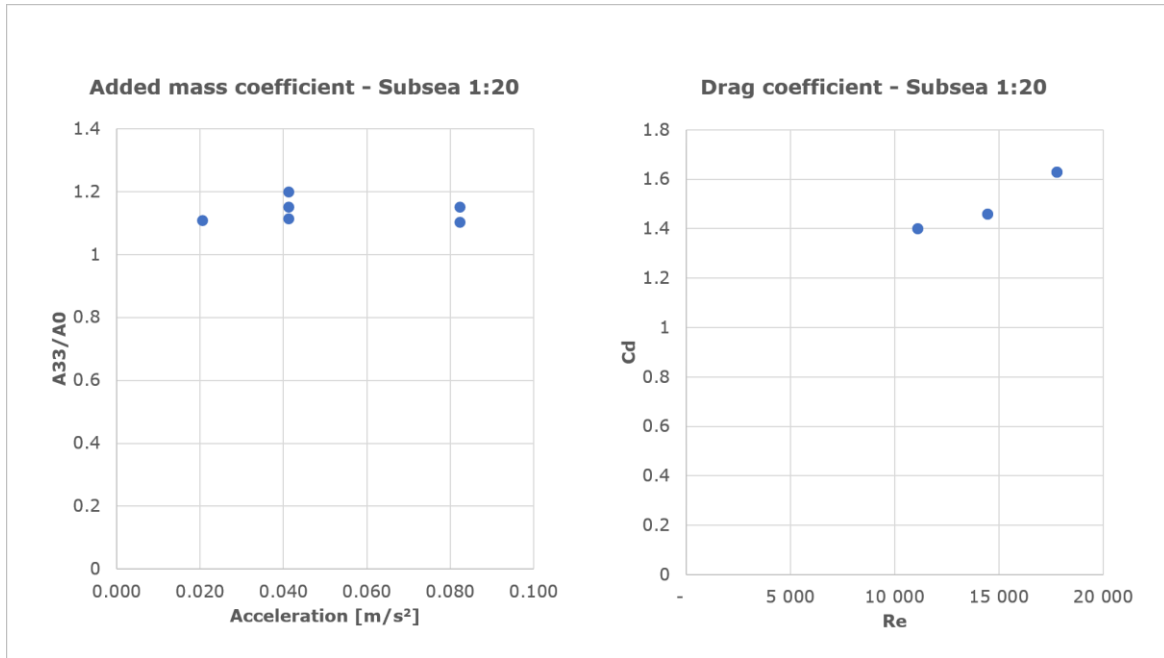
Figure 5.4 - Added mass coefficient, 1:20 subsea structure – lifting experiment

The results show an added mass of around 27 kg. As discovered from the forced lifting experiment of the mudmat, the added mass from this experiment may present false values. Instead of using the outer volume or the displaced volume, the added mass is made dimensionless by dividing it by the theoretical added mass A0.

The linear damping is approximated to be equal to 0, while the quadratic damping is around 75 Ns^2/m^2. The drag coefficient is then calculated with equation 3.8, in equation 5.1; giving a similar value as the coefficients in Figure 5.4.

$$Cd = \frac{2 \cdot B2}{\rho \cdot A} = \frac{2 \cdot 75 \frac{Ns^2}{m^2}}{999 \frac{kg}{m^3} \cdot 0.096 \, m^2} = 1.56 \tag{5.1}$$

The approximate values from the results are presented in Table 5.2.

Table 5.2 - Results from forced lifting experiment on 1:20 scaled subsea structure

Added Mass	Linear Damping	Quadratic Damping	A33/A0	Cd
27 kg	0 Ns/m	75 Ns^2/m^2	1.16	1.56

Assuming that the mudmat reference test is valid, the drag/damping results should be valid for Reynolds numbers in the same range. While the added mass values are a bit more uncertain, due to inertia and bottom effects. On the other hand, the added mass results should be more accurate than the mudmat results since the subsea structure is smaller than the mudmat and may, therefore, be positioned further from the sidewall – resulting in smaller wall effects.

5.2 Forced oscillation experiment

Results from forced oscillation experiments are presented as added mass from equation 4.5 and damping from equation 4.7. When suited, the added mass is made dimensionless with equation 3.6, and the damping is made dimensionless with equation 3.7.

The linear and quadratic damping is adapted to the measured results and given by equation 3.5, presented again below.

$$F_{damping} = B1 \cdot \dot{Z}(t) + B2 \cdot \left(\dot{Z}(t)\right)^2 \tag{3.5}$$

5.2.1 Mudmat experiments

The forced oscillation experiments with mudmat were the first oscillation experiment conducted, used to verify the method of forced oscillation. The results from the forced oscillation experiment on mudmat are presented in Figure 5.5 and dimensionless in Figure 5.6.
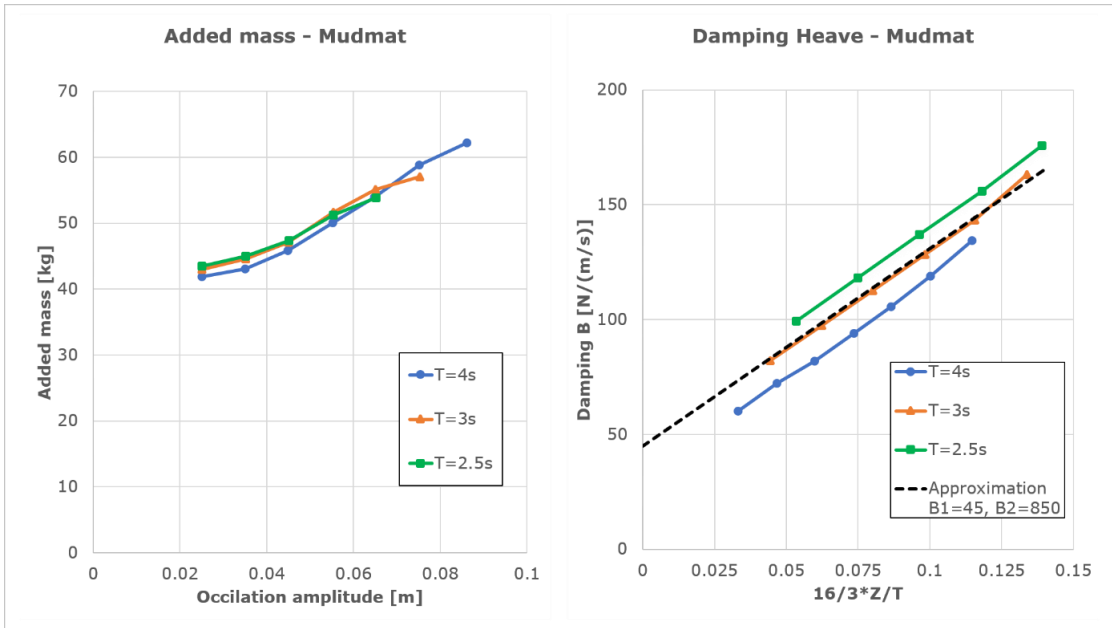
Figure 5.5 - Added mass and damping from mudmat, during oscillation experiment
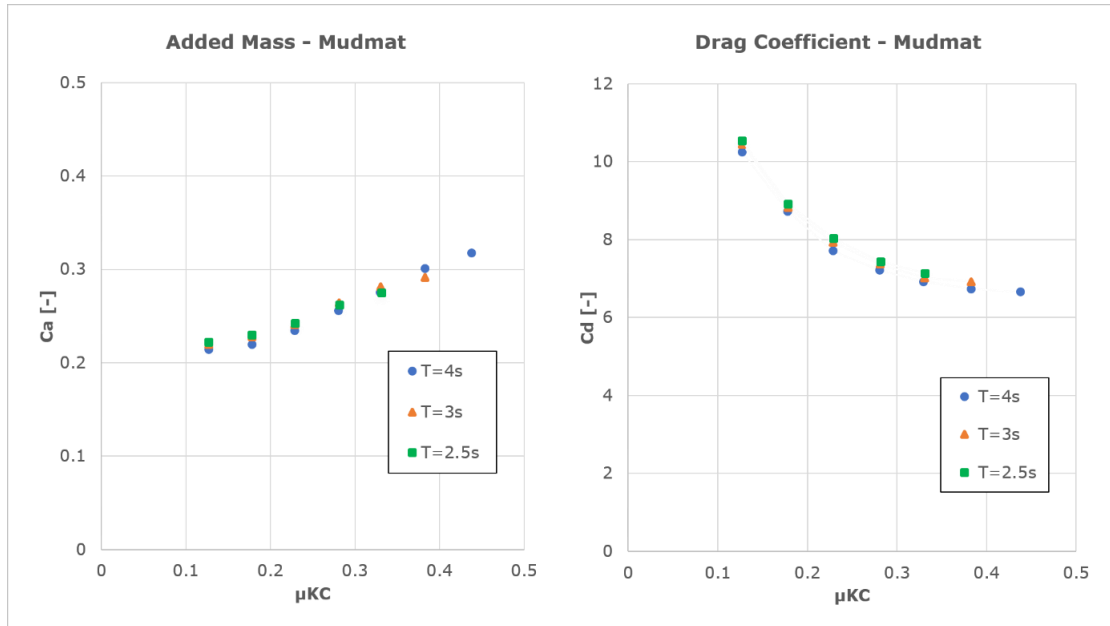
Figure 5.6 - Added mass coefficient from mudmat, during oscillation experiment

The results from the forced oscillation experiments, on mudmat in Figure 5.5, shows that the added mass is dependent by the oscillation amplitude, and not much by the period of the movement. While the damping is dependent on both the amplitude and the period since they set the velocity that the damping is connected to.

The added mass coefficient seems to be converging towards 0.2 when the porous KC number approaches zero; which is the same value as found in DNV-GL-H103, while it increases for higher KC numbers. It is uncertain how the DNV-GL coefficient is calculated. The drag coefficient seems to be converging towards 6 for higher porous KC numbers, but it could also decrease even more. Still, the drag coefficient acquired from these experiments is a lot higher compared with the one from DNV-GL-H103.

If the linear damping is assumed to be equal to zero, while the quadratic damping is around 850 Ns^2/m^2, the drag coefficient is then calculated with equation 3.8, in equation 5.2.

$$Cd = \frac{2 \cdot B2}{\rho \cdot A} = \frac{2 \cdot 850 \frac{Ns^2}{m^2}}{999 \frac{kg}{m^3} \cdot 0.299 \, m^2} = 5.7 \tag{5.2}$$

By estimating the drag coefficient this way, the linear damping contribution will not be missed out.

The results compared with the experimental results from SINTEF and Frøydis Solaas in Figure 5.7, shows that the damping is also a bit higher at the different periods. The results are overlapping in the plot, but the experiments conducted in this research are conducted at longer periods than SINTEF results. However, the linear damping seems to be quite alike, while the quadratic damping is unequal.

64

As presented in chapter 2.2.2, one could often neglect or simplify either the drag or added mass from oscillating movements. The KC number for the different combinations of amplitudes and periods in this thesis lies between 1 and 8. Therefore, the damping may often be neglected (KC<3) or linearized (3<KC<15), which means that the added mass is the most relevant for these forced oscillating experiments.

The added mass follows about the same slope as the results from Solaas, but with about eight kilograms less added mass. There could be several reasons for this, but one explanation could be due to that the mudmat is positioned close to the sidewall there is less water to accelerate. Also, having the same cross-section and perforation does not necessarily mean that the mudmat used in this research is identical to the ones used by DNV-GL and Solaas. Individual variations could lead to different results.
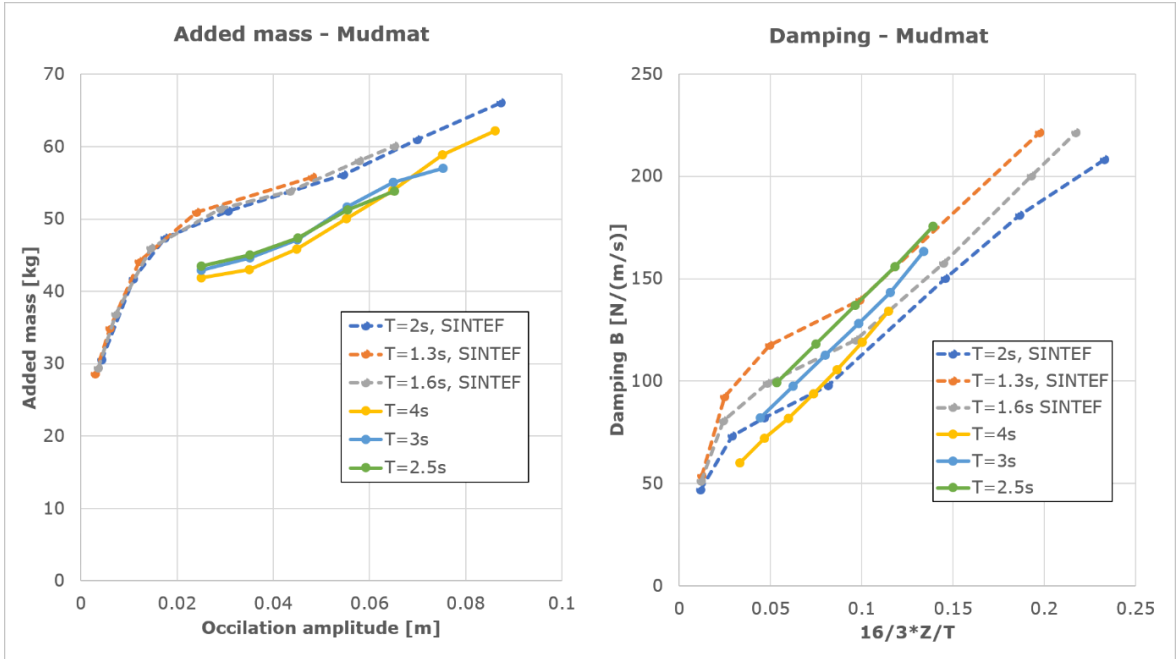
Figure 5.7 - Comparison of added mass and damping, oscillating mudmat experiment

Since the added mass and added mass coefficient variates, a fixed value is not set for them here. The approximate values from the results are presented in Table 5.3.

Table 5.3 - Results from forced oscillation experiment on mudmat

Linear Damping	Quadratic Damping	Cd
45 Ns/m	850 Ns^2/m^2	5.7

5.2.2 Solid cube experiments

A solid cube measured 150 mm in each direction was used as a test object to compare theoretical data to the experimental. The theoretical coefficients are collected form DNV-GL-H103 (DNV-GL, 2011). The results from the experiments are presented in Figure 5.8 and Figure 5.9.
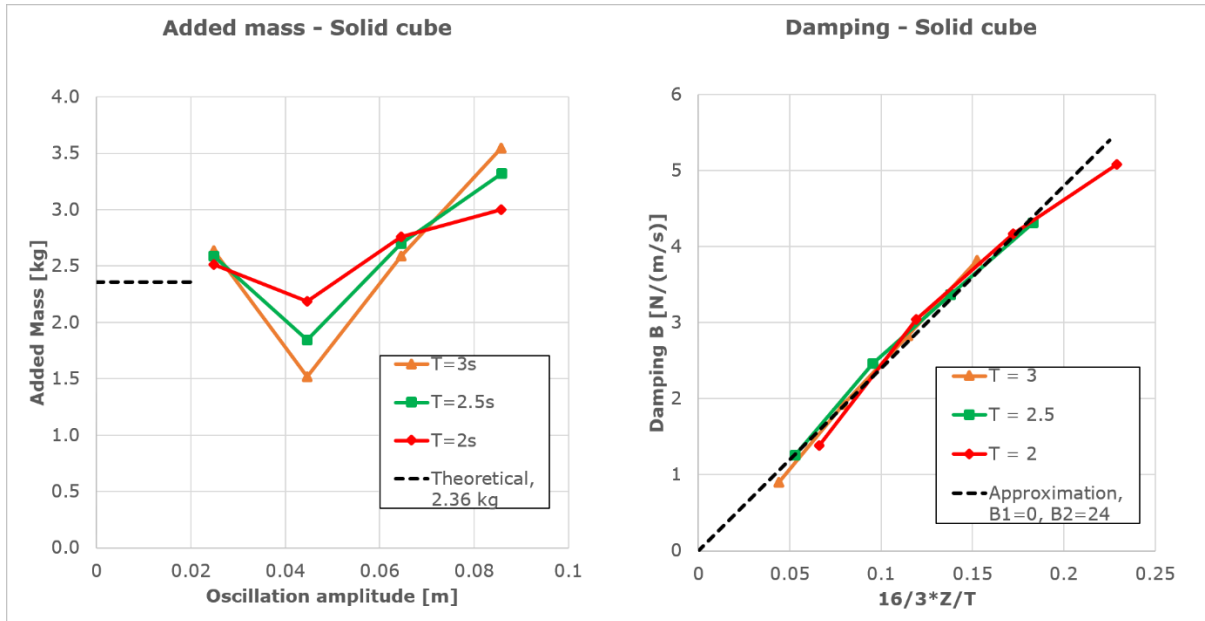
Figure 5.8 - Added mass and damping from solid cube – oscillation experiment
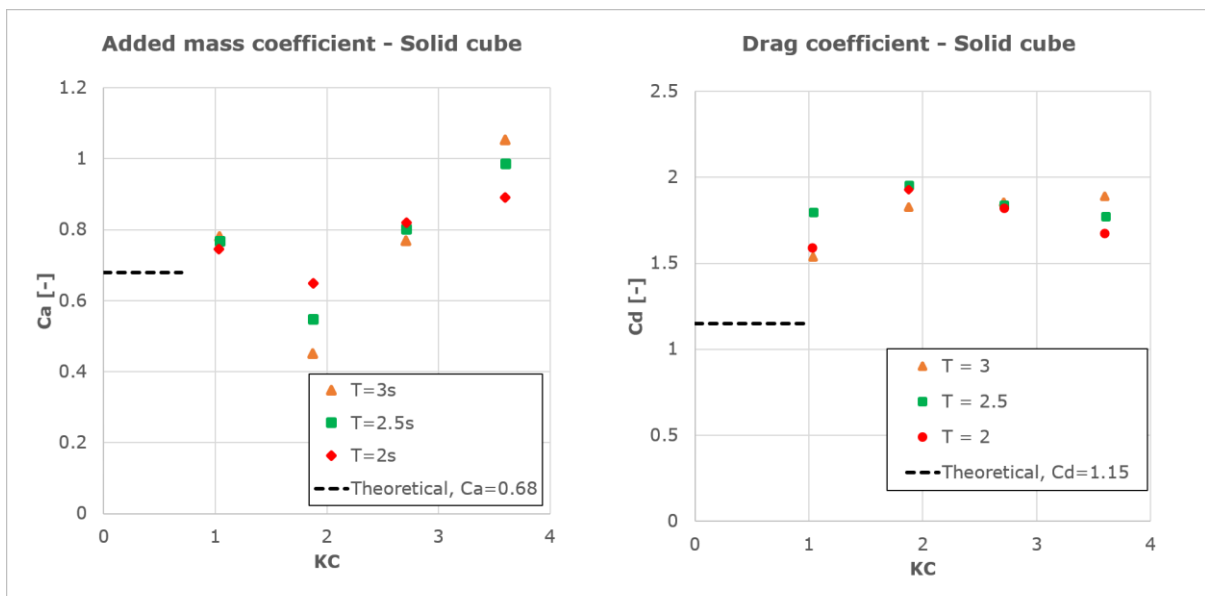
Figure 5.9 - Added mass- and drag coefficient from mudmat – oscillation experiment

The added mass and the added mass coefficient seem to be converging somewhere close to the theoretical value as the period decreases; at least for KC<3, where the added mass is dominant. While the damping and drag coefficient is a bit higher than the theoretical value. This could be due to a low KC number, which means that the damping is almost neglectable and therefore especially difficult to measure and calculate.

The approximate converging values from the results are presented in Table 5.4.

Table 5.4 - Results from forced oscillation experiment on solid cube

Added Mass	Linear Damping	Quadratic Damping	Ca	Cd
2.5 kg	0 Ns/m	24 Ns^2/m^2	0.75	1.7

5.2.3 Subsea structure experiments

The simplified subsea structure was produced in three working different scales, where all were tested with forced oscillation. Ultimately the results were scaled to full-scale for each scale, and then the results are compared. The results from the three different scaled subsea structures are presented in Figure 5.10, Figure 5.11, and Figure 5.12.

Figure 5.10 - Added mass and damping, 1:20 subsea structure - oscillation experiment

Figure 5.11 - Added mass and damping, 1:30 subsea structure - oscillation experiment
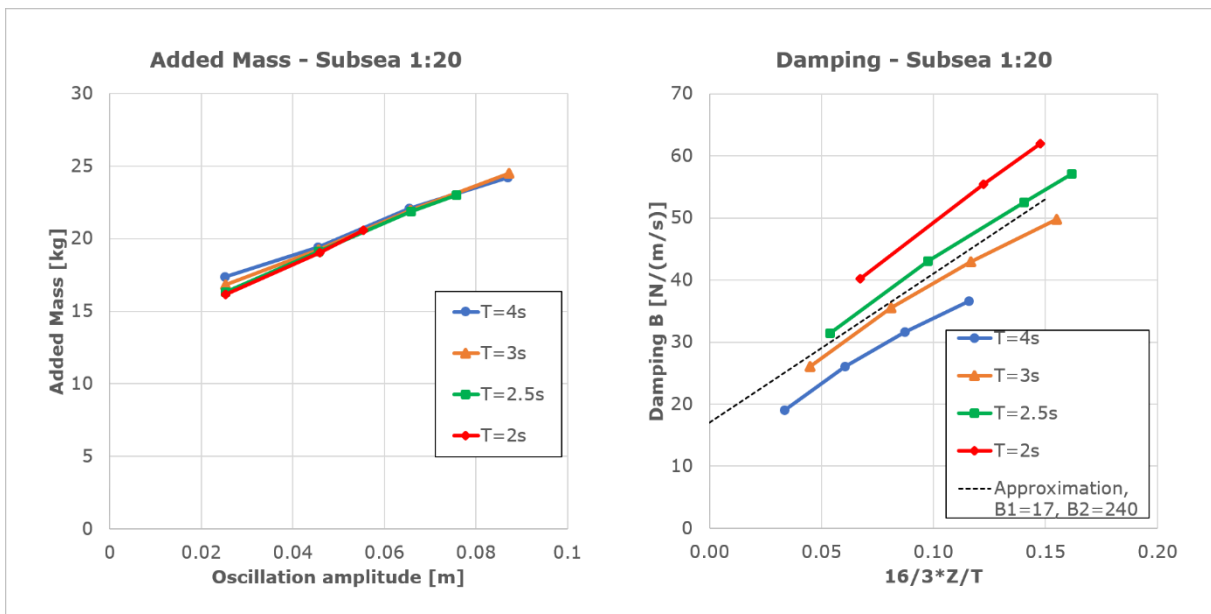
Figure 5.12 - Added mass and damping, 1:45 subsea structure - oscillation experiment

The results show that damping variate according to the period and amplitude. This is the same result found in the report of SINTEF and Solaas. While the added mass is quite consistent for the different periods, but variate according to the amplitude. These results from the different scaled subsea structures are then scaled with the Froude scaling introduced in chapter 2.2.1. By scaling the added mass and plotting it versus the porous KC number, the scale effects may be evaluated. This has been done in Figure 5.13. The plot for each scale is taken from the shortest period where four data points could be collected without chaotic movement on large amplitudes.

The added mass coefficient is also made dimensionless, in Figure 5.13, by dividing the added mass by the theoretical added mass A0.
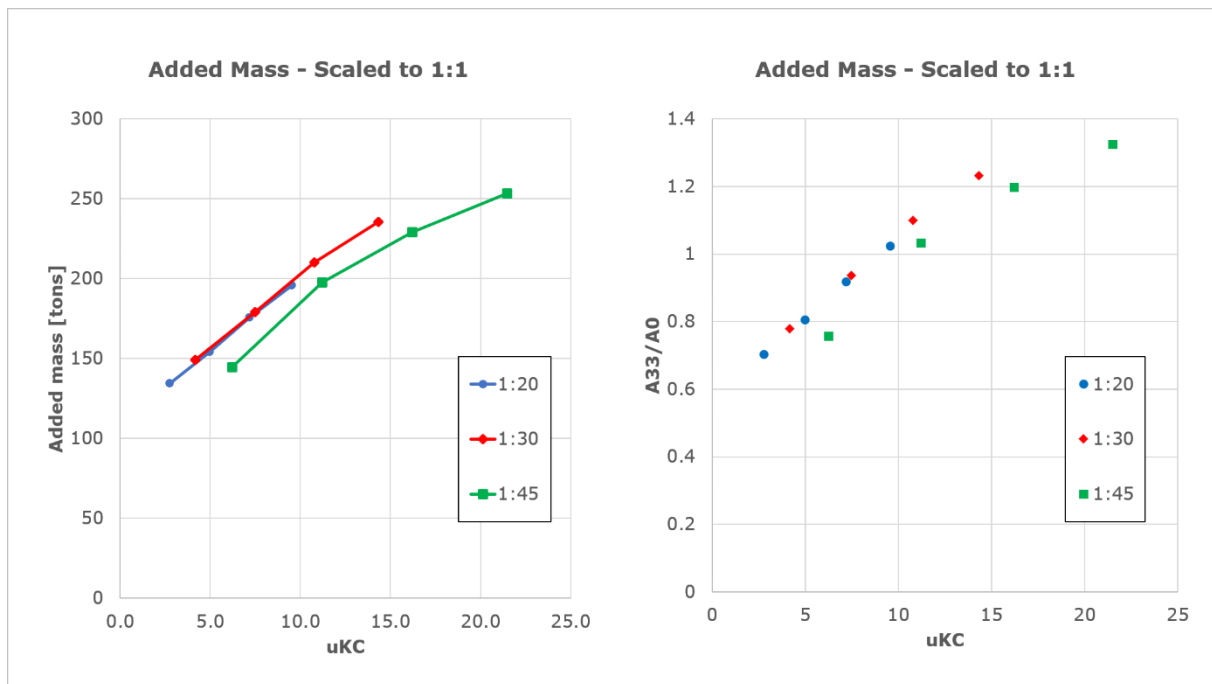
Figure 5.13 - Added mass and damping, 1:1 subsea structure – oscillation experiment

The results from the added mass scaled 1:1 shows that the added mass measured from the 1:20 and 1:30 scaled structure is much alike. While the results from the 1:45 scaled structure is a bit off. This is probably due to that the 1:45 scale is quite small, and the measured added mass is less than 0.3 N. The chance for errors increases as the force gets smaller since the vibration amplitude could get more significant than the force itself. Still, the three experiments give a quite equal added mass with the limited environment and large scaling in mind; where small differences in small scale make substantial differences when scaled up.

By scaling the damping according to Table 2.1 - Scaling factors, the scaling effects of damping could be compared for a full-scale model. The approximated measured results are presented together with the scaled results in Table 5.5. The comparison shows that the linear damping is quite alike when being scaled to full-scale, while the quadratic damping varies more. The reason for this could again be the low KC number, which makes it hard to estimate the drag since the added mass is dominant. Another reason for the variation could also be that the Froude number might not be entirely valid for perforated structures.

If the linear damping is assumed to be equal to zero, while the average quadratic damping of 850 Ns^2/m^2 is used, the drag coefficient may be calculated with equation 3.8, in equation 5.2. The same area used for the lifting experiment is also assumed here, this is the cross-section of the lower plate of the subsea structure - just scaled to full-scale.

$$Cd = \frac{2 \cdot B2}{\rho \cdot A} = \frac{2 \cdot 77.6\frac{kNs^2}{m^2}}{999\frac{kg}{m^3} \cdot 38.3 \; m^2} = 4.1 \tag{5.2}$$

By estimating the drag coefficient this way, the linear damping contribution will be missed out.

Table 5.5 - Measured and scaled damping, subsea structure - oscillation experiment

Scale	Measured Data		Scaled to 1:1	
	B1 [Ns/m] Linear Damping	B2 [Ns^2/m^2] Quadratic damping	B1 [kNs/m] Linear Damping	B2 [kNs^2/m^2] Quadratic damping
1:45	2	32	27.2	64.8
1:30	6	80	29.6	72.0
1:20	17	240	30.4	96.0

5.2.4 Suction anchor experiments

The suction anchor was produced in three different scales, as the subsea structure. Ultimately the results were scaled to full-scale for each test object, and then the results were compared. The results from the three different scaled suction anchors are presented in Figure 5.14, Figure 5.15, and Figure 5.16.
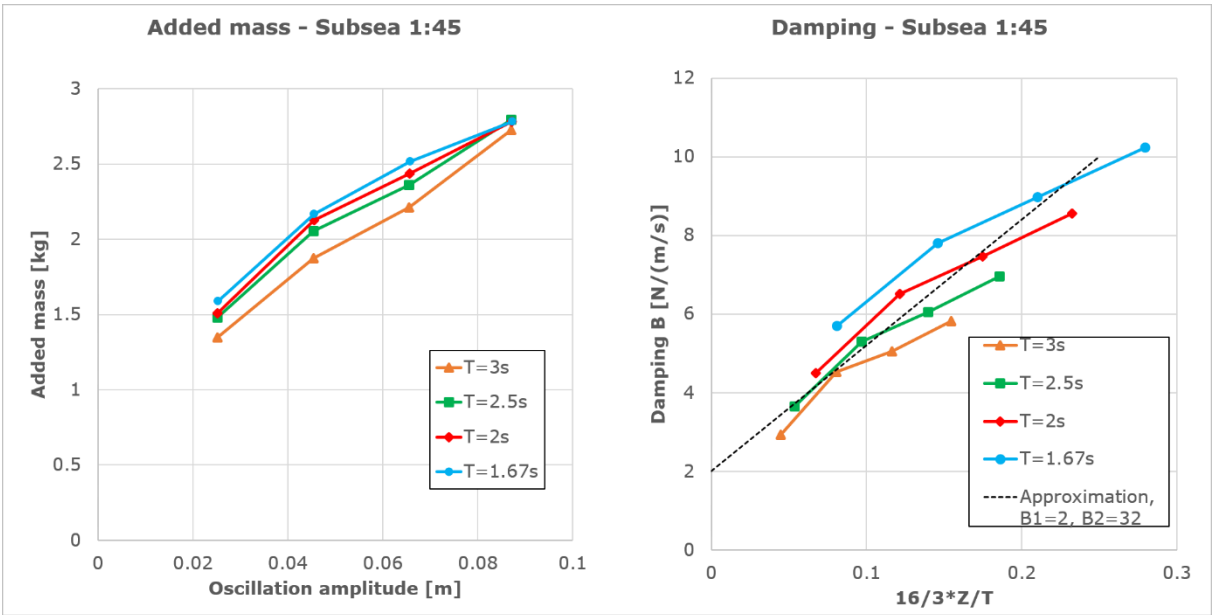

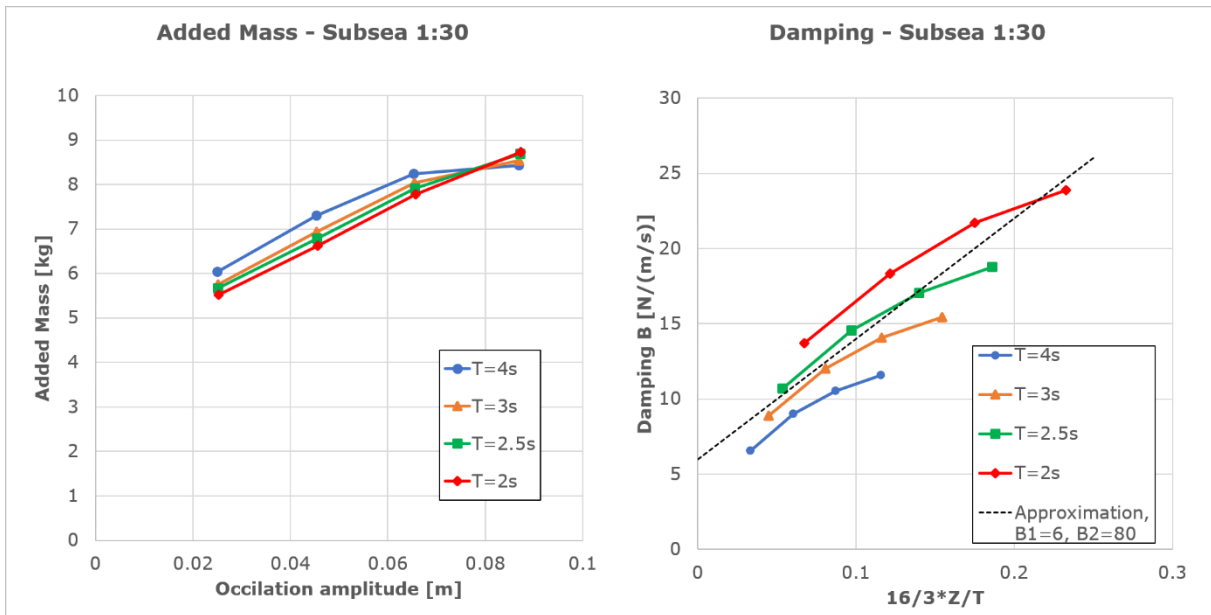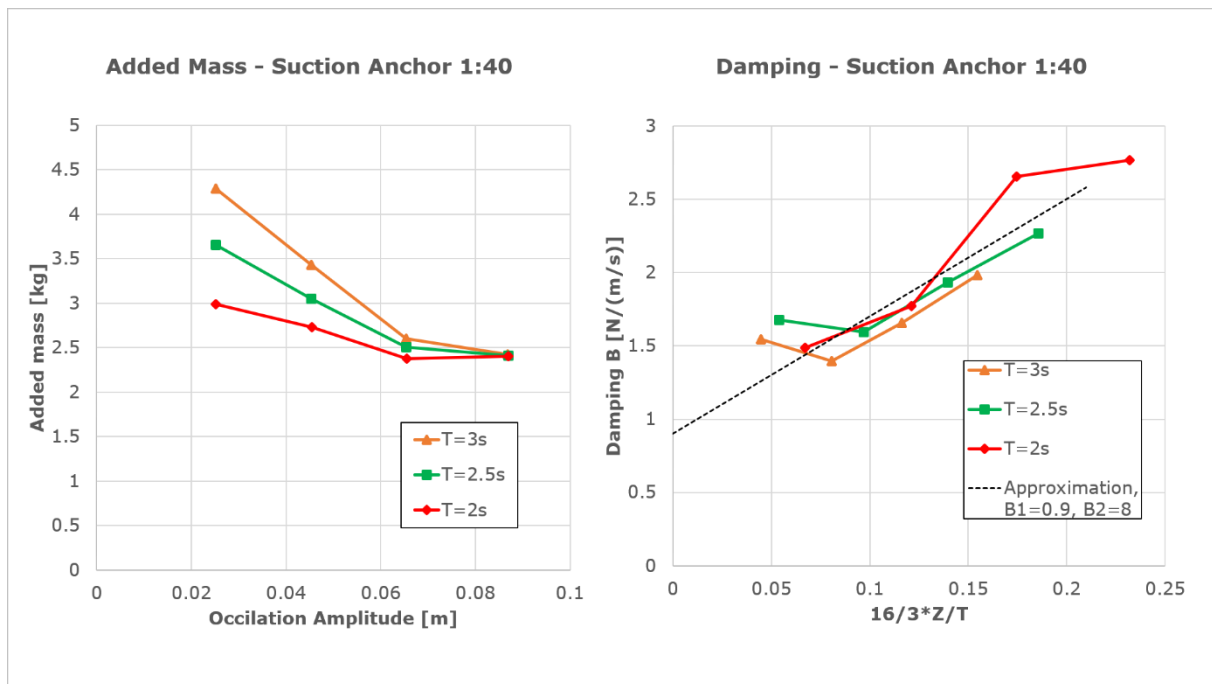**Figure 5.14 - Added mass and damping, 1:40 suction anchor – oscillation experiment**
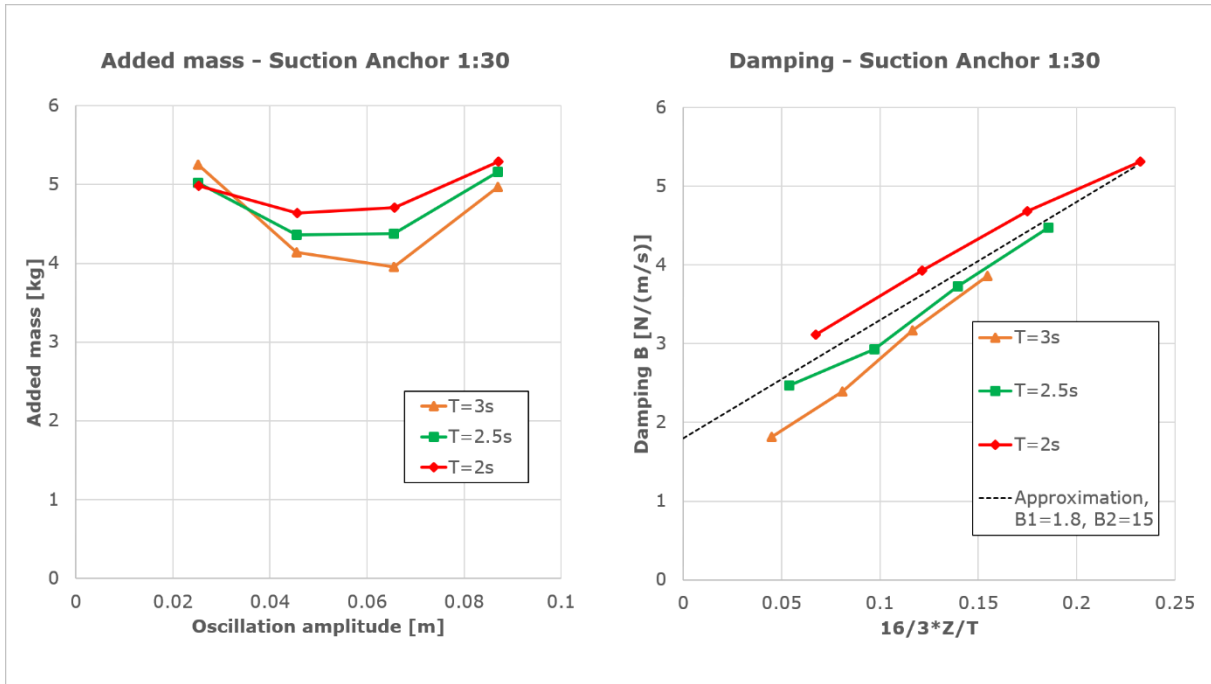
Figure 5.15 - Added mass and damping, 1:30 suction anchor – oscillation experiment
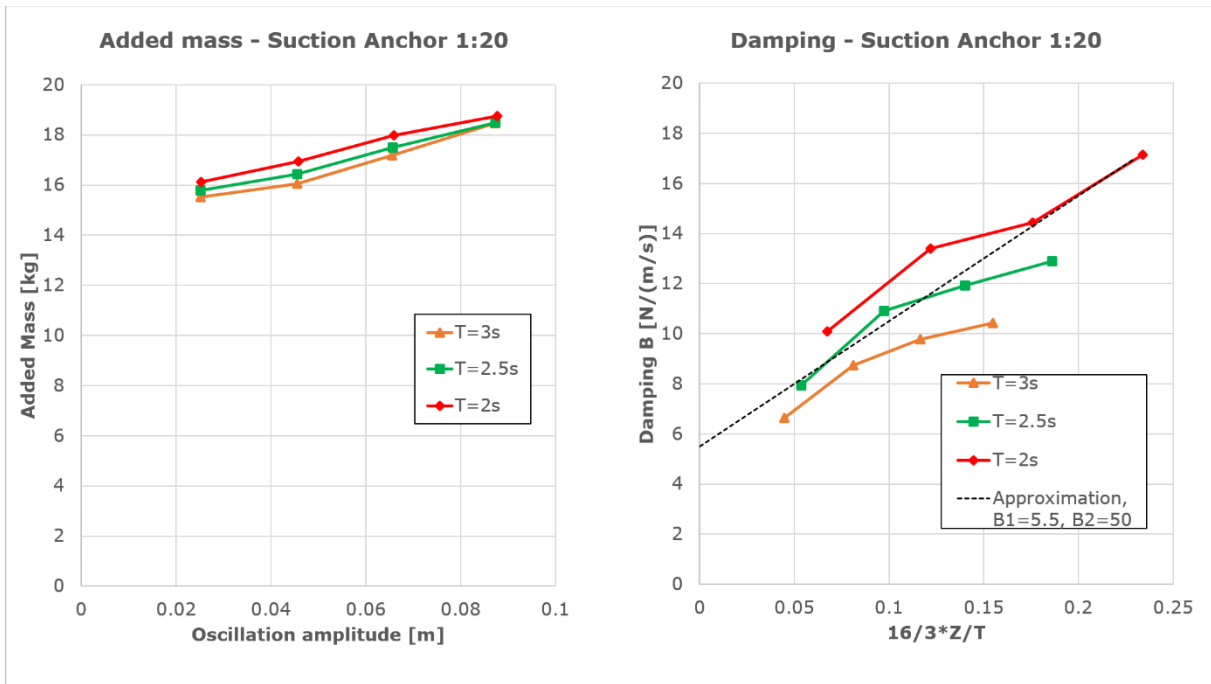
Figure 5.16 - Added mass and damping, 1:20 suction anchor – oscillation experiment

To evaluate the scale effects for the suction anchor, the added mass results from each suction anchor is scaled to full-scale values. The results may be compared by plotting the added mass versus the dimensionless ratio of heave-amplitude divided by anchor-diameter (Solaas, 2017). The result is presented in Figure 5.17.
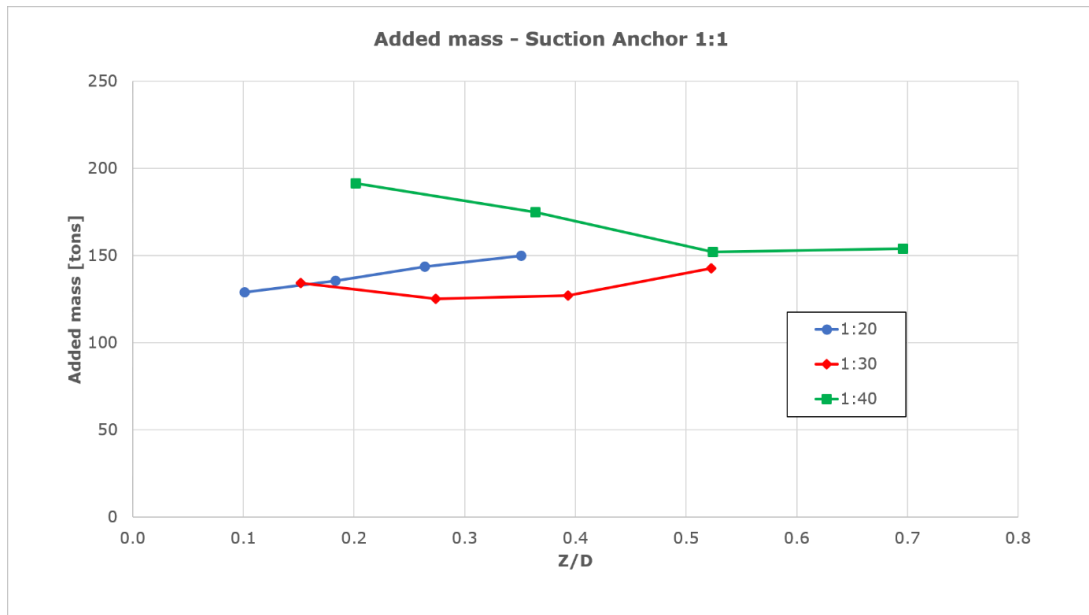
Figure 5.17 - Added mass, suction anchor scaled 1:1 – oscillation experiments

The results from the added mass scaled 1:1 shows that the added mass has some variations for the different scales. This could be due to that the added mass is quite small for the smaller scales, while the 1:20 scaled anchor shows a more consistent result. For larger amplitudes, the added mass from the three different scales seems to converge towards the same value.

The results are then compared in Figure 5.18, with experimental data from Solaas and SINTEF (Solaas, 2017). Solaas conducted experiments of a suction anchor with the same dimensions. The only difference is that her model had the hole perforation, not in the center of the anchor. It is unknown at which scale her experiments were conducted. For comparison of added mass, the experiment of the shortest period is used, since this was the ones that gave the most consistent results. The added mass for period T=2s is made dimensionless by dividing the added mass by the theoretical added mass A0.
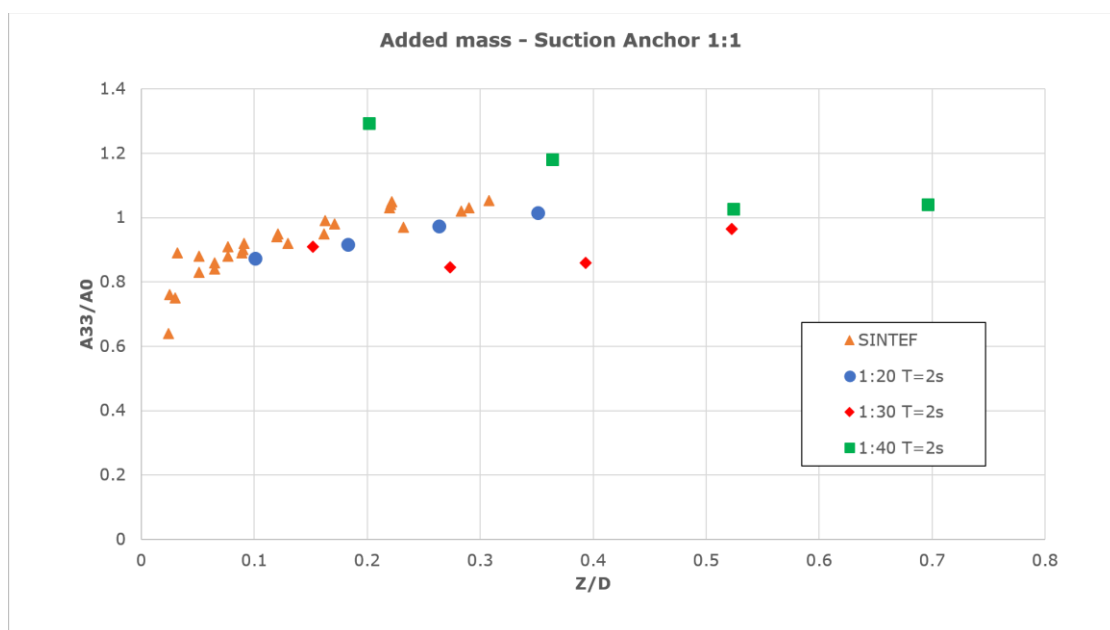
Figure 5.18 – Added mass compared with data from SINTEF

The results for the added mass are almost identical to the results from Solaas. Especially the results for the largest scale are matching quite well. For the smaller scales, there is a more substantial variation, but as the oscillation amplitude increases they seem to converge around the same value.

By scaling the damping, the scaling effects of damping could be compared for a full-scale model as well. The approximated measured results are presented together with the scaled results in Table 5.6.

Table 5.6 - Measured and scaled damping, suction anchor - oscillation experiment

Scale	Measured Data		Scaled to 1:1	
	$B1$ [Ns/m] Linear Damping	$B2$ [Ns^2/m^2] Quadratic damping	$B1$ [kNs/m] Linear Damping	$B2$ [kNs^2/m^2] Quadratic damping
1:40	0.9	8.0	9.1	12.8
1:30	1.8	15	8.9	13.5
1:20	5.5	50	9.8	20.0

The comparison shows that the linear damping is quite alike when being scaled to full-scale, while the quadratic damping varies more. The reason for this could again be the low KC number, which makes it hard to estimate the drag since the added mass is dominant.

If the linear damping is assumed to be equal to zero, while the quadratic damping is around 15.4 kNs^2/m^2, the drag coefficient is then calculated with equation 3.8, in equation 5.3.

$$Cd = \frac{2 \cdot B2}{\rho \cdot A} = \frac{2 \cdot 15.4 \frac{kNs^2}{m^2}}{999 \frac{kg}{m^3} \cdot 19.6 \, m^2} = 1.57 \tag{5.3}$$

By estimating the drag coefficient this way, the linear damping contribution will not be missed out.

The results for damping are, unlike the added mass, not similar to the results from Solaas. Results from SINTEF gave linear damping of 19 kN/(m/s) and quadratic damping of 30 kN/(m/s)^2. Again, this could be due to a low KC number where the added mass is dominant, or it could be due to that her experiments are conducted at different scales or KC numbers. However, the experiments in this thesis gave similar results between them for the linear damping for different scales.

6 Conclusion and Future Work

6.1 Conclusion

The objective of this thesis was to develop a test method for how 3D printing can be used to estimate hydrodynamical forces for subsea structures with the use of experimental methods. Lots of structures have been 3D printed, and about 500 experiments have been conducted in total. In the end, some aspects of the method have proven suitable and others not.

3D printing of complex subsea structures has proven to be close to impossible with the available equipment at NTNU Ålesund. Real-life subsea structures are quite large, which means that the structures must be scaled down quite a lot to fit a 3D printer. If the object is scaled down too much, plates that originally were 10 mm will become too thin for a 3D printer to produce. Therefore, the build volume of a printer utilized for this purpose should be at least the size of the Creality CR-10 S5 (500x500x500 mm) at NTNU Ålesund.

A subsea structure is also highly detailed and complex, which result in the need for some processing to make the structures more fitted for 3D printing. The removal of details was proven possible on the structures acquired from TechnipFMC. Still, when using the technology of fused deposition modeling the complex structures must be supported during 3D printing. The removal of PLA support structure is almost impossible, and therefore water dissolvent material or another 3D printing technology must be utilized. Since there is no other 3D printer of the needed size with either water dissolvent material or other printer technologies, no real-life subsea structures could be produced and tested. Instead, a simplified structure was made in addition to a suction anchor – which is a part of a typical subsea structure. A solution to be able to print real-life structures could be the technology of selective laser sintering (SLS); where a complex subsea structure would be fully supported by powder during production, which is easily removed after.

The forced lifting experiments gave quite accurate results for damping and drag coefficient when being validated with previous research. While the added mass was difficult to estimate due to that inertia forces for the system and object had to be subtracted analytically.

Forced oscillation experiments were conducted as a combination of two variations. Each object has been tested in both air and submerged, for each control variable. Then, the measured data series in the air is subtracted from the submerged data series, resulting in exclusively leaving the hydrodynamical forces. These experiments gave quite positive results in term of added mass, while the damping was harder to get right. However, due to limitations in relation to heave amplitude, all oscillation experiments are conducted at a low KC number. At low KC numbers, the added mass is dominant, and the damping could in many cases be neglected. This could explain why the damping is challenging to get correct.

There are several limitations with the experimental test setup, mostly connected to the size of the towing tank at NTNU Ålesund. By conducting experiments close to either the tank-bed, surface of the sidewall, the results are affected by bottom-, surface- and wall effects. The dept is a limitation in several ways, for the forced oscillation experiment both

the heave amplitude and the object size are limited. For forced lifting experiments, the acceleration and velocity are limited due to the short travel time between tank-bed and surface – which also sets a limitation for the size of the object.

The added mass for larger objects seems to be affected by the sidewall since there is less water to be accelerated as added mass while smaller objects tested with oscillating experiments gave quite positive results in term of added mass. Another challenge is that the smallest objects tested have a relatively small measured added mass; in these cases the added mass can be less than three kilograms. The vibrations and variations in friction may then become more substantial than the added mass, which easily may lead to false results.

With all the above results and discussion, the research questions will be answered. In relation to the first research question: "*How can 3D printed objects improve today's methods for estimating hydrodynamic coefficients*?", the method of using 3D printed structures in combination with experimental methods has potential as an improvement to today methods. Since hydrodynamical coefficients may be acquired with little investment and effort. However, more experiments must be conducted with other 3D printer technologies, as selective laser sintering, and the experiments must be conducted in a broader environment than the towing tank at NTNU Ålesund.

"*How to analyze and validate hydrodynamic coefficients from scaled experimental tests*?" was the second research question. The results from this research have shown that forced oscillation experiments have the potential to analyze hydrodynamic coefficients in relation to the added mass. The method could also possibly be used to estimate more accurate drag coefficients in a larger environment where experiments could be conducted at more significant KC numbers. However, the results show that complex structures are affected by both linear and quadratic damping. Since the linear damping not is included in a drag coefficient, it could be beneficial to express the drag as linear and quadratic damping instead of a drag coefficient. At the same time, this will be a more demanding method compared to typical coefficients. To validate the results, the setup must be thoroughly validated by performing experiments that may be validated with theoretical data and previous experimental studies. Another possibility could be computational fluid dynamics.

The third research question is: "*How does the scale effect influence the hydrodynamic coefficients*". Scale effect experiments were conducted on the subsea structure and the suction anchor with forced oscillation experiments. The results are then scaled with Froude scaling. The scaled added mass was quite consistent. Some deviations were found for experiments with a measured added mass less than about 5 kg, while larger values gave positive results when being scaled. In term of damping, the linear damping gave matching result when being scaled from the different scaled experiments. The quadratic damping had more considerable variations. It could be that the Froude scaling is not entirely consistent for perforated structures, but it could also be due to the overall low KC numbers.

6.2 Future work

The research in this thesis has found a potential for the method of using 3D printed subsea structures to estimate hydrodynamical characteristics. Still, there are several aspects within the field that must be further investigated before a final conclusion may be drawn for the method. To further study the potential of the method, the following recommendations for future work are given:

1. It would be interesting to conduct lifting experiments through the splash zone. This could be done with the existing setup, and the size of the tank would then not be such a limitation for these tests.

2. Experiments, where structures positioned in the splash zone at rest and affected by waves would be interesting to conduct. This may also be done with the existing setup. Here, either the force or the movement of the structure in the horizontal direction should be measured.

3. By either further developing the setup or moving it to another location, forced lifting experiments could be conducted with a counterweight. The requirement is that there is a large enough height either above the water surface or at another location to perform dry experiments. To remove the inertia and friction forces, the measured data from the dry experiment could be subtracted from the submerged data – as for the oscillation experiments. A simple method could be by draining the tank to conduct dry experiments.

4. The results from the model tests performed in this thesis may be verified with computational fluid dynamics (CFD) simulations. CFD could also be a tool to study the scale effects of different structures further.

5. A study where the acquired real-life subsea structures are 3D printed with selective laser sintering or other 3D printer technologies should be executed. Then it would be possible to estimate the hydrodynamical coefficients for a real model, where additionally full-scale data could exist.

6. It would be beneficial to perform the same sets of tests conducted in this thesis in a larger environment than the towing tank at NTNU Ålesund. This would remove the effect of bottom- wall- and surface effects. A larger basin would also allow for a setup with larger heave amplitudes for forces oscillation experiments, and longer intervals with constant acceleration and velocity for forced lifting experiments.

7. More experiments regarding scale effects should be conducted. These experiments should be with even larger structures. This would not have to be 3D printed structures, but typical perforated structures would be beneficial to the research. These experiments would also require a larger basin.

References

3D Matter, 2015. *What is the influence of infill %, layer height and infill pattern on my 3D prints?.* [Online]
Available at: http://my3dmatter.com/influence-infill-layer-height-pattern/
[Accessed 21 November 2018].

All3DP, 2018. *PLA Filament Guide – All You Need to Know.* [Online]
Available at: https://all3dp.com/1/pla-filament-3d-printing/
[Accessed 19 November 2018].

Bai, Y. & Bai, Q., 2018. *Subsea Engineering Handbook.* 2 ed. Houston: Zhejiang University.

Brockotter, R., 2018. *Key design considerations for 3D printing.* [Online]
Available at: https://www.3dhubs.com/knowledge-base/key-design-considerations-3d-printing#author
[Accessed 21 November 2018].

Chua, C. K., Leong, K. F. & Lim, C. S., 2003. *Rapid Prototyping.* 1 ed. Singapore: World Scientific.

DNV-GL, 2011. *DNV-RP-H103, Modelling and Analysis of Marine Operations,* s.l.: DNV-GL.

DNV-GL, 2014. *Introduction to Subsea Production Systems.* [Online]
Available at:
https://www.uio.no/studier/emner/matnat/math/MEK4450/h14/undervisningsmateriale/modul e-2/mek4450-dnvgl-05-templates-and-manifolds.pdf
[Accessed 22 November 2018].

FishSafe, 2018. *Subsea Templates and Manifolds.* [Online]
Available at: http://www.fishsafe.eu/en/offshore-structures/subsea-structures/subsea-templates-manifolds.aspx
[Accessed 23 November 2018].

Flynt, J., 2019. *All About SLS Printing: Advantages, Disadvantages, History, and more.* [Online]
Available at: https://3dinsider.com/sls-printing/
[Accessed 9 June 2019].

Gardan, J., 2015. *Additive manufacturing: State of the art and trends,* Troyes: Tandsonline.

Journée, J. & Massie, W., 2001. *Offshore Hydromechanics.* 5th ed. Delft: Delft University of Technology.

Keulegan, G. H. & Carpenter, L. H., 1958. Forces on Cylinders and Plates in an Oscillating Fluid. *Journal of Research of the National Bureau of Standards*, May, pp. 423-440.

Knott, E. F., 1993. *Radar Cross Section Measurements.* 1 ed. New York: Can Nostrand Reinhold.

Manning, M., 2016. *Offshore oil production in deepwater and ultra-deepwater is increasing.* [Online]
Available at: https://www.eia.gov/todayinenergy/detail.php?id=28552
[Accessed 22 November 2018].

MatterHackers, 2017. *3D Printing Filament Comparison Guide.* [Online]
Available at: https://www.matterhackers.com/3d-printer-filament-compare
[Accessed 25 Novemer 2018].

Mentzoni, F., Abrahamsen-Prsic, M. & Kristiansen, T., 2018. *HYDRODYNAMIC COEFFICIENTS OF SIMPLIFIED SUBSEA STRUCTURES,* Madrid: Conference on Ocean, Offshore and Arctic Engineering.

Morison, J., Johnson, J. & Schaaf, S., 1950. The forces exerted by surface waves on piles. *Journal of Petroleum Technology,* 2(05), p. 6.

NorskOljeMuseum, 2015. *Ormen Lange.* [Online]
Available at: https://www.norskolje.museum.no/ormen-lange/
[Accessed 23 November 2018].

Palermo, E., 2013. *What is Selective Laser Sintering?.* [Online]
Available at: https://www.livescience.com/38862-selective-laser-sintering.html
[Accessed 14 February 2018].

Reynolds, O., 1883. *An experimental Investigation of the Circumstances Which Determine Whether the Motion of Water Shall be Direct or Sinuous, and the Law of Resistance in Parallel Channels.* 1 ed. London: Philosophical Transaction of the Royal Society of London.

Siemens, 2018. *NX for Design streamlines and accelerates the product development process.* [Online]
Available at: https://www.plm.automation.siemens.com/global/en/products/nx/nx-for-design.html
[Accessed 21 November 2018].

Solaas, F., 2017. *MT2016 F-156 SFI MOVE RA2 Hydrodynamic coefficients for subsea,* Trondheim: Sintef Ocean AS.

Solheim, A., 1989. *The tommeliten subsea project,* Abredeen: Society of Petroleum Engineers.

Stampfl, J. & Hatzenbichler, M., 2014. *Additive manufacturing technologies: state of the art and trends.* [Online]
Available at: https://www.tandfonline.com/doi/pdf/10.1080/00207543.2015.1115909
[Accessed 10 Oktober 2018].

Statista, 2018. *Worldwide most used 3D printing technologies, as of July 2018*.* [Online]
Available at: https://www.statista.com/statistics/756690/worldwide-most-used-3d-printing-

technologies/
[Accessed 10 October 2018].

Stats Directe, 2019. *LOESS Curve Fitting (Local Polynomial Regression).* [Online]
Available at: https://www.statsdirect.com/help/nonparametric_methods/loess.htm
[Accessed 16 May 2019].

Tippee, J., 2016. *Shell takes ultra-deepwater to record depths with Stones.* [Online]
Available at: https://www.offshore-mag.com/articles/print/volume-76/issue-12/top-5-
projects/shell-takes-ultra-deepwater-to-record-depths-with-stones.html
[Accessed 22 November 2018].

Underwater Technology Foundation, 2018. *Subsea History.* [Online]
Available at: https://www.utc.no/utf/om_subsea/subsea_history/
[Accessed 19 November 2018].

Yu, Q., 2018. *Estimate Dynamic Facotrs for Subsea Lifting Operation by Using Experimental
Method - Rapd Prototyping,* Ålesund: NTNU.

Appendices

Appendix 1: Experimental Results

Appendix 2: MATLAB script

Appendix 3: 2D production drawings

Appendix 1: Experimental results

Table 1 - Experimental results from forced lifting experiments on mudmat

Velocity [m/s]	Acceleration [m/s²]	A33 [kg]	B [Ns/m]	Ca [-]	Cd [-]	Re [-]
0.044	0.021	64.6	17.9	0.33	2.7	6 663
0.074	0.021	76.4	36.5	0.39	3.3	11 106
0.074	0.041	70.5	36.5	0.36	3.3	11 106
0.096	0.041	76.4	47.4	0.39	3.3	14 437
0.096	0.021	74.4	47.4	0.38	3.3	14 437
0.118	0.021	70.5	60.2	0.36	3.4	17 769
0.118	0.082	66.6	60.2	0.34	3.4	17 769

Table 2 - Experimental results from forced lifting experiments on subsea structure

Velocity [m/s]	Acceleration [m/s²]	A33 [kg]	B [Ns/m]	A33/A0 [-]	Cd [-]	Re [-]
0.074	0.021	26.5	5.0	1.11	1.56	11 106
0.074	0.041	26.6	5.0	1.11	1.56	11 106
0.096	0.041	27.5	6.7	1.15	1.56	14 437
0.096	0.082	26.4	6.7	1.10	1.56	14 437
0.118	0.021	27.2	9.3	1.14	1.56	17 769
0.118	0.041	28.7	9.3	1.20	1.56	17 769
0.118	0.082	27.5	9.3	1.15	1.56	17 769

Table 3 - Experimental results from forced oscillation experiments on mudmat

Period [s]	Amplitude [m]	A33 [kg]	B [Ns/m]	Ca [-]	Cd [-]	μKC [-]	16/3*Z/T [m/s]
4	0.025	41.9	60.2	0.21	10.25	0.13	0.03
4	0.035	43.0	72.1	0.22	8.73	0.18	0.05
4	0.045	45.8	81.9	0.23	7.71	0.23	0.06
4	0.055	50.1	93.9	0.26	7.21	0.28	0.07
4	0.065	54.0	105.6	0.28	6.92	0.33	0.09
4	0.075	58.9	119.0	0.30	6.73	0.38	0.10
4	0.086	62.2	134.3	0.32	6.65	0.44	0.11
3	0.025	43.0	82.1	0.22	10.45	0.13	0.04
3	0.035	44.6	97.5	0.23	8.83	0.18	0.06
3	0.045	47.1	112.6	0.24	7.93	0.23	0.08
3	0.055	51.7	128.2	0.26	7.37	0.28	0.10
3	0.065	55.1	143.4	0.28	7.02	0.33	0.12
3	0.075	57.0	163.2	0.29	6.92	0.38	0.13
2.5	0.025	43.5	99.3	0.22	10.53	0.13	0.05
2.5	0.035	45.0	118.2	0.23	8.91	0.18	0.07
2.5	0.045	47.4	137.0	0.24	8.02	0.23	0.10
2.5	0.055	51.2	155.9	0.26	7.43	0.28	0.12
2.5	0.065	53.8	175.6	0.27	7.13	0.33	0.14

Table 4 - Experimental results from forced oscillation experiments on solid cube

Period [s]	Amplitude [m]	A33 [kg]	B [Ns/m]	Ca [-]	Cd [-]	KC [-]	16/3*Z/T [m/s]
3	0.025	2.63	0.90	0.78	1.54	1.04	0.04
3	0.045	1.52	1.92	0.45	1.83	1.87	0.08
3	0.065	2.59	2.83	0.77	1.86	2.71	0.11
3	0.086	3.55	3.82	1.05	1.89	3.60	0.15
2.5	0.025	2.59	1.26	0.77	1.80	1.04	0.05
2.5	0.045	1.85	2.47	0.55	1.95	1.88	0.10
2.5	0.065	2.70	3.37	0.80	1.84	2.72	0.14
2.5	0.086	3.32	4.31	0.99	1.77	3.61	0.18
2	0.025	2.51	1.39	0.75	1.59	1.03	0.07
2	0.045	2.19	3.05	0.65	1.93	1.88	0.12
2	0.065	2.76	4.17	0.82	1.82	2.72	0.17
2	0.086	3.00	5.08	0.89	1.67	3.60	0.23

Table 5 - Experimental results from forced oscillation experiments on subsea structure scaled 1:45

Period [s]	Amplitude [m]	A33 [kg]	B [Ns/m]	μKC [-]	16/3*Z/T [m/s]
3	0.025	1.35	2.93	6.20	0.04
3	0.045	1.87	4.53	11.17	0.08
3	0.066	2.21	5.04	16.12	0.12
3	0.087	2.73	5.82	21.41	0.15
2.5	0.025	1.48	3.66	6.20	0.05
2.5	0.045	2.06	5.30	11.17	0.10
2.5	0.066	2.36	6.05	16.12	0.14
2.5	0.087	2.80	6.96	21.41	0.19
2	0.025	1.51	4.49	6.20	0.07
2	0.046	2.13	6.52	11.20	0.12
2	0.066	2.44	7.47	16.14	0.17
2	0.087	2.78	8.56	21.43	0.23
1.6667	0.025	1.59	5.69	6.23	0.08
1.6667	0.046	2.17	7.81	11.22	0.15
1.6667	0.066	2.51	8.98	16.19	0.21
1.6667	0.087	2.78	10.23	21.48	0.28

Table 6 - Experimental results from forced oscillation experiments on subsea structure scaled 1:30

Period [s]	Amplitude [m]	A33 [kg]	B [Ns/m]	μKC [-]	16/3*Z/T [m/s]
4	0.025	6.0	6.6	4.1	0.03
4	0.045	7.3	9.0	7.4	0.06
4	0.065	8.2	10.6	10.7	0.09
4	0.087	8.4	11.6	14.3	0.12
3	0.025	5.8	8.9	4.1	0.04
3	0.045	6.9	12.0	7.4	0.08
3	0.066	8.0	14.1	10.7	0.12
3	0.087	8.5	15.5	14.3	0.15
2.5	0.025	5.7	10.7	4.1	0.05
2.5	0.046	6.8	14.6	7.5	0.10
2.5	0.066	7.9	17.0	10.8	0.14
2.5	0.087	8.7	18.8	14.3	0.19
2	0.025	5.5	13.7	4.2	0.07
2	0.046	6.6	18.3	7.5	0.12
2	0.066	7.8	21.7	10.8	0.18
2	0.087	8.7	23.9	14.3	0.23

Table 7 - Experimental results from forced oscillation experiments on subsea structure scaled 1:20

Period [s]	Amplitude [m]	A33 [kg]	B [Ns/m]	μKC [-]	16/3*Z/T [m/s]
4	0.025	17.4	19.0	2.8	0.03
4	0.046	19.4	26.1	5.0	0.06
4	0.066	22.1	31.6	7.2	0.09
4	0.087	24.2	36.6	9.5	0.12
3	0.025	16.8	26.0	2.8	0.04
3	0.046	19.3	35.5	5.0	0.08
3	0.066	22.0	42.9	7.2	0.12
3	0.087	24.5	49.8	9.5	0.16
2.5	0.025	16.3	31.5	2.8	0.05
2.5	0.046	19.1	43.1	5.0	0.10
2.5	0.066	21.9	52.5	7.2	0.14
2.5	0.076	23.0	57.0	8.3	0.16
2	0.025	16.1	40.2	2.8	0.07
2	0.046	19.0	55.4	5.0	0.12
2	0.055	20.6	61.9	6.1	0.15

C

Table 8 - Experimental results from forced oscillation experiments on suction anchor scaled 1:40

Period [s]	Amplitude [m]	A33 [kg]	B [Ns/m]	16/3*Z/T [m/s]
3	0.025	4.29	1.54	0.04
3	0.045	3.43	1.39	0.08
3	0.065	2.60	1.66	0.12
3	0.087	2.42	1.98	0.15
2.5	0.025	3.66	1.68	0.05
2.5	0.045	3.05	1.59	0.10
2.5	0.065	2.50	1.93	0.14
2.5	0.087	2.41	2.27	0.19
2	0.025	2.99	1.49	0.07
2	0.046	2.73	1.77	0.12
2	0.066	2.38	2.65	0.17
2	0.087	2.41	2.77	0.23

Table 9 - Experimental results from forced oscillation experiments on suction anchor scaled 1:30

Period [s]	Amplitude [m]	A33 [kg]	B [Ns/m]	16/3*Z/T [m/s]
3	0.025	5.25	1.81	0.04
3	0.046	4.14	2.39	0.08
3	0.066	3.95	3.17	0.12
3	0.087	4.97	3.86	0.15
2.5	0.025	5.03	2.47	0.05
2.5	0.046	4.36	2.93	0.10
2.5	0.066	4.38	3.73	0.14
2.5	0.087	5.16	4.47	0.19
2	0.025	4.98	3.12	0.07
2	0.046	4.64	3.92	0.12
2	0.066	4.71	4.68	0.18
2	0.087	5.29	5.31	0.23

d

Table 10 - Experimental results from forced oscillation experiments on suction anchor scaled 1:20

Period [s]	Amplitude [m]	A33 [kg]	B [Ns/m]	16/3*Z/T [m/s]
3	0.025	15.5	6.6	0.04
3	0.046	16.0	8.7	0.08
3	0.066	17.2	9.8	0.12
3	0.087	18.5	10.4	0.16
2.5	0.025	15.8	7.9	0.05
2.5	0.046	16.4	10.9	0.10
2.5	0.066	17.5	11.9	0.14
2.5	0.087	18.5	12.9	0.19
2	0.025	16.1	10.1	0.07
2	0.046	16.9	13.4	0.12
2	0.066	18.0	14.4	0.18
2	0.088	18.8	17.1	0.23

Appendix 2: MATLAB script

Forced lifting experiments

```
close all
clear
clc

filename = '1600RPM_556PMS_Subsea75pros.xlsx';
RPM = 1600;
RPMS = 556;

%Test Object Dimensions
% mudmat
% a = 0.83;
% b = 0.51;
% Vol = pi/4*a^2*b*0.71;
% Area = 0.299;
% L_car = (a+b)/2;

%Subsea 1:20
Vol = 0.0127;
Area = 0.096;
L_car = 0.15;

drum_diameter = 69.5*10^-3;
wire_diameter = 1.2*10^-3;
effective_radius = drum_diameter/2 + wire_diameter/2;
rho = 999;
visc = 1*10^-6;

Max_Velocity = RPM/60*2*pi*effective_radius/50;
Max_acceleration = RPMS/60*2*pi*effective_radius/50;
Re = Max_Velocity*L_car/visc;

%data import
data = xlsread(filename,1);
Time = data (:,1);
Tension = data(:,2);
Position = (data(:,4)/1000);

mass = 2.995;

%smoothing parameter
dt=Time(2)-Time(1);
span = 10*dt;    %smooth position and force 5
span2 = 7*dt;   %smooth acceleration 5
span3 = 10*dt; %smooth real force 15
span4 = 15*dt; %smooth Ca plot 15
span_accstart = 0.05; %0.05

%Velocity without smoothing
Velocity=diff(Position)/dt;
```

rloess smothing

```
force_smooth_loess = smooth(Time, Tension,span,'rloess');

Position_smooth_loess = smooth(Time, Position,span, 'rloess');
Velocity_smooth = diff(Position_smooth_loess)/dt;
Acceleration_smooth = diff(Velocity_smooth)/dt;
Acceleration_smooth_loess = smooth(Time(1:(length(Acceleration_smooth))), Acceleration_smooth, span2,'rloess');
Real_Force = force_smooth_loess - ([0;0;Acceleration_smooth_loess]*mass);
Real_Force_smooth = smooth(Time,Real_Force, span3, 'rloess');
```

f

Calculations

```
FCd = 1.1; %Manually tuned force to fit the linear area of the force plot with a=0

Cd = 2*FCd/(rho*Area*Max_Velocity^2);

% Find start stop acc
% find rise and fall time

data = Acceleration_smooth_loess;
max_data = 0.0206;
TimeAcc = Time(2:(end-1));

data = data-max_data*0.5;

data_smooth = smooth(TimeAcc, data,span_accstart,'rloess');

data_smooth = data_smooth./max_data;
data = data./max_data;

data_sign = round(0.5*(sign(data_smooth)+1));

ind = find(diff(data_sign)~=0);
nInd = size(ind,1);
null = zeros(nInd,1);

StartStop = TimeAcc(ind);

figure(3)
plot(TimeAcc,data)
hold on
plot(TimeAcc,data_smooth,'r','linewidth',2)
plot(TimeAcc,data_sign,'k','linewidth',2)
plot(TimeAcc(ind),null,'sk')

% Ca

i=0;
TimeStart = 0.0033;
TimeEnd = Time(length(Time));


for CaTime = (TimeStart):0.0033:(TimeEnd-0.5)

    i=i+1;
    checktime = round(CaTime/0.0033);
    logtime (i) = checktime;
    Ca_velocity = Velocity_smooth(checktime);
    Ca_Calc_Force = force_smooth_loess - (Max_acceleration*mass);
    FCa_int = Ca_Calc_Force(checktime) - 0.5*rho*Area*Cd*Ca_velocity^2;
    CaVector(i) = FCa_int/(rho*Vol*Max_acceleration);

end

PlotStart = round((StartStop(1)+0.75)/dt);
PlotStop  = round((StartStop(2)-0.5)/dt);

Ca_smooth = smooth(Time(1:length(CaVector)),CaVector,span4, 'rloess');
Ca_mean = mean(Ca_smooth(PlotStart:PlotStop));
Ca_max=max(Ca_smooth);
figure(1)
subplot(2,2,4)
plot(Time(PlotStart:PlotStop),Ca_smooth(PlotStart:PlotStop))
hold on
line([Time(PlotStart),Time(PlotStop)],[Ca_mean,Ca_mean])
title('Added Mass Coefficient')
```

g

```matlab
% Ploting
figure(1)

subplot(2,2,1)
%plot(Time,Position, '+r')
hold on
plot(Time,Position_smooth_loess, 'r', 'linewidth',2)
title('Position')

subplot(2,2,2)
%plot(Time(1:(length(Time)-1)),Velocity,'r+')
hold on
plot(Time(1:(length(Time)-1)),Velocity_smooth,'r', 'linewidth',2)
line([0,Time(length(Time))],[Max_Velocity,Max_Velocity])
%line([Time(Count),Time(Count)],[0,Max_Velocity])
line([Time(PlotStart),Time(PlotStart)],[0,Max_Velocity*1.2])
line([Time(PlotStop),Time(PlotStop)],[0,Max_Velocity*1.2])
title('Velocity')

subplot(2,2,3)
%plot(Acceleration_smooth,'+r')
hold on
plot(Time(1:(length(Time)-2)),Acceleration_smooth_loess,'r','linewidth', 1)
line([0,Time(length(Time))],[Max_acceleration,Max_acceleration])
line([Time(PlotStart),Time(PlotStart)],[-Max_acceleration,Max_acceleration*1.5])
line([Time(PlotStop),Time(PlotStop)],[-Max_acceleration,Max_acceleration*1.5])
%line([Time(Count),Time(Count)],[-Max_acceleration,(Max_acceleration*1.5)])
title('Acceleration')

figure(2)
%plot(Time, Tension,'+r')
hold on
plot(Time, force_smooth_loess,'r','linewidth',2)
plot(Time,Real_Force)
plot(Time,Real_Force_smooth,'b', 'linewidth',2)
line([0,Time(length(Time))],[FCd,FCd])
%line([Time(Count),Time(Count)],[0,max(force_smooth_loess)])
title('Force')

%row_header = {'Time', 'Position_smooth_loess', 'Velocity_smooth', 'Acceleration_smooth_loess','Tension_smooth_loes
%data = [Time'; Position_smooth_loess'; [0;Velocity_smooth]'; [0;0;Acceleration_smooth_loess]'; force_smooth_loess'
%output = [row_header data];
%xlswrite('smoothed_data',output,'Sheet1');
```

h

Forced oscillation experiment

```matlab
function Oscillation %Forced Oscillation Experiment
close all;
clear all;
clc

RPM = 750;
switch_pos_sub = 1; %0 or 1
switch_pos_dry = 0;

if 1
    fn1 = '750RPM_subsea33pros_dry_25mm.xlsx';
    fn2 = '750RPM_subsea33pros_sub_25mm.xlsx';

    data_dry = xlsread(fn1,1);

    time_dry = data_dry(:,1);
    tension_dry = data_dry(:,2);
    pos_dry = data_dry(:,4)/1000;
    save('measurement_dry','time_dry','pos_dry','tension_dry');

    data_sub = xlsread(fn2,1);

    time_sub = data_sub(:,1);
    tension_sub = data_sub(:,2);
    pos_sub = data_sub(:,4)/1000;
    save('measurement_sub','time_sub','pos_sub','tension_sub');
end

rho = 999;
omega0 = RPM/50/60*2*pi;
T = 2*pi/omega0


load('measurement_dry');
load('measurement_sub');



%Position dry
nData = size(time_dry);
ind_skip = 2000;

time_dry = time_dry(ind_skip:end);
pos_dry = pos_dry(ind_skip:end);

time_dry = time_dry - time_dry(1);

beta0 = [87e-3; omega0; 0; 0];
[pos_fitted_dry,beta_pos_dry] = my_fitting_method_position(time_dry,pos_dry,beta0);


beta_pos_dry;
yoff_dry = beta_pos_dry(4);
period_dry = 2*pi/beta_pos_dry(2);

pos_new_dry = pos_fitted_dry - yoff_dry;

if switch_pos_dry == true
    b_d=1.5;
else
    b_d=1;
end

time_trim_dry = -beta_pos_dry(3)/beta_pos_dry(2)+period_dry*b_d;
time_new_dry = time_dry-time_trim_dry;

%Tension dry
tension_dry = tension_dry(ind_skip:end);

beta1 =[4;4;omega0;0];
[tension_fitted_dry,beta_tension_dry] = my_fitting_method_force(time_new_dry,tension_dry,beta1);
beta_tension_dry;

tension_yoff_dry = beta_tension_dry(4);
tension_new_dry = tension_fitted_dry - tension_yoff_dry;
```

```matlab
%Position submerged
time_sub = time_sub(ind_skip:end);
pos_sub = pos_sub(ind_skip:end);

time_sub = time_sub - time_sub(1);

beta2 = [87e-3; omega0; 1; 0];
[pos_fitted_sub,beta_pos_sub] = my_fitting_method_position(time_sub,pos_sub,beta2);


beta_pos_sub;
yoff_sub = beta_pos_sub(4);
period_sub = 2*pi/beta_pos_sub(2);

pos_new_sub = pos_fitted_sub - yoff_sub;

if switch_pos_sub == true
    b_s=1.5;
else
    b_s=1;
end

time_trim_sub = -beta_pos_sub(3)/beta_pos_sub(2)+period_sub*b_s;
time_new_sub = time_sub-time_trim_sub;

%Tension submerged
tension_sub = tension_sub(ind_skip:end);

beta3 =[4;4;omega0;0];
[tension_fitted_sub,beta_tension_sub] = my_fitting_method_force(time_new_sub,tension_sub,beta3);
beta_tension_sub;

tension_yoff_sub = beta_tension_sub(4);
tension_new_sub = tension_fitted_sub - tension_yoff_sub;


vel = diff(pos_fitted_sub)/(time_new_sub(2)-time_new_sub(1));
acc = diff(vel)/(time_new_sub(2)-time_new_sub(1));

max_acc=max(acc)
max_vel=max(vel)
amp = (abs(beta_pos_sub(1))+abs(beta_pos_dry(1)))/2;

% %Object dimensions mudmat
% a = 0.83; %mudmat width
% b = 0.51; %mudmat length
% A = 0.299; %effective area
% D = a; %characteristic dimension
% p = 0.29; %perforation
% vol = pi/4*a^2*b*(1-p)

%Object dimensions subsea
height = 0.0666667;
% width = 0.15;
D=height;
% A = 0.15^2;
% vol=0.15^3;
p=0.16;

%Relative Coefficients

force_added_mass  = beta_tension_sub(1) - beta_tension_dry(1);
force_damping     = beta_tension_sub(2) - beta_tension_dry(2)

beta_tension_sub(1)
beta_tension_dry(1)
beta_tension_sub(2)
beta_tension_dry(2)

% Ca = abs(force_added_mass)/(rho*max_acc*vol) %mudmat
% Cd = 2*abs(force_damping)/(rho*A*max_vel^2)  %mudmat

%Ca = abs(force_added_mass)/(rho*max_acc*pi/4*0.05^2*0.5) %cylinder
%Cd = 2*abs(force_damping)/(rho*0.05*0.5*max_vel^2)
```

j

```matlab
A33 = abs(force_added_mass)/max_acc;
uKC = amp/D*(1-p)/(2*p^2)
% KC = max_vel*T/D;
B   = force_damping/max_vel
eov = 16/3*amp/T %equivalent oscillation velocity

% data = [T; amp; Ca; Cd; A33; uKC; B; eov] %mudmat
data = [T; amp; A33; uKC; B; eov;]            %subsea template
% data = [T; amp; KC; A33; B; eov;]           %suction anchor
% data = [T; amp; Ca; Cd; A33; KC; B; eov;] %solid cube

%Plot Dry
figure (1)
subplot(211)
hold on
plot(time_dry,pos_dry)
plot(time_dry,pos_fitted_dry)
plot(time_new_dry,pos_new_dry,'r','linewidth',2)
grid on
xlim([0 15])
title('Position [mm] Dry')

subplot(212)
hold on
plot(time_dry,tension_dry)
plot(time_dry,tension_fitted_dry)
plot(time_new_dry,tension_new_dry,'r','linewidth',2)
grid on
xlim([0 15])
%ylim([-10 10])
title('Tension [N] Dry')


%Plot Submerged
figure (2)
subplot(211)
hold on
plot(time_sub,pos_sub)
plot(time_sub,pos_fitted_sub)
plot(time_new_sub,pos_new_sub,'r','linewidth',2)
grid on
xlim([0 15])
title('Position [m] Submerged')

subplot(212)
hold on
plot(time_sub,tension_sub)
plot(time_sub,tension_fitted_sub)
plot(time_new_sub,tension_new_sub,'r','linewidth',2)
grid on
xlim([0 15])
%ylim([-10 10])
title('Tension [N] Submerged')

% Merged Tension Plot
figure (3)
%subplot(211)
hold on
plot(time_new_dry,tension_new_dry,'b','linewidth',2)
plot(time_new_sub,tension_new_sub,'r','linewidth',2)
yyaxis right
plot(time_new_sub(1:end-1),vel)
plot(time_new_sub(1:end-2),acc)
grid on
xlim([0 15])
%ylim([-10 10])
title('Tension [N]')
legend ('Dry','Submerged','vel','acc')

figure(4)
%subplot(212)
hold on
plot(time_new_dry,pos_new_dry,'b','linewidth',1)
plot(time_new_sub,pos_new_sub,'r','linewidth',1)
grid on
xlim([0 15])
title('Position [m]')
legend ('Dry','Submerged')
end
```

k

```matlab
function [pos_fitted,beta_fitted] = my_fitting_method_position(time_input,pos_input,beta0)

    fun = @(beta,t) beta(1).*sin(beta(2).*t + beta(3))+beta(4);

    beta_fitted = nlinfit(time_input,pos_input,fun,beta0);

    pos_fitted = fun(beta_fitted,time_input);

end

function [force_fitted,beta_force] = my_fitting_method_force(time_input,force_input,beta1)

    fun = @(beta,t) beta(1).*sin(beta(3).*t) + beta(2).*cos(beta(3).*t)+beta(4);

    beta_force = nlinfit(time_input,force_input,fun,beta1);

    force_fitted = fun(beta_force,time_input);

end
```
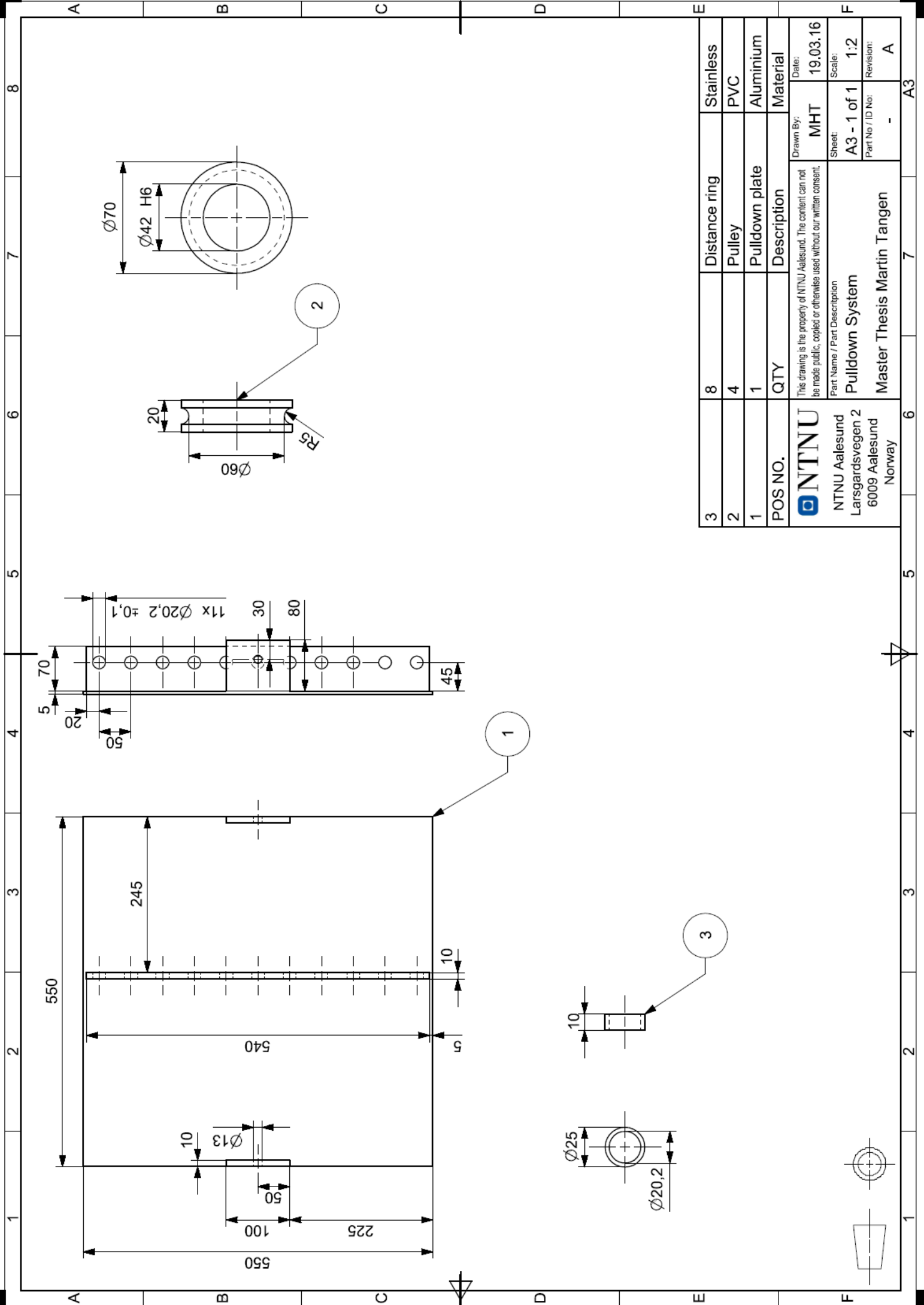
Appendix 3: 2D production drawings

Technical drawing — Pulldown System

Dimensions and annotations visible:

- Ø70
- Ø42 H6
- 20
- R5
- Ø60
- 2
- 11x Ø20,2 ±0,1
- 30
- 80
- 70
- 5
- 20
- 50
- 45
- 1
- 245
- 550
- 540
- 10
- 5
- 10
- 3
- Ø25
- Ø20,2
- 10
- Ø13
- 50
- 100
- 225
- 550

POS NO.	QTY	Description	Material
3	8	Distance ring	Stainless
2	4	Pulley	PVC
1	1	Pulldown plate	Aluminium

This drawing is the property of NTNU Aalesund. The content can not be made public, copied or otherwise used without our written consent.

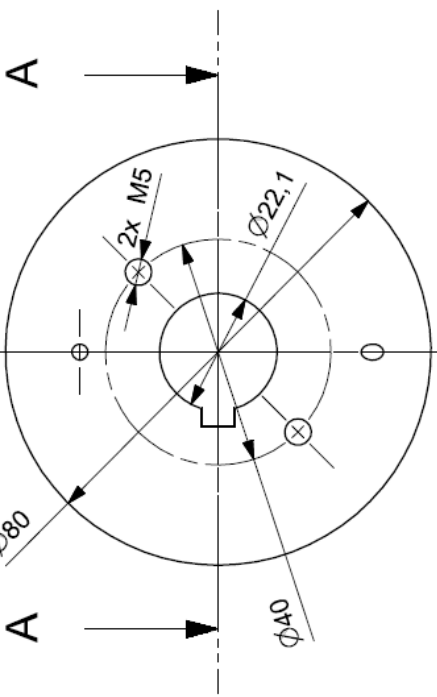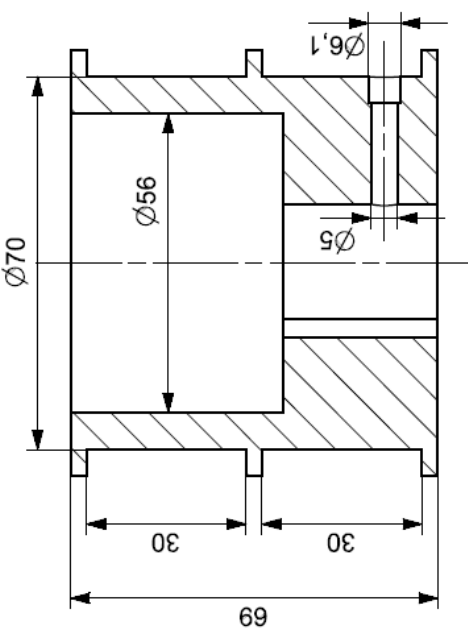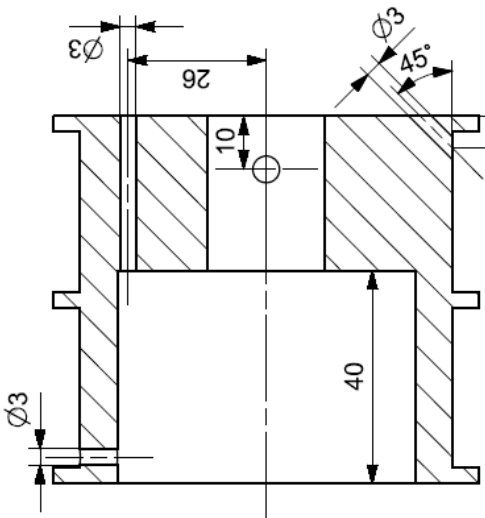Part Name / Part Description: Pulldown System

Master Thesis Martin Tangen

Drawn By:	MHT	Date:	19.03.16
Sheet:	A3 - 1 of 1	Scale:	1:2
Part No / ID No:	-	Revision:	A

NTNU Aalesund
Larsgardsvegen 2
6009 Aalesund
Norway

A3

SECTION B-B

32

SECTION A-A

ϕ13
ϕ13
18

45
50
25
24,5

A
A

B
B

50
550
32
47

Drawing dimensions and annotations:

- 70
- 30
- 150
- 200
- 15
- 30
- 2x M4
- 50
- 90
- Ø100
- Ø84
- 4x Ø7
- 250
- 142
- 71
- 6x Ø10
- 120
- 60
- 180
- 20
- 22
- 43
- 100

Balloon references: 1, 2, 3, 4

PC NO	QTY	PART NAME			MATERIAL
4	1	Feste kondensator		6 mm	Aluminium
3	2	Vinkel		8 mm	Aluminium
2	1	Motorfeste		8 mm	Aluminium
1	1	Brakett mot tank		8 mm	Aluminium
				PLATE THICKNESS	

Part Name / Part Description
Brakett
Slepetank

Drawn By: Martin Tangen
Date: 26.02.18
Scale: 1:2
Sheet: A3 - 1 of 1
Revision: A
Part No / ID No: -

A3

Toleranser etter NS-ISO 2768-1 Middels

SECTION B-B

SECTION A-A

Ø3
26
Ø3
45°
10
6
40
Ø3

A
B
2x M5
Ø22,1
Ø80
Ø40
A
B

Ø70
Ø56
Ø6,1
Ø5
30
30
69

7x M5

Ø22

M 5

40

120

6

10 | 10 | 25

13

20

Kilespor etter standard

Toleranser etter NS-ISO 2768-1 Middels
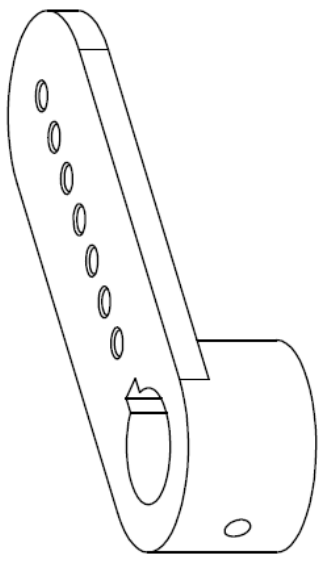
PC NO	QTY	PART NAME	MATERIAL
2	1	Festebrakett	S235JR
1	1	Sylinder med kile	S235JR

Martin Håbet Tangen

Master's thesis

NTNU
Norwegian University of
Science and Technology